METHODS FOR GENERATION, MANIPULATION AND CHARACTERIZATION OF HIGH REPETITION RATE OPTICAL FREQUENCY COMBS

A Dissertation

Submitted to the Faculty

of

Purdue University

by

Supradeepa Venkata Subbaiah Ramakrishna

In Partial Fulfillment of the

Requirements for the Degree

of

Doctor of Philosophy

May 2011

Purdue University

West Lafayette, Indiana

To my family

ACKNOWLEDGMENTS

I would like to thank my advisor Professor Andrew M. Weiner for his guidance, support, and patience throughout my graduate study. It was a great opportunity to be a member of his group, to learn from him and to do research on exciting topics. I also would like to thank Professor Daniel Elliott, Professor David Nolte and Professor William Chappell for serving as my Ph.D. committee members and for their helpful comments.

My special thanks go to Dr. Daniel E. Leaird for his invaluable technical support and guidance throughout. I would like to thank my current and former colleagues Dr. Ehsan Hamidi, Dr. Chen-bin Huang, Dr. Albert Vega, Dr. Hao Shen, Rui Wu, Fahmida Ferdous, Dr. Christopher Long, Dr. Victor Torres-Company, Dr. Li Xu, Dr. Dong-sun Seo, Dr. Houxun Miao, Dr. Gladys Minguez-Vega and Dr. Shawn Wang for valuable discussions (both technical and social) when I needed them. I would like to thank Dee Dee Dexter and all the other staff at the School of Electrical and Computer Engineering at Purdue University for invaluable help on official matters.

Finally, on a personal front, I would like to thank all my good friends at Purdue, who made my stay fun and productive. I would always be grateful to my family for being there for me, whatever I choose to do.

TABLE OF CONTENTS

Page

Page

LIST OF FIGURES

Figure Page

Figure Page

Figure Page

Figure Page

LIST OF ABBREVIATIONS

ASE	Amplified spontaneous emission
AWG	Arrayed waveguide grating
BS	Beam splitter
CW	Continuous wave
DCF	Dispersion compensating fiber
DDF	Dispersion decreasing fiber
EDFA	Erbium doped fiber amplifier
FSR	Free spectral range
FWHM	Full width at half maximum
FWM	Four wave mixing
HNLF	Highly non-linear fiber
IM	Intensity modulator
OAWG	Optical arbitrary waveform generation
OSA	Optical spectrum analyzer
PBS	Polarizing beam splitter
PC	Polarization controller
PM	Phase modulator
PMCW	Phase modulated continuous wave laser
PS	Microwave phase shifter
RF	Radio frequency
SLM	Spatial light modulator
SMF	Single mode fiber
SNR	Signal-to-noise ratio
VIPA	Virtually imaged phased array

ABSTRACT

Venkata Subbaiah Ramakrishna, Supradeepa. Ph.D., Purdue University, May 2011.
Methods for Generation, Manipulation and Characterization of High Repetition Rate Optical Frequency Combs. Major Professor: Andrew M. Weiner.

In recent years, driven by metrological applications, there has been significant development in lasers producing very short pulses periodically with stabilized repetition rates and center frequencies. In frequency domain such lasers have discrete spectral lines with fixed frequency positions and are known as optical frequency combs. Utilizing such sources together with the well established techniques of Femtosecond pulse shaping, individual spectral lines can be controlled independently allowing for 100% duty factor very high complexity waveform generation. This is known as optical arbitrary waveform generation (OAWG) and promises to have significant impact in optical science and technology.

The key components of an OAWG system primarily involves –

1. A source generating a high repetition rate frequency comb
2. An apparatus which can manipulate the comb on a line-by-line basis
3. Characterization techniques to analyze the modifications done to the comb

The work presented here has spanned all these three aspects. Firstly, a new class of pulse shapers which can achieve more than a magnitude improvement in achievable waveform complexities compared to previous techniques will be demonstrated. Next, two different characterization techniques (applicable in different situations) for high repetition rate frequency combs and arbitrary waveforms will be demonstrated. The last part of the dissertation would be on new ideas utilizing phase modulation for generating high stability, broadband optical frequency combs which are easily tunable in center frequency and repetition rate. Building upon recent ideas to generate frequency combs starting from continuous wave (CW) lasers, frequency comb sources with record spectral

flatness and pulse quality are demonstrated. Techniques for significant enhancement in bandwidth of such sources using nonlinear optics in fibers will also be discussed.

1. INTRODUCTION

Optical arbitrary waveform generation (OAWG), also known as line-by-line pulse shaping is a methodology to make very high complexity optical waveforms. It combines the area of optical frequency combs together with femtosecond pulse shaping. Our research till date has focused on development work on different aspects of OAWG, including generation, characterization and systems applications. This will be the main theme of this dissertation. In order to understand the process of OAWG, it is necessary to have an understanding of optical frequency combs. To this effect, we will briefly talk about optical frequency combs in section 1.1. In section 1.2 we will describe in detail the principles behind OAWG. Section 1.3 describes the different aspects of our work and how the motivation for it arises from OAWG. Section 1.4 provides a general organization of this dissertation.

1.1 Optical frequency combs

An optical frequency comb [1, 2] is a name given to a pulsed laser source emitting a periodic waveform with a stabilized repetition rate. In frequency domain, such a source is constituted of a discrete set of frequencies spaced by a constant period. This looks like a comb and hence the origin of the name. Traditionally, mode locked lasers which emit a periodic train of short pulses have been the primary sources of optical frequency combs. Attributes that are desirable in a frequency comb include having stable frequency positions of individual comb lines and knowing the exact frequency position of the individual comb lines. By suitable locking mechanisms, the frequency positions of the comb lines can be stabilized, however exact determination of individual frequencies is hard. This happens because the absolute optical frequencies constituting the comb will not be exact multiples of the repetition rate owing to difference between the phase and

group velocities in the laser cavity. The individual comb lines are given by the equation [1]

$$f_m = mf_{rep} + \varepsilon \tag{1.1}$$

Where f_{rep} is the repetition rate of the laser and ε is known as the carrier envelope offset, whose value is not easy to obtain and because of which, exact determination of frequencies becomes difficult. Fig 1.1 schematically shows this. Fig 1.1(a) shows an ideal frequency comb with an infinite bandwidth. Fig 1.1(b) shows a schematic of a realistic spectrum from a mode locked laser with a Gaussian envelope where the comb lines are offset from multiples of the repetition rate by the carrier envelope offset frequency. Fig 1.1(c) shows the envelope of time domain trace corresponding to the comb.

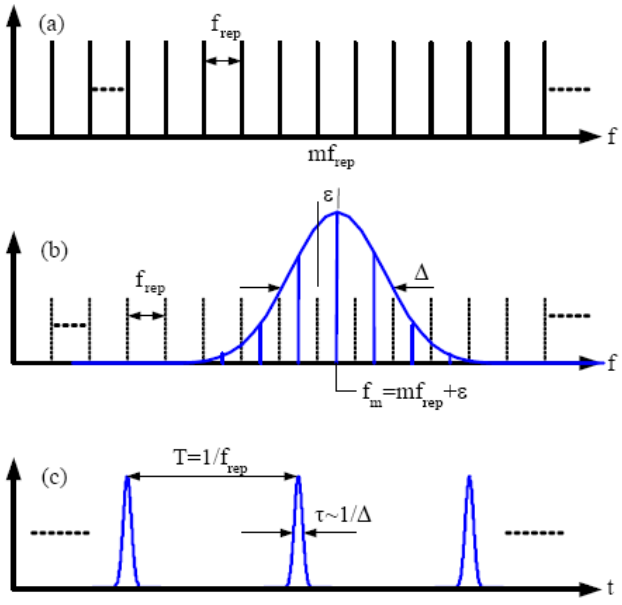

Fig 1.1 (a) Ideal frequency comb, (b) Representative output spectrum of a mode locked laser with a Gaussian envelope, (c) corresponding time domain representation

In the last decade, driven by metrological applications, there were significant developments in frequency combs and a method to measure and lock the carrier envelope offset was proposed. Such combs are called self referenced frequency combs and they have stabilized frequency lines with known frequency positions [1, 2].

However, the laser output is still a series of bandwidth limited pulses and for various applications, it is necessary to shape the waveforms into user defined shapes.

This can be achieved with the well established technique of Femtosecond pulse shaping [3]. However, the true strength of using frequency combs as sources in pulse shapers come when spectral lines constituting the comb can be controlled individually [4]. This in time domain corresponds to potentially 100% duty factor shaped waveforms with arbitrary user defined features. This regime is known as optical arbitrary waveform generation and we will discuss this further in section 1.2.

Before we go into the next section, there is an important point that needs to be discussed. An optical frequency comb can refer to any source with a stabilized repetition rate and stable carrier frequencies. This can be at very small repetition rates (i.e. kHz) all the way to THz. However, for practical applications, for e.g. in optical communications, the interesting regime will be in repetition rates of 10s of GHz corresponding to the data rates used. Also, in order to be able to address individual spectral lines in a pulse shaper, it is necessary to have relatively wider spacing (again of the order of GHz). So when we refer to OAWG, we are usually talking about relatively high repetition rate frequency combs. However, mode locked lasers don't scale well into these repetition rates while maintaining frequency stability. Due to this reason, there has been significant development of alternate frequency comb sources with high repetition rates [5-8]. This also forms an important aspect of our work and a detailed description of our contribution is discussed in chapter 4.

1.2 Optical Arbitrary Waveform Generation (OAWG)

As we described in the previous section, by shaping the amplitude and phase of individual lines of a frequency comb, 100% duty factor waveforms can be generated and this is known as optical arbitrary waveform generation (OAWG). Figure 1.2 schematically shows the difference between conventional pulse shaping ("group of lines regime") and OAWG ("line-by-line regime"). In the group of lines case, in time domain shaped pulses are isolated in time, where as in the line-by-line regime they occupy the entire time window leading to 100% duty factor waveforms.

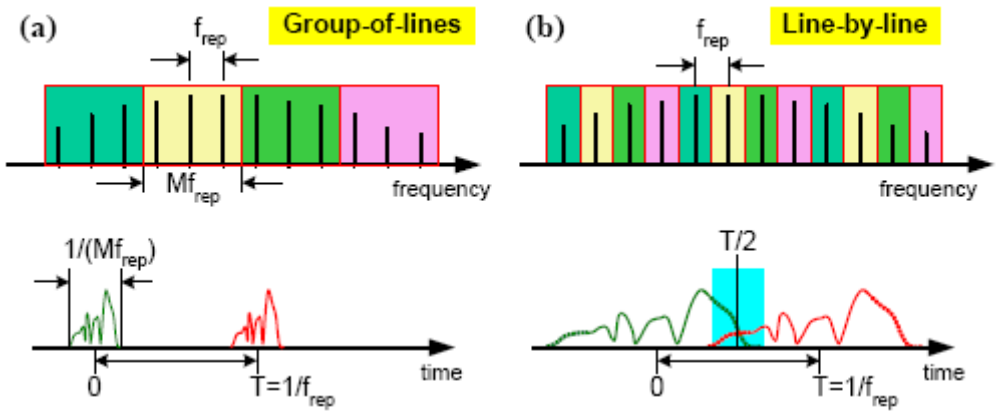

Fig 1.2 Pulse shaping (a) Group of lines regime, (b) Line-by-line regime

Another interesting extension of this regime is the case when the pulse shaping operation is modified at the repetition rate of the comb. In this case, the waveform updates on a frame to frame basis allowing for potentially infinite record length, very high complexity waveforms. This is schematically shown in fig 1.3.

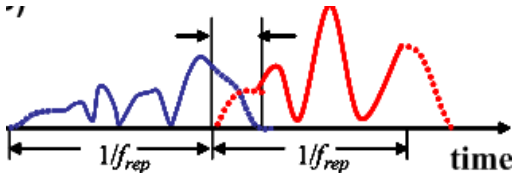

Fig 1.3 OAWG with frame to frame update

Potential applications of OAWG include wide bandwidth optical communications (for e.g one can think of simultaneously encoding all the channels in a dense wavelength division multiplexed system (DWDM) together), secure communications in phase and amplitude modulation (for e.g. optical CDMA [9-10]), optical signal synthesis, ultra-high resolution remote sensing, LIDARs, spectroscopic sensing and coherent control.

Let us now briefly describe the operating principle of femtosecond pulse shaping [3] by which the waveforms are generated. In a Fourier pulse shaping apparatus, the spectrum of an incident pulse is spread spatially using a spectral disperser (for e.g. a diffraction grating) and focused onto a spatial light modulator (SLM), which transfers spatial phase and amplitude information onto the complex optical spectrum. This Fourier synthesis procedure results, after the optical frequencies are recombined, in programmable user-defined waveforms.

An important requirement of the OAWG setup is the ability to spectrally resolve individual comb lines. This can be achieved in conventional grating based pulse shapers using bigger beams and finer groove spacing on the gratings. Fig 1.4 shows the schematic of a grating based high resolution pulse shaper aligned in a reflective configuration used to address comb lines individually.

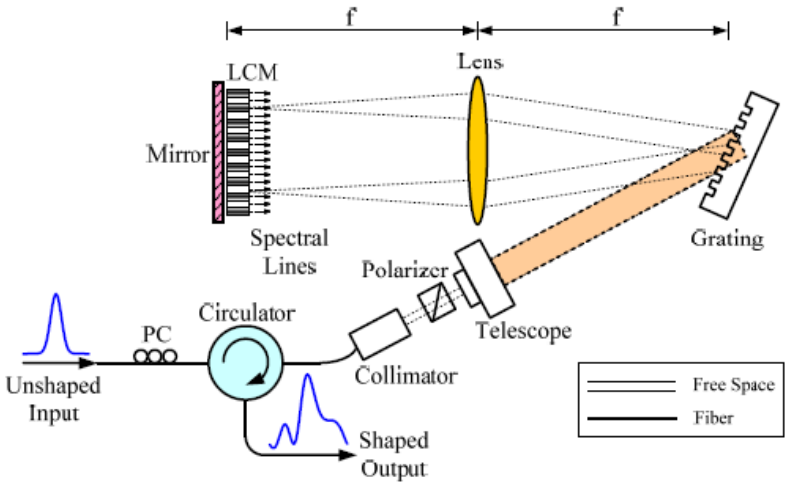

Fig 1.4 Grating based high resolution Fourier pulse shaper

Other possibilities include using high spectral resolution spectral dispersers (like the virtually imaged phased array (VIPA)) [11, 12]. However, either way there is a compromise required between the achievable spectral resolution and total bandwidth. This limits the complexity of the synthesized waveforms. In chapter 2, we will be demonstrating a new configuration which overcomes this constraint.

1.3 Key components of an OAWG system – Motivation for our work

The key components of OAWG systems are –

- A high repetition rate frequency comb source.

- An apparatus to encode information by manipulating the amplitude and phase of individual lines of the comb.

- Characterization apparatii which can measure the changes made and also provide decoding techniques in system applications.

Now, let us look into each of these in more detail and describe how our work contributes to further the existing technologies in each of these aspects.

As we discussed in the previous sections, the first aspect of interest is a frequency comb source which provides us the initial waveform. For OAWG applications as well as other applications in optical communications, LIDAR, RF photonics etc, we desire the following key attributes –

- **High repetition rate**. This can be in the order of 10GHz and above. This is necessary to ensure that the OAWG system can resolve the lines for encoding purposes. In the context of other applications, (like optical communications for example), the frequency comb is a phase locked multi-wavelength source and each line is used to encode data. This necessitates that the spacing be relatively high to ensure high data rate communications.
- **Optical frequency stability.** One of the key attributes of OAWG is the coherent synthesis of waveforms for various applications. In such a system, it is very important to ensure that the optical frequencies stay fixed.
- **Easy tuning of repetition rate and center frequency.** Different applications might require different repetition rates and optical center frequencies. So, our source should be in a position to easily tune both the center frequency as well as repetition rate.

Modelocked lasers are the sources of choice for generating low repetition rate frequency combs. However, it is difficult to scale their repetition rates to the required multi-GHz level while maintaining the same fidelity of operation obtained in low repetition rates. These lasers become more complex and the performance (in terms of generated bandwidth and stability) is reduced. Tunability is very hard to achieve and repetition rate as well as optical center frequency is fixed. Further more, they drift over time and complex control schemes are necessary to stabilize them. Owing to these

reasons, in recent years, there has been significant interest in generating frequency combs by direct phase modulation of an input CW laser. This technique allows for convenient tuning of center frequency and repetition rate as well. However, so far the spectral flatness and complex schemes necessary to create a pulse train from the source has become a limiting factor hampering its use for many applications. In our work, we will propose techniques to overcome this and demonstrate how frequency combs with very flat spectra and high quality pulse sources can be obtained using phase modulation.

The next step is to be able to control the individual lines of the comb in a programmable fashion both in amplitude and phase. Desirable attributes would be to be able to address as many lines as possible. We achieve this proposing a new class of hybrid pulse shaping configurations utilizing two spectral dispersers in cross dispersing configurations. A performance improvement of an order can be obtained with such a configuration compared to previous methods.

Simultaneous to generation capabilities of high repetition rate frequency combs and optical arbitrary waveforms, it is necessary to have techniques to characterize them. These sources and waveforms pose unique challenges for characterization rendering existing pulse measurement techniques largely incapable of handling them. We will discuss this further in chapter 3 and propose two new ideas for characterization of these waveforms. These two methods are applicable in different regimes and even as standalone methods, provide solutions to interesting applications. This will also be discussed further in chapter 3.

In summary, our work provides a tested recipe to establish a complete OAWG system. This is achieved by new ideas and techniques for generation, manipulation and characterization of high repetition rate frequency combs.

1.4 Organization of the dissertation with summary of our contributions

The organization of this dissertation will largely follow a chronological order. The early work was mainly done on frequency comb manipulation techniques and this is covered in chapter 2. Here, we will propose a new pulse shaping configuration to achieve high complexity waveform generation by simultaneously using a spectral disperser called the

virtually imaged phased array (VIPA) and a diffraction grating in a two dimensional geometry. We will demonstrate results with both low repetition rate and high repetition rate frequency combs. Also covered in this chapter are theoretical and experimental studies into temporal dispersion characteristics of a VIPA when used in a pulse shaper. The last section of this chapter will cover methods to achieve programmability utilizing 2-D spatial light modulators. Our new 2-D pulse shaping configuration achieves a significant increase in waveform shaping complexity (measured by number of controllable features) compared to previous demonstrations. Further more, this technique has the potential to achieve octave spanning bandwidths and waveform complexities several orders greater than currently achievable.

Chapter 3 will be dedicated to characterization techniques for optical arbitrary waveforms. After a brief discussion on challenges for charactering these waveforms, we will present two different characterization techniques. We will also extend one of the techniques to single shot regime in which waveforms are rapidly updated on a frame by frame basis. This is the first demonstration of single shot measurements of complex waveforms (bandwidth > 1THz (1ps temporal resolution) and record length of 100ps) emanating from high repetition rate frequency combs. Previous demonstrations were largely limited to low repetition rate sources (< 10s of MHz) and this work improved on it by three orders. Several challenges were overcome to achieve this objective. Also covered in this chapter will be applications of these characterization techniques for fast monitoring of dispersion and dispersion slope of long optical fiber links and characterization of novel optical frequency comb sources. This was the first demonstration of coherent measurement techniques of link properties in the several km of fiber regime. All previous demonstrations were significantly limited to an order of few meters of fiber (three orders smaller).

Chapter 4 will be about generation techniques for high repetition rate frequency combs starting from continuous wave (CW) lasers. We will first discuss methods to spectrally equalize phase modulated CW combs and methods to generate high quality pulse trains from them. We will then discuss techniques to enhance the bandwidth of such frequency combs utilizing non-linear fiber optics. Previous demonstrations of

frequency comb generation from CW lasers suffered from poor spectral quality. There was a compromise between achievable bandwidth with a required level of spectral flatness. In this work we improve over previous demonstrations significantly. Compared to previous demonstrations with similar comb flatness as we have, we achieve bandwidths of > 10 times. With respect to previous demonstrations having similar bandwidths, we achieve significant flatness enhancement of > 5 (defined by ratio of tall lines to short lines in the comb spectrum). Our work is also the first to demonstrate very high quality pulse generation from these combs without complex schemes to correct distortions. We expect that the ability to achieve broad-bandwidths together with the convenience of these frequency comb sources makes them a very promising candidate was a variety of frequency comb and short pulse applications.

Chapter 5 will be summarizing our work and discussing future work.

2. HIGH COMPLEXITY FREQUENCY COMB MANIPULATION AND WAVEFORM GENERATION

In this chapter we will demonstrate a new pulse shaping configuration which utilizes two different spectral dispersers (a virtually imaged phased array (VIPA) and a diffraction grating) working in two spatial dimensions to achieve high complexity optical waveform generation. This configuration derives its strength from simultaneous use of high resolution spectral dispersion properties of the VIPA with broad operating bandwidth of diffraction gratings thus providing the benefits of either. In section 2.1 we will discuss this further by highlighting the limitations of one dimensional pulse shapers and how this is overcome in 2D. In section 2.2, we will briefly describe the operation of the VIPA. In section 2.3 we will describe the experimental setup of the 2D shaper. In the process of building the 2D pulse shaper, new temporal dispersion behavior detrimental to operation of the pulse shaper was observed due to the VIPA. This aspect of the VIPA had to be understood quantitatively before it could be used together with other spectral dispersers. We will briefly describe the observations and together with a quantitative model in section 2.4. In section 2.5 and 2.6 we will describe experimental results done with low repetition rate Femtosecond fiber lasers and high repetition rate optical frequency combs. Section 2.7 will demonstrate methods to achieve programmability. The work on the 2D shaper has been presented in our publications [13, 14].

2.1 Limitations of one dimensional Fourier pulse shapers

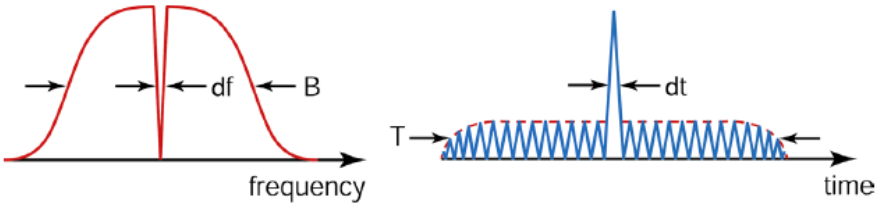

Fig 2.1 Relation between frequency domain and time domain in Fourier pulse shaping (from [3])

In Fourier pulse shaping there is a reciprocal relation between the smallest frequency feature that can be controlled and the total temporal width of the shaped waveform. In the schematic shown in fig 2.1, the smallest frequency feature is ‘df’ and this is inversely

proportional to the total temporal width, denoted in the figure by ‘T’. Similarly, the total bandwidth addressable in the frequency domain (shown as ‘B’) is inversely proportional to the finest temporal feature ‘dt’. So in order to achieve high complexity waveform generation it is desirable is to have both high resolution of operation together with a wide addressable bandwidth. In one dimensional configurations this is not possible due to two reasons, firstly any spectral disperser used requires a compromise between achievable spectral resolution and total bandwidth and secondly the number of control elements on one dimensional spatial light modulators (which is limited to a few hundred) limits the total number of addressable frequency features.

Diffraction gratings have long been the primary spectral disperser used in pulse shaping. They have been successfully used in pulse shapers working with very short pulses done to few carrier cycles which in frequency domain correspond to very wide bandwidths. However to achieve higher spectral resolution, it is usually necessary to simultaneously reduce the line spacing on the grating and increase the size of the beam incident on the grating [4]. Reducing the line spacing is a hard task since conventional gratings are made using photo lithographic techniques and the wavelength of light used in manufacture fundamentally limits the achievable line spacing. Also, with increasing spectral resolution (which leads to higher spatial separation between wavelength components) light starts to get dispersed in a wide region which though is not a limitation in theory, causes difficulties in practical implementation. Due to these effects, the maximum achievable spectral resolution in grating based pulse shapers has been limited to ~5GHz operating over bandwidths of < 1THz [4]. We see that though the spectral resolution achievable is quite high, as a compromise the bandwidth is significantly reduced.

An alternate route to achieve high spectral resolution is to use a high resolution spectral disperser. A key example is a VIPA which we will be using in our experiments though there are others, for e.g. Arrayed Waveguide Gratings (AWG) [15] and cascaded fiber bragg gratings [16]. A programmable 1D pulse shaper based on a VIPA spectral disperser that achieves ~700 MHz spectral resolution – a significant enhancement compared to grating based shapers has been reported [12]. However, the VIPA is characterized by a free spectral range (FSR), at most a few hundred GHz, and this limits the bandwidth over which spectra may be independently manipulated.

From the above discussion we see that using a single disperser operating in one spatial dimension it is impossible to simultaneously achieve both high resolution and broad bandwidth. However we can imagine a situation where if both a grating and a

VIPA are used together, benefits of both can be obtained. In the next sections, after a brief description of the VIPA device, we will discuss how this can be done.

2.2 Virtually Imaged Phased Array (VIPA)

An important component we will use in our experiment is a virtually imaged phased array (or a VIPA) [11]. A VIPA is a side entrance Fabry-Perot etalon which achieves spectral dispersion with high resolution using multiple beam interference.

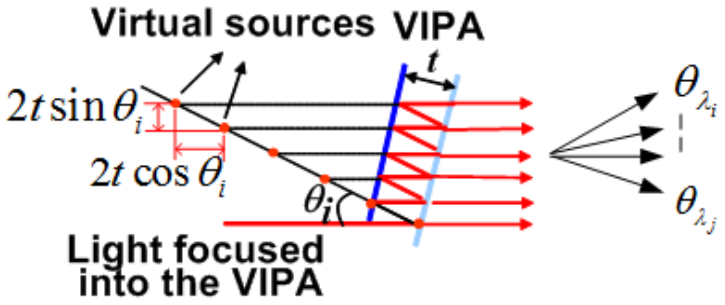

Fig 2.2 Schematic of a virtually imaged phased array (VIPA)

Fig 2.2 schematically shows a VIPA. The front side of the VIPA is 100% reflecting, while the back side is ~95-98% reflecting. Light is coupled into the VIPA using a cylindrical lens and it bounces around in the etalon leaking a bit of power in each bounce. In the figure 't' refers to the thickness of the VIPA and θ_i refers to the input angle. As shown in the figure, the VIPA can be modeled as a set of virtual sources spatially separated from each other. These sources act as a phased array creating constructive interferences for different wavelengths in different directions, hence acting as a spectral disperser.

Using the VIPA in a pulse shaping configuration, high spectral resolutions down to 700MHz have been demonstrated [12], however similar to any Fabry-Perot device, the VIPA has a free spectral range (FSR) of the order of few hundred GHz, which gives us a measure of bandwidth over which the spectral dispersion by the VIPA is unique. Otherwise, frequencies separated by an FSR apart have the same angular dispersion. This aspect of the VIPA limits its applicability for a lot of applications particularly for short pulses which have bandwidths much wider than the FSR of the VIPA.

2.3 A two dimensional pulse shaping configuration using a virtually imaged phased array (VIPA) and a diffraction grating

Before we describe the experimental setup, a brief description of the operating principle would be useful. When the input signal to a VIPA has a bandwidth broader than its FSR, the spectral dispersion wraps on itself with periods of one FSR, meaning frequencies separated by one FSR (which can be a few 100GHz) occupy the same spatial position. So with a VIPA alone though spectral resolution obtained is high, this aspect of its spectral dispersion limits the total accessible bandwidth. However 100s of GHz is significantly large enough to be separated using a grating based pulse shaper. So, the idea is to use a grating aligned in a perpendicular direction to the direction of the VIPA such that the different overlapping FSRs after dispersion by the VIPA are spatially separated in a perpendicular direction by the grating. Now instead of having a line of dispersed frequencies, it's a two dimensional matrix. This 2D arrangement as a spectral disperser has been previously used for experiments in optical communications for wavelength demultiplexing [17], wavelength-parallel polarization sensing [18], and frequency-comb spectroscopy[19], but prior to now has not been demonstrated for optical pulse shaping.

Figure 2.3 shows the experimental setup. For the source we utilize either a 50MHz repetition rate mode-locked erbium fiber laser generating 150 fs bandwidth-limited pulses or a 10 GHz repetition rate optical frequency comb consisting of more than 500 comb lines (within 30dB) corresponding to bandwidth-limited 415 fs pulses [8]. The pulse shaper consists of a VIPA-grating spectral disperser, cylindrical lens focusing elements, and a retroreflecting mirror, with the output extracted through an optical circulator. The VIPA used is air spaced and has a FSR of 200GHz. The transmission grating has a pitch of 940 lines/mm. After the VIPA and the grating, two cylindrical lenses are used, one for each of the dispersers. This step is necessary because of the need to obtain a zero net temporal dispersion configuration for either spectral disperser independently. Reflective grating based pulse shapers employ a single lens in a 4-f configuration, where the grating-lens and lens-mirror distances are each set equal to the focal length for zero net temporal dispersion. However, VIPA based pulse shapers require a different distance to have zero temporal dispersion. Hence, to achieve net zero dispersion for both dispersers

together, the degree of freedom offered by using two lenses is necessary. We will discuss this further in the next section and characterize the zero dispersion condition for VIPA based pulse shapers. Fig 2.4 shows the output spectrum and intensity crosscorrelation in the zero dispersion configuration. We see that the input and out spectra are similar indicating no spectral distortion introduced by the pulse shaper. The output crosscorrelation is a bandwidth limited pulse similar to the input indicating absence of any temporal dispersion. The total loss of the pulse shaper including the circulator was ~15dB. To better represent this number, VIPA only pulse shapers have a loss of ~12dB; the increase in loss moving to a 2D setup is approximately 3dB.

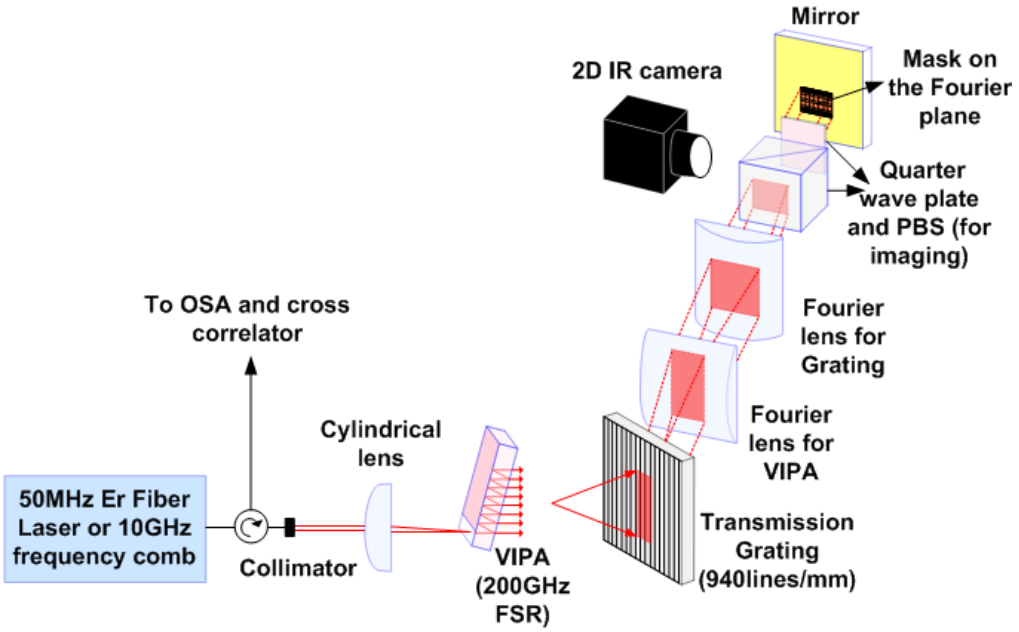

Fig 2.3 - The experimental setup - after undergoing dispersion by the VIPA (free spectral range (FSR) of 200GHz) and the grating (940lines/mm) in perpendicular directions, and spatial Fourier transforms by the respective lenses, the light forms a 2D pattern on the Fourier plane where a patterned mask shapes the input spectrum. An adjustable fraction of the light is diverted to an imaging camera for aligning and monitoring the mask.

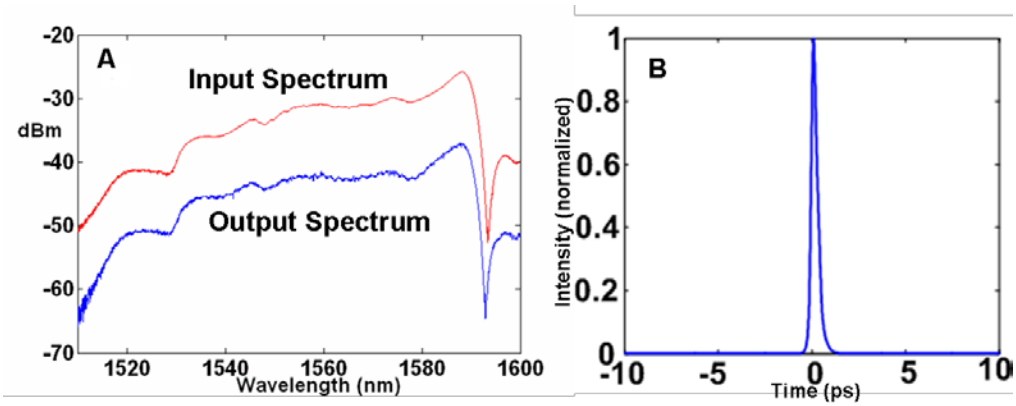

Fig 2.4 Output characteristics for the Femtosecond fiber laser observed at zero dispersion configuration for (A) Comparison between input and output spectrum showing no distortion, (B) Intensity cross correlation of the output pulse showing bandwidth limited pulse

For this current set of experiments, we implement pulse shaping using an amplitude only mask that is patterned in 2D using standard photolithographic techniques. Our final goal is to have both amplitude and phase control and to do this efficiently a 2D spatial light modulator is necessary. This will be further discussed in section 2.7. However since amplitude masks are relatively easy to make, we use them for a first demonstration of the operation of the 2D shaper. Further, it is relevant to note that for a variety of experiments (for e.g. in spectroscopy), amplitude control alone is sufficient.

In a two dimensional configuration, there is an additional alignment degree of freedom necessary to put the mask in correct orientation. Therefore, a continuous real-time monitoring tool is essential to properly orient the mask. This monitoring was provided by the IR camera (shown in fig 2.3) which images the Fourier plane of the pulse shaper. A polarizing beam splitter followed by a quarter wave plate makes it possible to control the amount of power going to the camera and minimizes losses for the shaper. The 2D IR camera used in these experiments to obtain the images of the Fourier plane acquires images in a grey scale format. Minor processing has been performed on the images to be shown in the following figures which include reducing the ambient noise, increasing the contrast, and changing the color scheme to improve readability of the images. Otherwise, the images are exact representations of the Fourier plane in the experiment.

Figure 2.5 (A) shows the Fourier plane image for the 50MHz repetition rate Erbium fiber laser source without masking. In the figure, all the frequency components of the input source are present and the image appears to be continuous streaks which are different VIPA FSRs spatially separated by the grating. The laser repetition rate of 50MHz is significantly smaller than the spectral resolution in our setup which is ~3GHz, hence, though the spectrum consists of discrete frequency components, the Fourier plane image appears as continuous streaks. Fig. 2.5 (B) shows the Fourier plane image with an amplitude mask designed to introduce both coarse and fine features into the optical spectrum, while also suppressing all but the main diffraction order of the VIPA. Ideally the mask can be made to simultaneously shape identical frequency components from different orders, however this is difficult to achieve in a fixed mask configuration (without programmable control) and so in our current set of experiments we block all the VIPA orders except the dominant order.

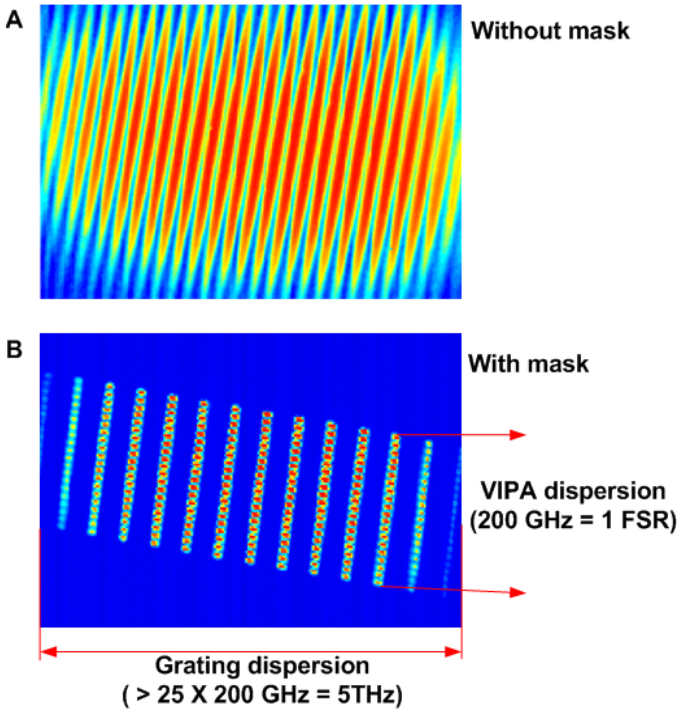

Fig 2.5, (A) Image of the Fourier plane without a mask, (B) with a mask.

2.4 New temporal dispersion aspects manifested by a VIPA based pulse shaper

Before we go into experimental results with the 2D shaper, it is important to describe some new aspects of temporal dispersion manifested by a VIPA based pulse shaper.

For a brief background - an important attribute desirable from the pulse shaping apparatus is that there should be no additional amplitude or phase effects other than the ones which are user defined. This would ensure that the waveform shaping is purely user defined without any extraneous effects. Another way of looking at this is, in the absence of a mask, the output and input fields should be identical. Usually with reasonable choice of components, the spectral amplitude effects due to the apparatus are minimal; however it is more involved when it comes to spectral phase effects. The origins of phase effects lie in the well known fact that when ever there is angular dispersion of spectral components there is a possibility of temporal dispersion, which in the frequency domain corresponds to additional spectral phase of second order and higher (linear spectral phase is a delay in time) [20, 21]. Physically this is associated with the fact that whenever there is spectral dispersion, there is a possibility that the different frequency components which are now travelling in different paths can travel different distances leading to chromatic dispersion. In pulse shapers since there is spectral dispersion and recombination before and after masking respectively, it becomes necessary to ensure that the apparatus does not introduce any additional temporal dispersion of the input light. In such a configuration the input and output in the absence of masking will be identical and this is called the zero dispersion configuration.

The most common spectral disperser used in pulse shaping is a diffraction grating and the zero dispersion configuration here is well characterized and known as the 4-F configuration [3]. In this configuration the lens which focuses the light spectrally dispersed by the grating on the Fourier plane (where the mask is placed) is in between them at an equal distance of one focal length (F) from each. In either of the two main schemes which exist for recombination, 1) Reflective geometry, where a mirror at the Fourier plane reflects the light back in the same path as the incident light or 2) Transmission geometry, where a 2^{nd} pair of identically placed lens and grating is used after the Fourier plane, light travels a distance of 4F between its first and second

incidence on a grating and hence the origin of the configuration's name. The 4-F configuration provides a dispersion free configuration when using diffraction gratings over reasonably broad bandwidths and has been used for a long time now.

In order to use a VIPA in a pulse shaping apparatus, it becomes necessary to understand the temporal dispersion characteristics and look for the zero dispersion configuration. As it turns out, for a VIPA the 4-F configuration is significantly away from zero dispersion. Fig. 2.6(A) shows the input pulse with a pulse width of ~150fs to the pulse shaper and fig. 2.6(B) shows a section of one VIPA free spectral range (FSR) size of the input spectrum which in this case is 200GHz(~1.6nm at 1550nm). The input pulse is a bandwidth limited pulse and the spectrum is flat. Since the VIPA is a Fabry Perot etalon based device, the frequency response is periodic at the free spectral range and in experiments when the input bandwidth is greater than the FSR, the modifications introduced by the VIPA are periodic at the FSR. Because of this reason, representing one FSR is sufficient since all the information about the modifications introduced by the VIPA is contained in it. At the output (fig 2.6(C)) we see a pulse train under a wide temporal envelope which significantly differs from the input. This is indicative of large temporal dispersion by the pulse shaper. To clarify why we are seeing a pulse burst instead of a broadened pulse we note that the short input pulse has a bandwidth much wider than the FSR of the spectral disperser. So any modification that happens is repeated at periods of one FSR and hence if the pulse shaper is introducing temporal dispersion, which in frequency domain is a spectral phase effect, this phase is periodically repeated. The net effect is a pulse train where the individual pulse widths are still the same as the input pulse width but under a temporal envelope whose width is dependent on the amount of dispersion introduced. So the observed pulse burst behavior is a manifestation of significant temporal dispersion [22]. If the initial bandwidth of the pulse was equal to or smaller than the FSR of the disperser, then a more straightforward effect would have been seen where the input pulse would have been broadened to a pulse whose width is equal to the width of the envelope in fig. 2.6(C) similar to effects of temporal dispersion observed in grating based pulse shapers. We see from the width of the temporal envelope that at the 4-F configuration a ~150fs input pulse is broadened to more than 100ps and

hence is very far from being dispersion free. Another interesting effect observed is that, in the spectrum now (fig 2.6(D)) we have deep ripples. Since temporal dispersion is purely a spectral phase effect, it is surprising to see spectral amplitude effects. As we will explore in more detail in appendix A, this effect occurs due to multiple diffraction orders by the VIPA which in presence of temporal dispersion lead to wavelength dependent phase differences between different diffraction orders causing an interference phenomena which leads to the formation of these spectral ripples.

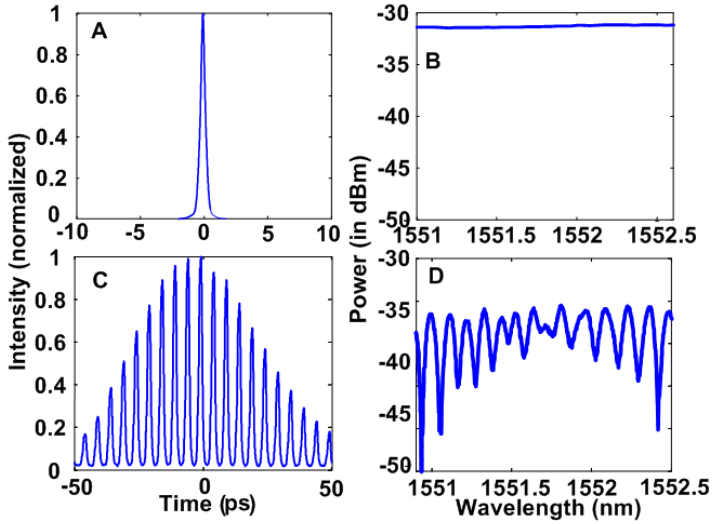

Fig. 2.6 (A) input pulse, (B) input spectrum, (C) output pulse, (D) output spectrum.

A main factor contributing to this modified temporal dispersion behavior is the pronounced non linearity in the frequency to space mapping by a VIPA spectral disperser in contrast to gratings which have a linear mapping for reasonable bandwidths. In fact most high resolution spectral dispersers show pronounced non linear frequency to space mapping even in small bandwidths. In presence of this non linearity, additional effects need to be taken into consideration to characterize temporal dispersion.

Here we will provide a qualitative description on why the dispersion characteristics of the VIPA are different and predict the zero dispersion condition. In appendix A, we will rigorously model the dispersion behavior and prove that the zero dispersion condition we obtain is correct. Also discussed in appendix A will be the spectral manifestation of dispersion which we will not be going into here.

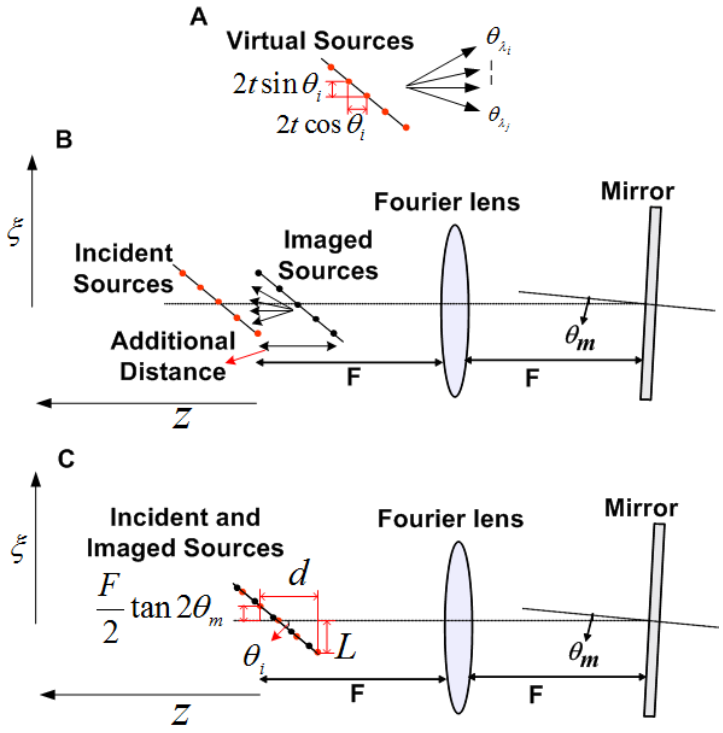

Fig. 2.7 (A) Schematic of spectral dispersion by a VIPA, (B) 4-F configuration of a VIPA shaper, (C) Zero dispersion condition for a VIPA shaper.

As previously described in section 2.2, a VIPA can be described as a series of virtual sources horizontally and virtually separated from each other and spectral dispersion occurs due to interference between these sources. Fig 2.7(A) shows a schematic of that. Now, in a pulse shaping configuration, with a Fourier lens and a mirror, the 4-F configuration is defined when the distance between the source and the Fourier lens is F. In case of a VIPA, this is not very clear since spectral dispersion is not happening from one point in space and so the 4-F configuration is defined as a distance of F from the first virtual source to the lens. This case is shown in fig 2.7(B). If we look at the line joining the incident set of sources and the reflected set of sources as an extended object in the optical system, we see that they fall in different places. As a result, there is additional dispersion as shown in fig 2.7(B). If we ask the question on what input configuration of sources leads to zero dispersion, we expect it to be the situation when the reflected set of sources superimpose onto the incident set of sources. Without a rigorous analysis it is hard to relate the offset distance between the incident and virtual sources to the amount of temporal dispersion, but it is intuitively clear that if they overlap, we would expect no

additional temporal dispersion. We calculated the location of incident virtual sources which allows this to happen, we obtain the zero dispersion condition for the VIPA shaper. The equation is –

$$L + \frac{F}{2}\tan 2\theta_m - d\tan\theta_i = 0 \quad (1)$$

Where, 'L' is the distance by which the first virtual source is offset from the optic axis. 'θ_m' is the tilt of the mirror, 'd' is distance by which the first virtual source is closer to the Fourier lens that F and 'θ_i'is the input angle to the VIPA. We will rigorously show in appendix A that this is the case.

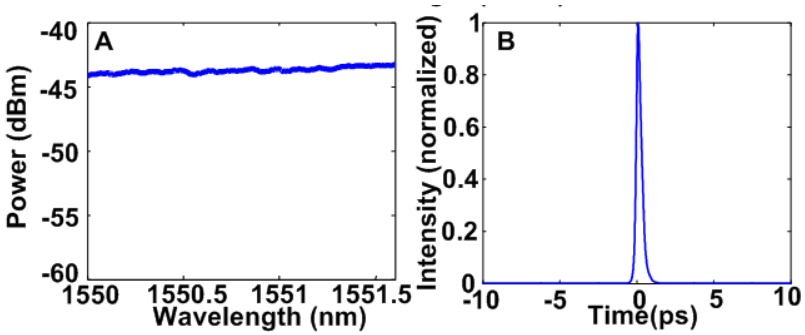

Fig. 2.8 Zero dispersion configuration for a VIPA shaper (A) Output spectrum, (B) Output intensity crosscorrelation.

Fig 2.8 (A) and (B) show the output spectrum and intensity crosscorrelation of a VIPA shaper aligned in the new zero dispersion configuration. We see a dispersion free bandwidth limited output pulse as expected and a flat spectrum without any ripples. This gives us the confidence that in future experiments the pulse shaping is happening purely due to user defined operations.

2.5 Experimental results with a low repetition rate Femtosecond fiber laser

In this section we will demonstrate pulse shaping results with the 2D pulse shaper using a 50MHz erbium fiber laser which produces short pulses of ~150fs. This allows us to demonstrate the increase in achievable complexities in waveform generation clearly owing to large available bandwidth from the source. It is important to point out here is that since 50MHz is much smaller than the spectral resolution of the VIPA, we are not

working at the line-by-line regime, but rather at a group of lines regime which in time domain corresponds to shaped pulses which are comparatively isolated in time.

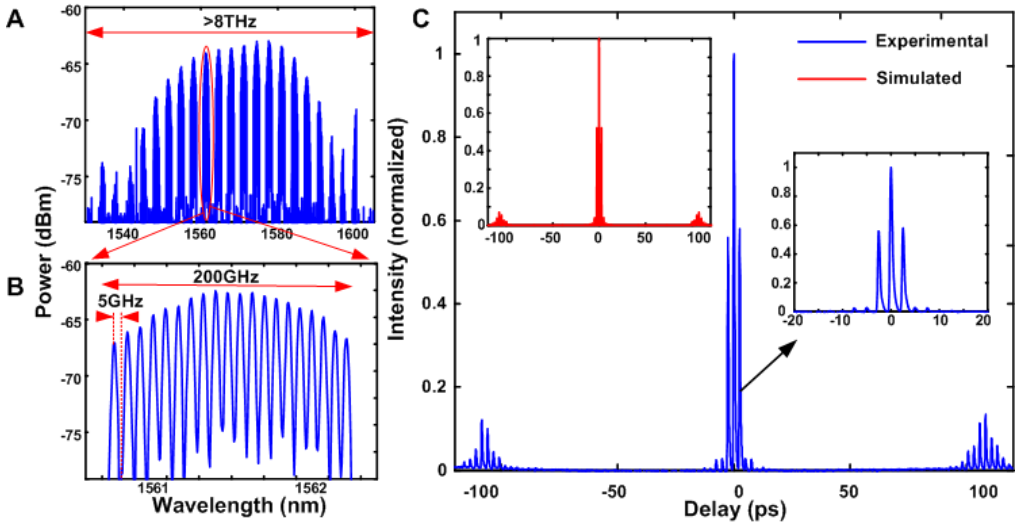

Fig 2.9 - (A) the full spectrum of the shaped pulse. (B) magnified portion of the spectrum circled in red in Fig. 2.9(A). The smallest features are 5GHz, and over a bandwidth of 8THz (> 64nm), there are more than 1600 controllable spectral features. (C) time domain cross correlation trace. An initially bandwidth limited pulse of 150fs is shaped over a time window exceeding 200ps.

Figure 2.9(A) shows an OSA measurement of the shaped spectrum, and Fig. 2.9(B) shows a magnified view of one FSR (circled in red in Fig. 2.9(A)) corresponding to the mask shown in Fig. 2.5(B). The mask blocks out every alternate FSR of the VIPA (indicated in the image by a doubling of the FSR-to-FSR spacing), introducing a coarse periodicity of 400 GHz. Within each transmitted FSR the mask creates on-off sections with a width of 5 GHz each (hence a 10 GHz fine periodicity). The magnified portion of the spectrum in Fig. 2.9(B) shows this on-off operation within a single FSR. The initial 10dB bandwidth covers more than 8 THz (>64nm). With the 5 GHz minimum feature size, the spectrum contains more than 1600 potentially controllable features, corresponding to substantially higher complexity than any previous pulse shaping demonstration to the best of our knowledge. The intensity cross-correlation trace shown in Fig. 2.9(C) demonstrates that the initial 150 fs pulse is now redistributed over a total time aperture of more than 200ps. The inset in red shows the simulated output which is in excellent agreement with the measurement. A small amount of 2nd and 3rd order spectral phase was added to the simulations of shaped waveforms to take into account the

small residual dispersion of the dispersion compensated fiber links. The same residual phase value was maintained for all simulations and was initially obtained by comparing the calculated cross-correlation assuming flat spectral phase with the cross-correlation of the pulse shaper output without any applied mask. The second inset shows the fine temporal features near the main pulse which arise due to the coarse periodicity in the mask. Even greater pulse shaping complexity is possible using this apparatus, limited in the present experiments by the input optical bandwidth.

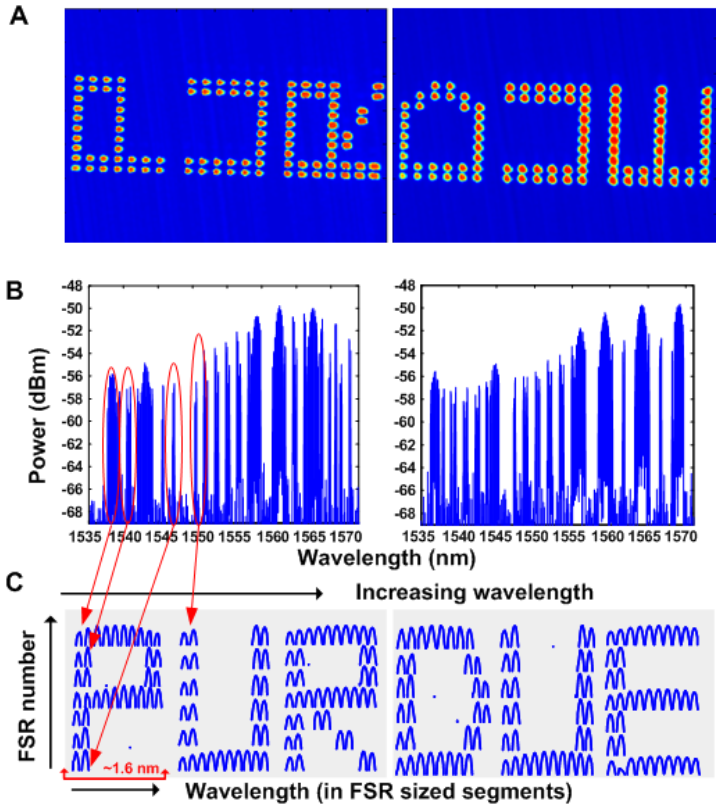

Fig 2.10 – (A) images of the Fourier plane for the two halves of the mask; the corresponding spectra are shown in (B). The smallest spectral feature is 10GHz and the total number of features in either spectra is around 450. To better represent the features determined by the mask, both spectra are split into three sections, each consisting a few FSRs of the VIPA. Each section is then plotted in segments of one FSR (200 GHz) lined vertically as shown in (C). The clear correspondence between the applied mask and the spectrum demonstrates enhanced spectral control made possible by the ability to control fine spectral features over a large bandwidth.

Figure 2.10 shows an example of a pure spectral shaping experiment. Fig. 2.10(B) shows OSA spectra obtained with the two masks whose images are shown in Fig. 2.10(A). Complicated structure is observed, with features as fine as 10 GHz spread over

4.5THz of bandwidth. Fig. 2.10(C) shows the same spectra, re-plotted in a row-column format, with one FSR (200GHz) per row and three columns per spectrum. Now an image emerges from the OSA spectra, spelling out the word 'PURDUE.' This example illustrates the direct correspondence between the applied spatial mask and the spectral transfer function and demonstrates the ability to achieve nearly arbitrary intensity control of the optical spectrum. We would like to point out here that this idea has been adapted by others [23] as part of a system to achieve very fast acquisition cameras. In this case, a dynamic entity that needs to be imaged is placed in the Fourier plane. This information then gets mapped onto the spectrum and the spectrum is measured using fast schemes. This then allows for rapid imaging of the dynamic system.

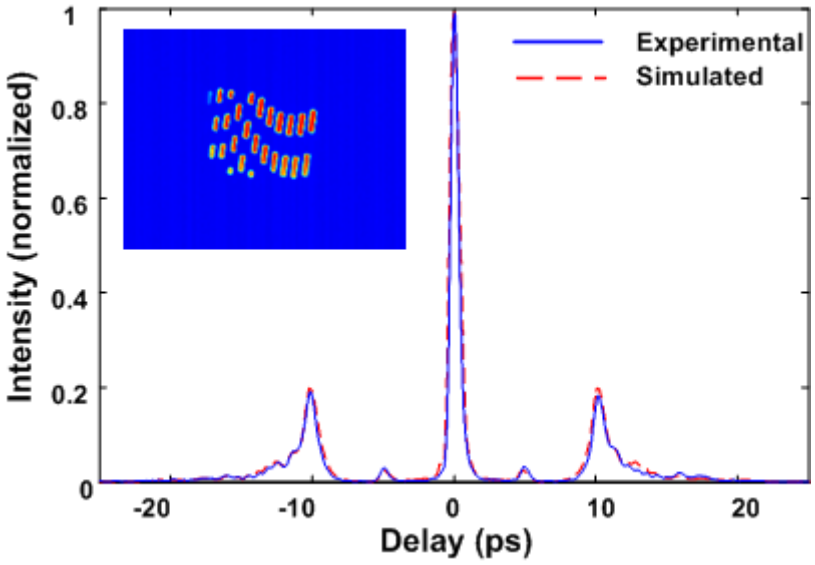

Fig 2.11 - An experimental cross correlation trace (solid blue) and the simulated (dashed red) trace are superimposed; excellent agreement between the two traces is observed. Both satellite pulses have been broadened, indicating a quadratic spectral phase with the acquired tail indicating a cubic spectral phase. The image on the inset shows the Fourier plane with the mask in place.

Fig. 2.11 demonstrates an interesting example which begins to exploit spectral phase. Because the masking operation implemented currently is strictly amplitude-only, we follow a design approach based on computer generated holography [24], where phase information is encoded as a slow modulation in the periodicity of a nearly periodic amplitude pattern. In our experiment the mask modulates the initial spectrum in an on-off fashion, with a period that varies slowly over the optical bandwidth. This results in a mixture of quadratic and cubic spectral phase, which may be discerned qualitatively from

the curvature evident in the Fourier plane image (inset). Readout of this spectral hologram [25] results in a time domain trace consisting of an unshaped peak at t=0 with equal but time-reversed shaped signals at positive and negative time offsets, respectively. These features correspond to the undiffracted zero-order beam and to the real and conjugate images generated from 1^{st}- and -1^{st}-order diffraction in the spatial holography analog. Here in our time domain experiment, the satellite pulses exhibit a clear asymmetric tail as expected from the designed cubic spectral phase as well as a small broadening associated with quadratic phase.

2.6 Experimental results with a high repetition rate frequency comb

Now we will demonstrate results with the 2D shaper in the regime of line-by-line shaping or arbitrary waveform generation. Our configuration allows for significant enhancement of the number of controllable frequency lines. As we previously mentioned in chapter 1, this regime is particularly interesting for a variety of applications like optical communications, coherent LIDAR, massively parallel, novel spectroscopic sensing techniques e.t.c.

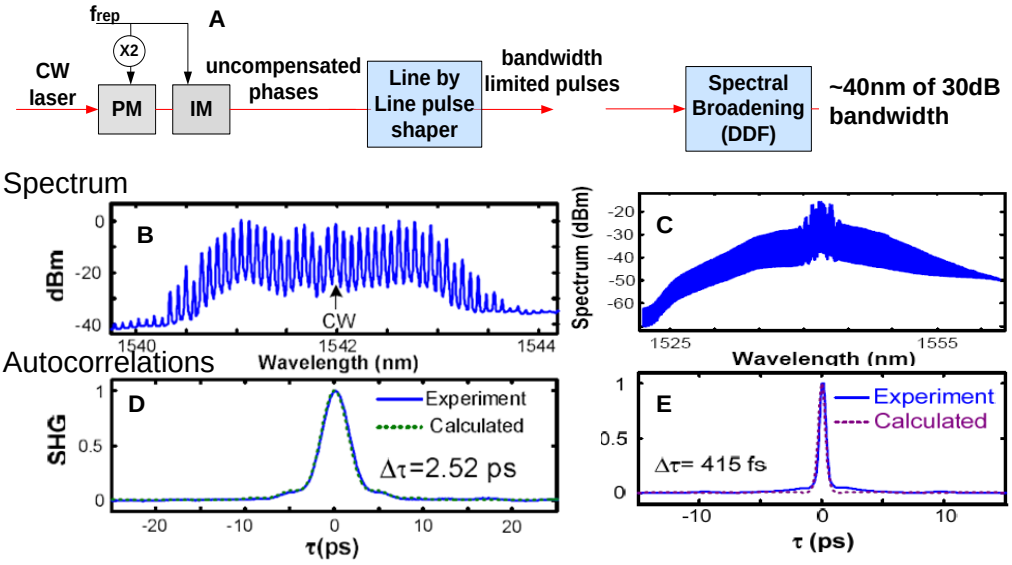

Fig 2.12 – (A) Experimental scheme for generation of the frequency comb. (B), (D) Spectrum and output autocorrelation after cascaded modulators and phase correction. (C), (F) Spectrum and autocorrelation after spectral broadening using DDF

Fig 2.12(A) shows the scheme used for generating the frequency comb source [8]. A continuous wave (CW) laser is sent through a strongly driven phase modulator followed by an intensity modulator. At this point, though a frequency comb is generated, the temporal envelope is still wide owing to phase variations between different lines. This is corrected using a line-by-line pulse shaper generating bandwidth limited pulses of ~2.5 ps duration (usable bandwidth of ~300GHz). The bandwidth limited nature of the pulse is supported by a close match between the simulated autocorrelation assuming flat spectral phase and the measured autocorrelation (figs 2.12(B) and (D)) [8]. These pulses are then spectrally broadened and compressed using a soliton based dispersion decreasing fiber which generates a broadened spectrum of ~40nm 30dB bandwidth and ~415 fs pulses (figs 2.12 (C) and (E)).

Figure 2.13(A) presents a small section of the spectrum both before and after applying a pulse rate quadrupling mask. After applying the mask, the initial 10 GHz comb spacing is increased to 40GHz. Fig. 2.13(B) shows the image of the masked Fourier plane and the corresponding time domain cross correlation trace. The discrete or comb-like nature of the optical spectrum is evident as discrete spots at the Fourier plane. The central spots are brighter due the shape of the source spectrum. In the time domain, the pulse-to-pulse separation is 25ps corresponding to the 40GHz line spacing determined by the mask. Fig. 2.13(C) shows the image of the Fourier plane with a pulse rate doubling mask and the corresponding time domain trace. In the time domain, pulses repeating every 50ps are observed as expected. In Fig. 2.13(D), a slight modification of the pulse rate doubling mask is implemented: at the edge of every FSR, two successive lines are either selected or skipped. This modification significantly reshapes the time domain output: instead of a single pulse at the midpoint of the cross-correlation, a pulse doublet is now observed. The trace shown in red is the simulated output, which is in excellent agreement with the experimental cross-correlation.

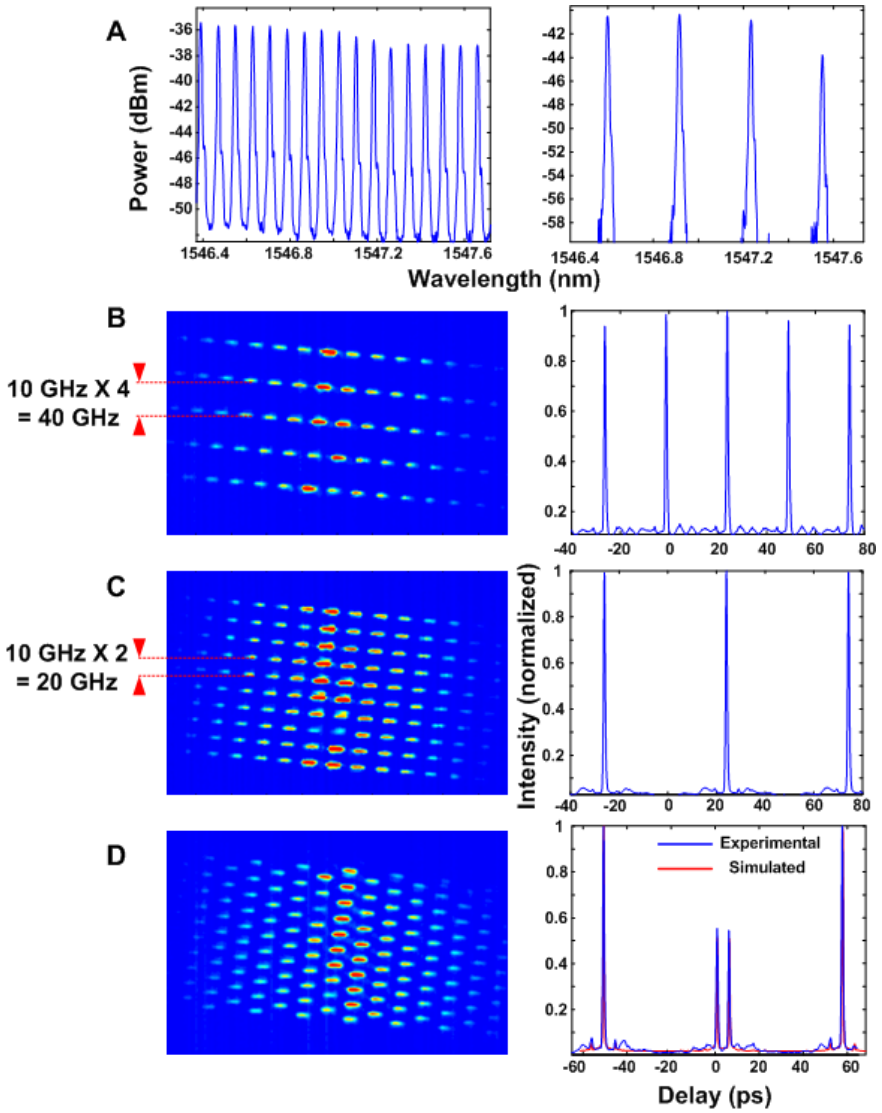

Fig 2.13 - (A), a portion of the input frequency comb and the same section after application of a pulse rate quadrupling mask. The line-to-line spectral spacing of the input is 10GHz, which is the temporal repetition rate of the source. After application of the mask, the line-to-line spacing is manipulated to be 40GHz. (B), the image of the Fourier plane with the quadrupling mask and the corresponding time domain cross correlation trace. The pulse-to-pulse separation is 25ps corresponding to the 40GHz repetition rate. (C), The image of the Fourier plane with a pulse rate doubling mask showing a spot-to-spot separation of 20GHz separation. In the time domain the pulse-to-pulse separation is 50ps as expected. (D), a mask is utilized which is a slight modification of the pulse rate doubling mask. The pattern is staggered by inserting irregularities every 20 spectral lines. In the time domain this results in a significant change, where a double pulse structure is observed near zero delay instead of a single pulse as in the pulse rate doubling case (C). Excellent agreement between the simulated (red) and the experimental (blue) cross correlation traces is observed.

2.7 Achieving programmability using a spatial light modulator

The mask used in the previous experiments was an amplitude only mask made using photolithography. Ideally, we would like to have simultaneous control of both the spectral amplitude and phase in order to achieve generation of the entire range of waveforms possible. However, spectral phase control using such masks is a very difficult task. Also, the pulse shaping operation is not programmable. Both these limitations can be overcome by using spatial light modulators instead of fixed masks.

Two dimensional spatial light modulators are now widely available over a wide range of operating wavelengths. The most promising technology is based on liquid crystal on silicon and two dimensional arrays with >2million pixels are available [25]. However an important point to note is that, a single liquid crystal array will only allow for shaping either the spectral phase profile or the amplitude profile. In order to control both amplitude and phase independently, two liquid crystal layers are needed and these are the type of devices used in 1D [26]. However, in two dimensions such dual layer devices aren't available and all two dimensional liquid crystal modulators (LCM) are phase only modulators. These devices used in a conventional manner can only provide either amplitude or phase, but we would like to have both. Interestingly, there exist methods which can provide simultaneous amplitude and phase shaping using a phase only SLM by utilizing diffraction.

Whenever an optical beam hits a periodic phase pattern (a grating) with a period much finer than the size of the beam, a part of the light is diffracted away into different direction referred to as the 1^{st}, 2^{nd} … orders of diffraction. The reflected light (called 0^{th} order of diffraction) has now a reduced intensity. By changing the amplitude of the periodic phase function, the amount of light diffracted and the amount of light reflected can be controlled and this provides a methodology to control the amplitude of the light beam. Phase control can be achieved by superimposing a much slower (significantly larger than the focused spot size on the SLM) profile programmed onto the SLM. Fig 2.14 shows an intuitive way of understanding this control scheme. This is shown here in 1-D, though we utilize this scheme in 2-D. The SLM surface is divided into larger super-pixels which are much larger in size to the focused spot size. The slow phase variation

programmed onto the SLM varies super-pixel to super-pixel and manifests as a frequency dependent phase shift providing phase shaping. A high period grating is also programmed superimposed on the slow phase variation of each super pixel. The amplitude of the grating allows for controllable diffraction of the intensity of light into the different orders (as shown in the figure) and this provides a convenient way to control amplitude.

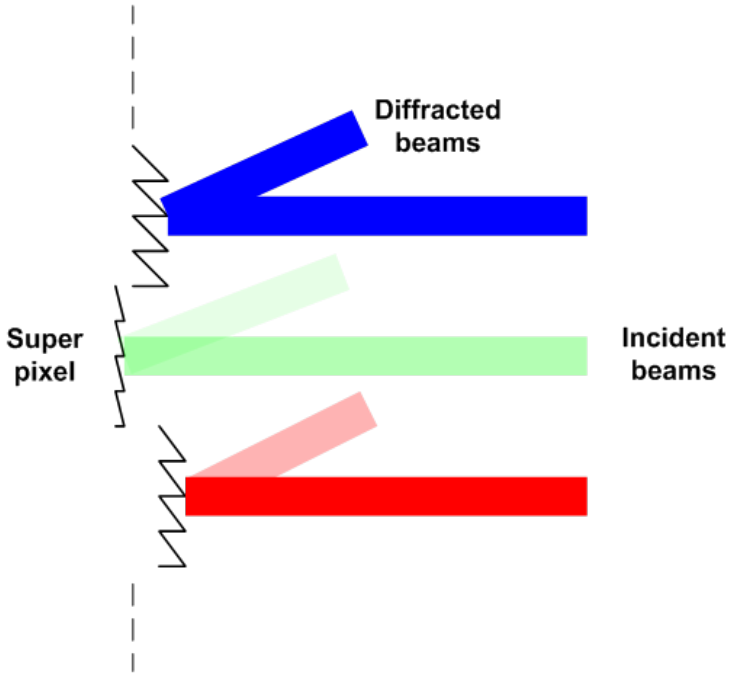

Fig 2.14 Schematic showing control of amplitude and phase with a phase only spatial light modulator using diffractive effects

In this technique, for amplitude control, two primary methods exist. The first is to collect the light returned in the 0^{th} order and the other is to look at the light diffracted into the first order. In our experiments, we collect the light diffracted into the 1^{st} order instead of the 0^{th} order. The advantage is that parasitic reflections from the non uniformity and dead spaces on the SLM are large in the 0^{th} order and are more suppressed in the 1^{st} order [26].

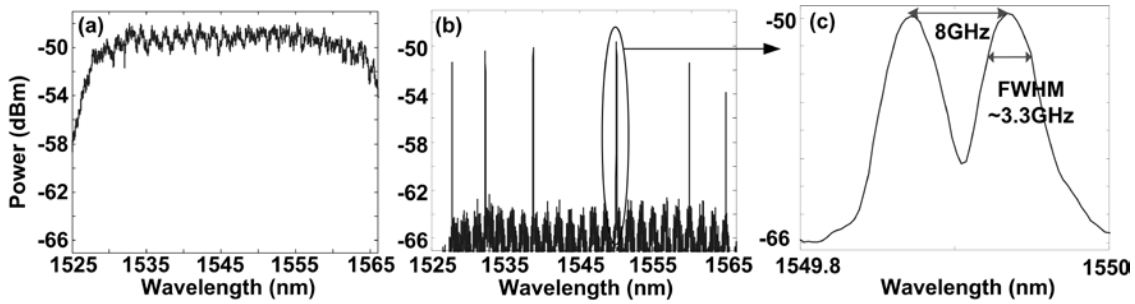

Fig. 2.15**.** Output spectra with the ASE source (a) with no masking and (b) with a mask allowing only a few narrow spectral features to pass. (c) The zoomed version of the circled section in (b) shows fine feature control with FWHMs as low as ~3.3GHz.

The first experiment is to demonstrate the programmable control of the spectrum with high resolution and broad bandwidth utilizing the 2-D SLM in the 2-D pulse shaper. Fig 2.15(a) shows the output spectrum with a spectrally flattened ASE source input for the case where no additional shaping is applied. A relatively featureless spectrum is observed with some amplitude distortions. This comes about due to the dead spaces between the pixels of the SLM and future work would involve reduction of these effects. We then apply a mask which allows only a few narrow spectral features to pass and turns off everything else. The output spectrum is shown in fig 2.15 (b), with the circled region also expanded in fig 2.15 (c). We see that the narrow features are as small as 3.3GHz and the total bandwidth is >40nm limited only by the bandwidth of the source. The zoomed region also shows how narrow features spaced very close to each other (~8GHZ) can be independently controlled.

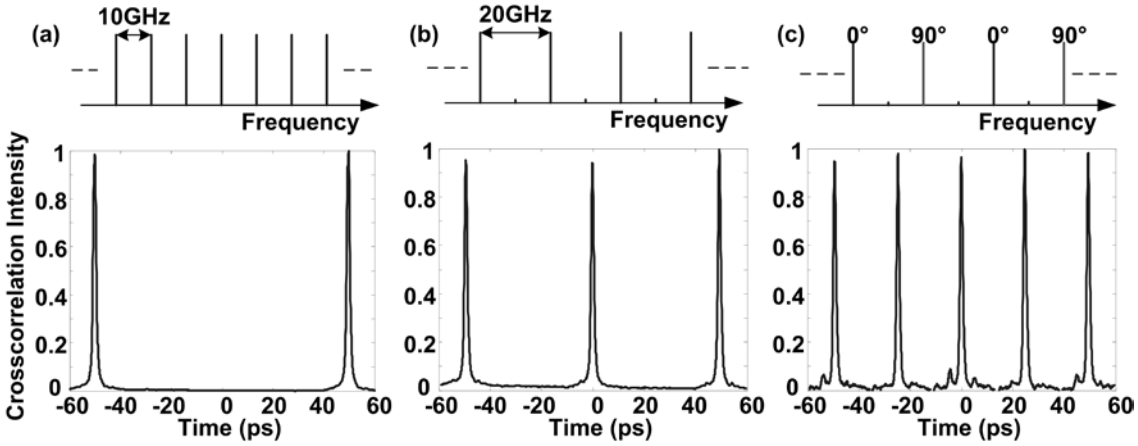

Fig. 2.16. (a) Schematic showing the comb source and the experimental crosscorrelation trace with pulses spaced by 100ps corresponding to 10GHz, (b) Every alternate line is suppressed and now the crosscorrelation shows pulses spaced by 50ps, (c) By using phase shaping to create 0 and 90 degree phase shift between lines spaced 20GHz apart, the repetition rate is quadrupled to pulse to pulse spacing of 25ps

The next experiment is to demonstrate simultaneous amplitude and phase control. To do this we utilize a frequency comb source and demonstrate a proof of concept experiment of pulse rate multiplication utilizing both amplitude and phase shaping capabilities. The source used is a 10GHz comb discussed in the previous section. In the absence of any shaping, in the time domain we expect pulses 100ps apart corresponding to 10GHz repetition rate. This is seen in the experimental intensity crosscorrelation trace in fig 2.16(a) obtained with a short unshaped reference pulse. The corresponding schematic shows no shaping. As shown in the schematic in fig 2.16(b), we then cut every alternate line utilizing amplitude shaping, increasing the repetition rate to 20GHz which corresponds to pulses spaced 50ps apart. This is again verified in the experimental crosscorrelation trace. To demonstrate simultaneous amplitude and phase control, we retain only every other line as in 2.16(b), but we further apply an alternating 0, 90deg phase between them (2.16(c)). This corresponds to an additional doubling of the repetition rate with the relative pulse heights being a good indicator of the accuracy of the phase shaping. In the experimental crosscorrelation trace we see the pulses are now equally tall, spaced by 25ps indicating good, simultaneous control of amplitude and phase.

In summary, we have demonstrated a fundamentally new pulse shaping geometry which disperses optical frequencies along a two-dimensional grid, resulting in a

substantial increase in achievable pulse shaping complexity. It should be possible to scale this scheme for high spectral resolution shaping of octave spanning optical sources. For example, for a 10 GHz repetition rate, octave spanning laser frequency comb centered at 1.55 μm wavelength, independent control of the approximately twenty thousand spectral lines comprising the comb should be possible. We demonstrated how we can make this programmable by integrating a 2-D spatial light modulator developed for display applications with millions of pixels in the pulse shaper.

3. CHARACTERIZATION TECHNIQUES FOR HIGH REPETITION RATE FREQUENCY COMBS AND OPTICAL ARBITRARY WAVEFORMS

Simultaneous to the development of generation capabilities, we have worked on characterization techniques and this chapter will be on that. In section 3.1 we will discuss on challenges in characterization of these waveforms and difficulties in adapting existing techniques. In section 3.2 we will present a low power fast acquisition apparatus and we will use this further in section 3.3 to monitor dispersion characteristics of long fiber links. In section 3.4, we will extend this technique to measure rapidly varying waveforms by increasing the measurement capability to single shot. In section 3.5 we present another new technique for applications which require a self referenced measurement scheme and in section 3.6 we will use this to characterize some novel optical frequency comb sources. The work relating to section 3.2 has been published in [27], the work in section 3.3 in [28] , the work in section 3.4 in [29] and the work in section 3.5 in [30].

3.1 Challenges in characterization of optical arbitrary waveforms

OAWG leads to new challenges in waveform characterization associated with the unique attributes of fields generated through line by line pulse shaping. In particular, such fields may exhibit 100% duty cycle, with shaped waveforms spanning the full time domain repetition period of the frequency comb, and with spectral amplitude and phase changing abruptly from line to line. Such fields are also characterized by large time-bandwidth product, equal approximately to the number of lines in the shaped frequency comb. Although methods for full characterization of ultrashort pulse fields are well developed, e.g., [31-34], such methods are typically applied to measurement of low duty cycle pulses that are isolated in time, with spectra that are smoothly varying, and with relatively low time-bandwidth product. These properties correspond to low spectral resolution insufficient to capture the rapid spectral changes that are a hallmark of line by

line pulse shaping. In general, it is also desirable that characterization methods for OAWG fields offer high sensitivity (low power requirement) and fast data acquisition. These properties will be needed when pulse shaping is operated at rapid waveform updates [35] and also to capture interesting waveform transients expected with both high (line by line) spectral resolution and very rapid waveform update [36].

A few efforts towards waveform characterization for OAWG have been reported. For example, in [37] spectral phase was measured by observing the phase of the RF beat signal obtained when a line by line shaper was used to select two adjacent comb lines at a time from a 10 GHz frequency comb. In [38] signals from a 20 GHz optical comb were characterized by an X-FROG [39] technique in which the sum frequency signal generated through the interaction of shaped and unshaped fields was spectrally resolved and measured as a function of delay. However, both of these techniques require a series of measurements performed sequentially, which slows measurement time.

3.2 Waveform characterization using dual-quadrature spectral interferometry (DQSI)

Spectral interferometry [34] is a well known pulse characterization technique which measures an unknown signal waveform with respect to a characterized reference pulse by looking at the spectrally resolved interference between them. Owing to its linear nature, it adapts well to low power applications. The fact that it is not a self-referenced technique, and needs a well characterized reference pulse is not a significant limitation since a short pulse used as reference can be characterized by other well established self referenced techniques. However, in conventional implementations of spectral interferometry, in order to unambiguously retrieve the phase information from one component of the interference signal (either in phase or quadrature), a large delay is necessary between the signal pulse and the reference pulse. This leads to very high demands on spectral resolution (many times more than the spectral features in the signal waveform) particularly for optical arbitrary waveforms which already have fine spectral content. In fact, from a fundamental perspective, for a periodic waveform with a 100% duty cycle, it is impossible to achieve time separation greater than the temporal aperture of the

waveform since delay will also be periodic at the repetition rate. Hence we adapt a version of spectral interferometry called dual-quadrature spectral interferometry which uses polarization demultiplexing to measure the complete interference signal (both in-phase and quadrature) allowing for zero-delay operation simultaneously minimizing spectral resolution requirements.

Before we go into the experimental setup, let us briefly describe mathematically the operating principle. In dual-quadrature spectral interferometry, in-phase and quadrature interferograms ($I_1(\omega)$ and $I_2(\omega)$) can be written in terms of the signal and reference power spectra ($|A_s(\omega)|^2$ and $|A_r(\omega)|^2$) and the phase difference between them ($\Delta\psi(\omega)$) as [34]

$$I_1(\omega) = |A_s(\omega)|^2 + |A_r(\omega)|^2 + 2|A_s(\omega)||A_r(\omega)|\cos(\Delta\psi(\omega)) \tag{3.1}$$

$$I_2(\omega) = |A_s(\omega)|^2 + |A_r(\omega)|^2 + 2|A_s(\omega)||A_r(\omega)|\sin(\Delta\psi(\omega)) \tag{3.2}$$

The reference spectrum and phase and the two interferograms are known and from the two equations we need to retrieve the signal spectrum and the signal phase. In general the above equations give two solutions for the signal spectrum and phase which are

$$|A_s|^2 = \frac{(I_1 + I_2)}{2} \pm \frac{\sqrt{(I_1 + I_2)^2 - 2(I_1^2 + I_2^2) - 4|A_r|^4 + 4|A_r|^2 (I_1 + I_2)}}{2} \tag{3.3}$$

with the corresponding $\Delta\psi(\omega)$ for each $|A_s(\omega)|^2$ given by

$$\Delta\psi(\omega) = \arg\left(\frac{(I_1(\omega) - |A_s(\omega)|^2 - |A_r(\omega)|^2) + j(I_2(\omega) - |A_s(\omega)|^2 - |A_r(\omega)|^2)}{2|A_s(\omega)||A_r(\omega)|}\right) \tag{3.4}$$

This however prevents unambiguous retrieval with a single measurement and requires an auxiliary measurement, e.g., of the signal power spectrum. In previous demonstrations a separate measurement of the signal spectrum was in fact carried out [34, 40]. Here we show that with an additional constraint which can be easily implemented in the experiment, Eq. (3.1) and Eq. (3.2) are sufficient to unambiguously retrieve both the signal spectrum and the phase information.

Adding Eq. (3.1) and Eq. (3.2) we have,

$$|A_s|^2 = \frac{(I_1+I_2)}{2} - (|A_r|^2 + \sqrt{2}|A_s||A_r|\sin(\Delta\psi + \pi/4)) \le \frac{(I_1+I_2)}{2} - (|A_r|^2 - \sqrt{2}|A_s||A_r|) \quad (3.5)$$

Now if we require that the level of the signal spectrum is less than the reference spectrum everywhere by at least 3dB (i.e. $|A_s(\omega)|^2 \le |A_r(\omega)|^2/2$ for all ω), then $|A_r(\omega)|^2 - \sqrt{2}|A_s(\omega)||A_r(\omega)| \ge 0$, and so from Eq. (3.5) we have $|A_s(\omega)|^2 \le \frac{(I_1(\omega)+I_2(\omega))}{2}$. This forces the negative sign for the signal spectrum in Eq. (3.3) and thus ensures uniqueness for the spectrum and the corresponding spectral phase. Also, our new constraint is not hard to implement since in most spectral interferometry implementations, the signal and reference are derived from the same source; it is therefore sufficient to ensure that the net gain in the signal arm is less than that in the reference arm by 3dB.

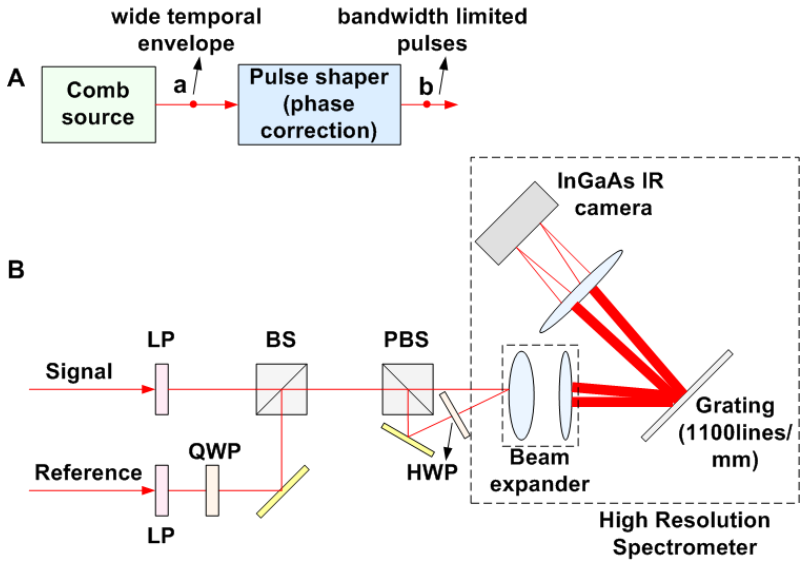

Fig. 3.1. [A] Schematic showing the generation of bandwidth limited pulses. At point (a) the frequency comb has a wide temporal envelope which is then phase corrected to obtain compressed bandwidth limited pulses at point (b). [B] Experimental setup, LP : linear polarizer, QWP : quarter wave plate, HWP : half wave plate, BS : beam splitter, PBS : polarizing beam splitter.

Before we describe the experimental setup, we will briefly describe the source used in our experiments. It is the same source we described in the previous chapter, a detailed account can be found in [8]. The frequency comb source we use is generated by sending a continuous wave (CW) laser through a strongly driven phase modulator followed by an intensity modulator. At this point, though a frequency comb is generated,

the temporal envelope is still wide owing to phase variations between different lines (shown schematically as point (a) in fig 3.1(A)). This is corrected using a line-by-line pulse shaper generating bandwidth limited pulses of ~2.5 ps duration (usable bandwidth of ~300GHz) (at point (b) in fig 3.1(A)). The bandwidth limited nature of the pulse is supported by a close match between the simulated autocorrelation assuming flat spectral phase and the measured autocorrelation.

Fig. 3.1 shows the dual quadrature spectral interferometry setup. The signal to be measured is linearly polarized at a 45deg angle while the reference is circularly polarized. These two beams are combined followed by a high resolution spectrometer consisting of a 10X beam expander, an 1100lines/mm grating, and an InGaAs IR CCD camera. The pixel dimension of the camera in the dispersed direction is 25microns, which corresponds to a spectrometer resolution of 3.33GHz per pixel. This gives a line to line spacing of 3 pixels on the camera (corresponding to the frequency comb spacing of 10GHz). The spectrometer simultaneously measures the interferograms in both polarizations (corresponding to the in-phase and quadrature terms) by mapping them to different physical locations on the camera. The measured spectrometer crosstalk arising from a single adjacent line three pixels away is ~5% and ~8%, respectively, for the two channels. For each of the polarizations, the 30 lines of the frequency comb spread across 90 pixels of the camera. We retrieve waveform information from a single frame of CCD data with 1.4 μs integration time, which defines our data acquisition time. In our measurements we have verified good waveform retrieval at an average signal and reference power of 10 μW and 20 μW. In this case, since the total energy per measurement is a product of the signal power and the gating time, we are only using around 14pJ of signal energy per measurement. This corresponds to an average signal energy of less than 0.5pJ per spectral line. The fast acquisition time significantly reduces sensitivity to environmental fluctuations. For example, at 1.4 μs integration time optical phase fluctuations associated with the relatively long (detailed in section 3.3) lengths of optical fibers did not appear to degrade our spectral interferometry data.

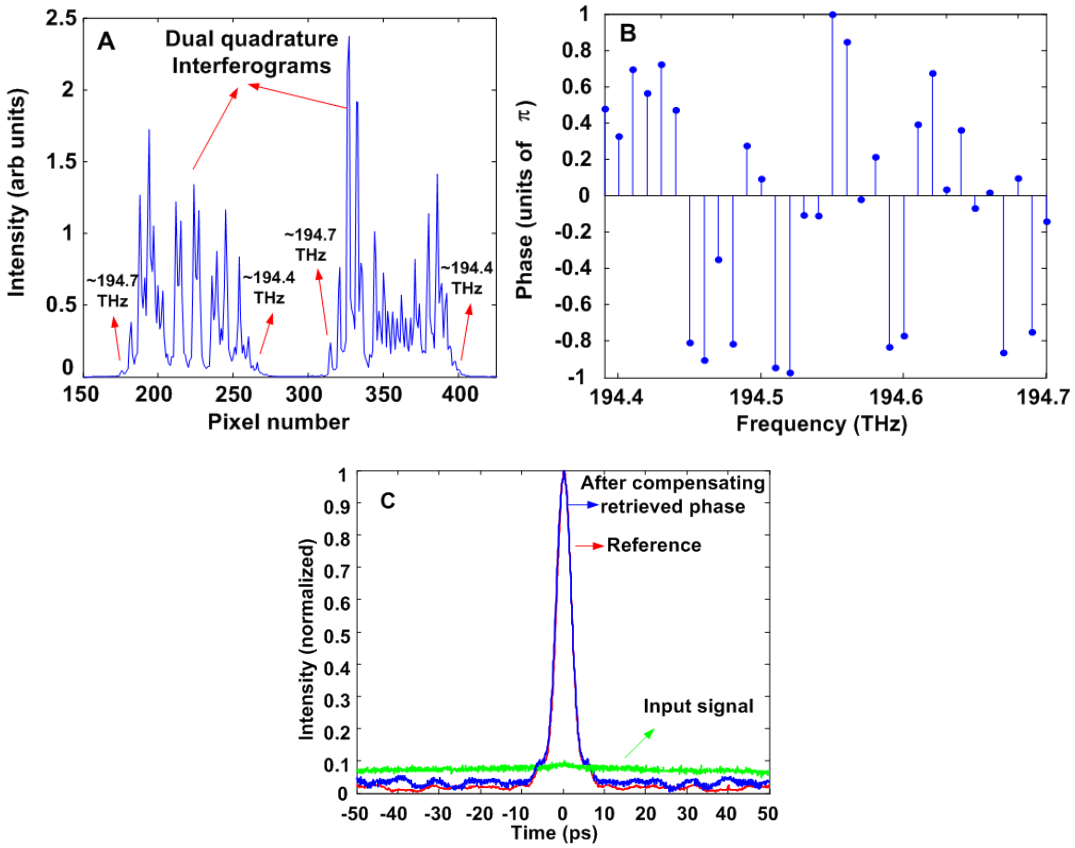

Fig. 3.2. [A] Raw interferogram data obtained by the camera showing the two quadratures. [B] Retrieved spectral phase. [C] Experimental autocorrelations showing the reference pulse and the signal before and after applying the inverse of the retrieved phase.

In Fig. 3.2 we describe the results of an experiment that demonstrates the ability to characterize fields spanning the full 100ps waveform period at 100% duty cycle. As noted before, although a frequency comb is formed after the modulators, in the time domain the envelope is still spread over most of the 100 ps period. This situation corresponds to strong spectral phase variation. The bandwidth-limited reference pulse formed by compressing the comb (extracted from point (b) in Fig. 3.1(A)) is then used to measure a signal field corresponding to an uncompressed version of the frequency comb (extracted from point (a) in Fig. 3.1(A)) through the dual-quadrature spectral interferometry. The inverse of the retrieved phase is applied to the signal field via a second line-by-line shaper (not shown), and the output autocorrelation is measured. If the phase retrieval is good, the autocorrelation should be that of a bandwidth-limited output pulse matching that of the reference pulse. In Fig. 3.2(A) we show representative raw interferogram data obtained from the camera showing both the channels. Each pixel

corresponds to ~3.33GHz, which corresponds to a spacing of 3 pixels between adjacent lines of the frequency comb. Abrupt changes in the intensities of the interferograms indicate the strong phase variation which occurs on a line by line basis. In Fig. 3.2(B), we have the retrieved spectral phase. We see a strongly modulated phase pattern with abrupt phase jumps. Fig. 3.2(C) shows the autocorrelations of the input signal field (uncompensated comb), which has a nearly flat envelope and occupies the entire 100ps repetition period, as well as those of compressed reference and signal pulses. The autocorrelations of the reference pulse compressed via the second harmonic optimization method [8] and of the signal pulse compressed under spectral interferometry control are closely matched and correspond to bandwidth-limited pulses ~3 ps in duration. The slight increase in the wings of compressed pulse autocorrelation compared to those of the reference pulse can be attributed to small errors in the spectral interferometry measurement.

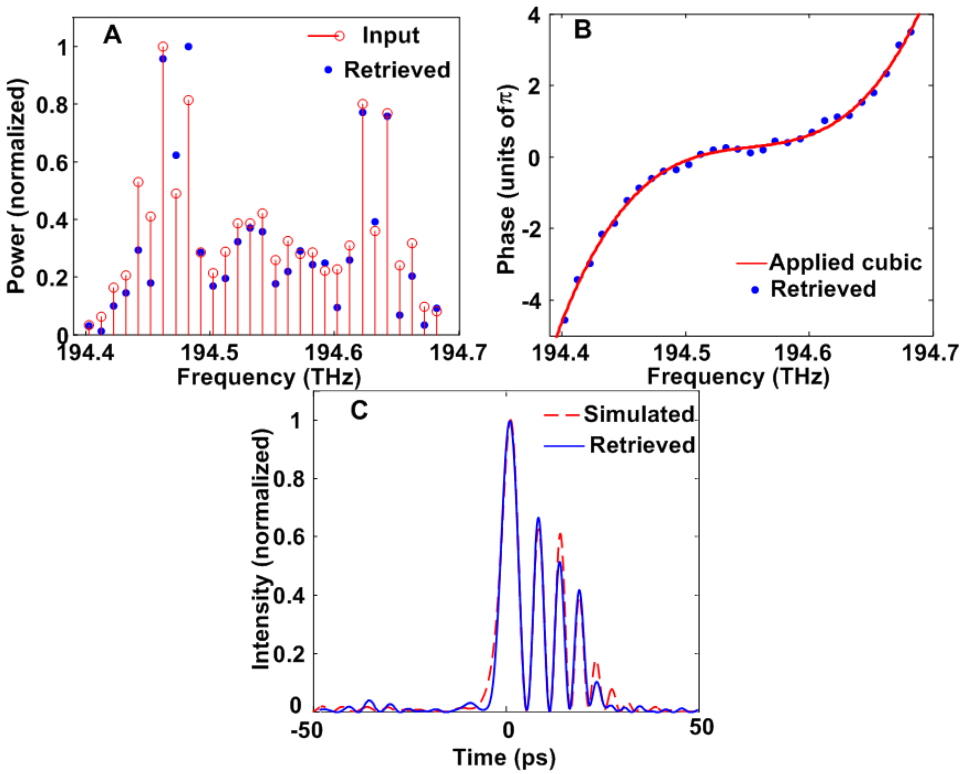

Fig. 3.3. [A] Input and retrieved spectra. [B] Applied cubic phase and the retrieved spectral phase. [C] Time domain intensities generated using the retrieved spectrum and phase (retrieved) and the input spectrum and applied phase (simulated).

Fig. 3.3 demonstrates the use of dual quadrature spectral interferometry for retrieval of the power spectrum and phase of a signal field to which known user defined spectral phase was applied. Here the compressed pulse (at point (b) in Fig. 3.1(A)) is split to yield identical reference and signal pulses. Cubic spectral phase was then applied using a second line by line shaper operating only on the signal field. In Fig. 3.3(A), the input spectrum (measured independently on an OSA) and the retrieved spectra are plotted. Fig. 3.3(B) shows both the applied phase (i.e., the phase programmed onto the pulse shaper) and the retrieved phase. The retrieved phase is in good agreement with the applied cubic phase; the difference has a standard deviation of 0.11π radians. Simulations show that the difference between the applied spectrum and phase and the retrieved spectrum and phase arise mainly due to the crosstalk in the spectrometer. By further reducing the crosstalk, improvement should be possible. In Fig. 3.3(C), we show a comparison of calculated time domain intensity profiles obtained using the input power spectra (measured separately) and the applied spectral phase or that retrieved through spectral interferometry. The close agreement indicates that the phase measurement through spectral interferometry is sufficiently accurate to yield a meaningful prediction of field profile in the time domain.

3.3 Fast monitoring of dispersion and dispersion slope parameters of long optical fiber links using DQSI

In recent years there has been significant work on novel paradigms in optical communications where the phase of the optical carriers is controlled to obtain better spectral efficiency with reduced crosstalk [41-42]. There also has been significant renewal of interest in coherent optical communications [43] where again the phase plays an important role. In practical systems involving installed fiber, the link dispersion is not expected to remain fixed but vary slightly over time. This will also be the case with reconfigurable optical networks where the data might be carried by different links, each with different dispersion properties. Dispersion along these links will not only manifest itself as temporal distortion but also as frequency dependent phase variations of the transmitted signal. Therefore a real time dispersion monitoring tool which can perform

fast measurements with low power requirements is desirable. Another area where this would be useful is in timing and frequency transfer over fiber links [44-46]. Fiber delay fluctuations which occur in sub millisecond time scales manifest themselves as phase noise in the transmitted signal. In situations where broad bandwidths (i.e. short pulses) are used, dispersion variations which cause frequency dependent delay fluctuations would also have to be compensated faster than the fluctuation time scales.

Measuring dispersion properties in fiber is well established [47]. However, common shortcomings are relatively long acquisition times and difficulty in precisely measuring large dispersions expected in long fiber links. In temporal domain measurements, large dispersion manifests itself as large pulse broadening where exact determination of dispersion becomes difficult due to varying pulse shapes. Other methods like the radio-frequency phase shift technique [46] require wavelength scanning and are hence slow.

Using our DQSI based measurement technique, fast measurement(<1.4 μs, limited only by camera integration time) of both dispersion and dispersion slope can be made directly by measuring the 2^{nd} and 3^{rd} order spectral phase of a high repetition rate optical frequency comb after dispersive propagation over ~25 km length of fiber. Two primary factors contribute to the success of our experiment; one is the use of high repetition rate frequency combs and the second is going to a zero delay scheme of spectral interferometry. Firstly, conventional spectral interferometry has been used previously for dispersion measurement but with using white light sources (see [48] for example); however the need to resolve interferometric fringes associated with nonzero delay constrained the fiber length to a few meters. In our experiments we exploit the periodic nature of delay and the long coherence lengths associated with optical frequency combs to perform direct interferometric measurements of spectral phase for lengths up to 50 km of standard SMF, many orders of magnitude longer than previous spectral interferometry experiments. Secondly, as discussed previously, in conventional implementations of spectral interferometry, even with a frequency comb removing the effect of delay based fringes, phase retrieval becomes difficult owing to the requirement of a large delay between interfering pulses. This significantly increases resolution requirements and for

dispersed high repetition rate pulses (>50% duty factor) becomes impossible. This difficulty is mitigated by going to a zero delay version.

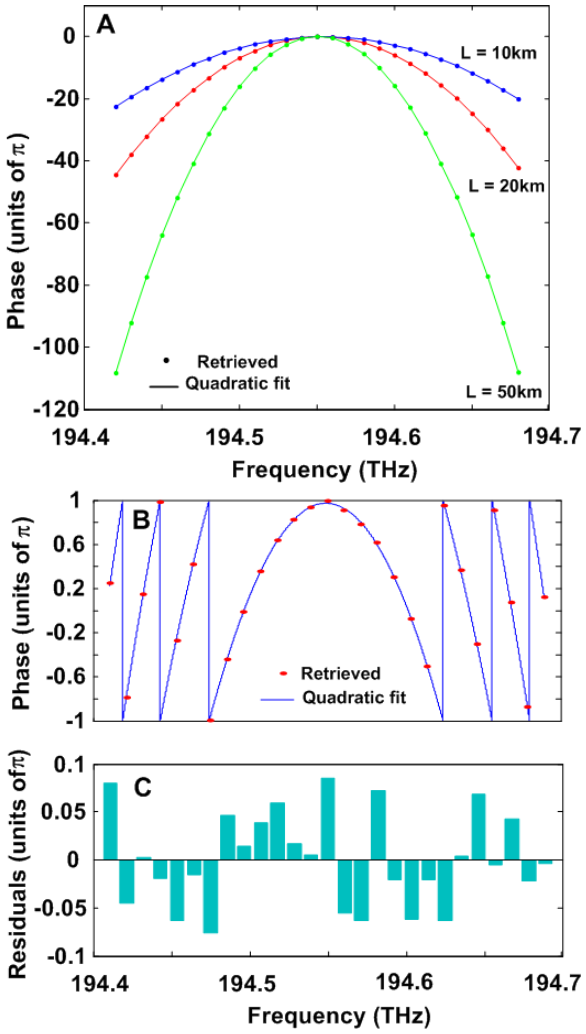

Fig. 3.4. [A] Retrieved spectral phases after propagation over 10km, 20km and 50km of optical fiber. The solid lines represent the quadratic fit. [B] The retrieved phase and the quadratic fit, shown without the unwrapping and [C] the corresponding residuals for the 10 km fiber.

Fig. 3.4(A) shows the measured spectral phase of the signal field after propagation through 10km, 20km and 50km of standard single mode optical fiber. The quadratic fit to the data is also shown. The standard deviation of the error between the measured phases and the quadratic fit is 0.05π, 0.04π, 0.07π respectively corresponding to 10km, 20km and 50km. The amount of cubic phase present in these cases is small. The measured values of quadratic phase give a dispersion measure of ~164ps/nm, 328ps/nm and 810ps/nm respectively for the three spools. As verification, from the retrieved phase and the knowledge of the length of the each fiber spool, the dispersion coefficients were

calculated to be 16.4ps/nm km, 16.4ps/nm km and 16.2ps/nm km. These independent estimates are all very close and are consistent with the known dispersion of standard single mode fiber.

The total dispersion corresponding to the three different fiber spools turn out to be ~400ps, 800ps and 2000ps, respectively, which are all significantly higher than the pulse period of 100ps. This means that the net change in phase over the entire bandwidth is significantly higher than 2π. Therefore, the underlying quadratic phase moves over many 2π ranges over the frequency range, with the variation becoming more rapid as we move away from the center. Our measurement samples this nominal quadratic function periodically at 10GHz intervals. To indicate this, Fig. 3.4(B) shows the retrieved phase and the corresponding quadratic fit for the case of 10km fiber length, but in this case without the unwrapping. As expected, the retrieved phase lies close to the wrapped quadratic fit. We notice that as we move away from the center frequency in Fig. 3.4(B), the measurement points sample the quadratic phase only one or two times per 2π variation. We might expect this to raise questions about the adequacy of the sampling frequency and whether a subset of the data from the above figure (say farther away from the center frequency) is sufficient to unambiguously provide the underlying quadratic phase.

To address this issue, we would like to point out that the choice of starting the unwrapping with smallest variation near the center was arbitrary which would make the points away from the center seem to have greater variation from point to point. We could have started the unwrapping near any point in which case, the phase variation would be minimum near that point. The underlying reason here is that the different quadratic fits that are obtained while we vary the choice of the data point to start unwrapping differ only by a linear phase (because shifting the center frequency for a function which is quadratic in frequency gives a term linear in frequency). Hence, even a subset of the data from the above figure uniquely determines the underlying quadratic phase and by subtracting different amounts of linear phase, can be made to look symmetric(having minimum variation) around any point. This point is further clarified in Fig. 3.4(C) where we plot the residuals (difference between the quadratic fit and retrieved phase) for each

data point. The magnitude of the residuals don't show any pronounced character while moving away from the center frequency and the variations are of the same order indicating the similarity of each retrieved data point. Similar behavior is observed in the residuals of the 20km and 50km fiber measurements.

In the previous set of experiments, the frequency comb source used was the one generated using cascaded modulators and this does not generate enough bandwidth to clearly observe the dispersion slope of the fiber links which manifest as a cubic spectral phase. So to measure this, we now use a different optical frequency comb source called an optical frequency comb generator (OFCG). Here the frequency comb is generated by creating periodic sidebands of a driving CW laser through a phase modulator inside a cavity [5] (more on this section 3.6).

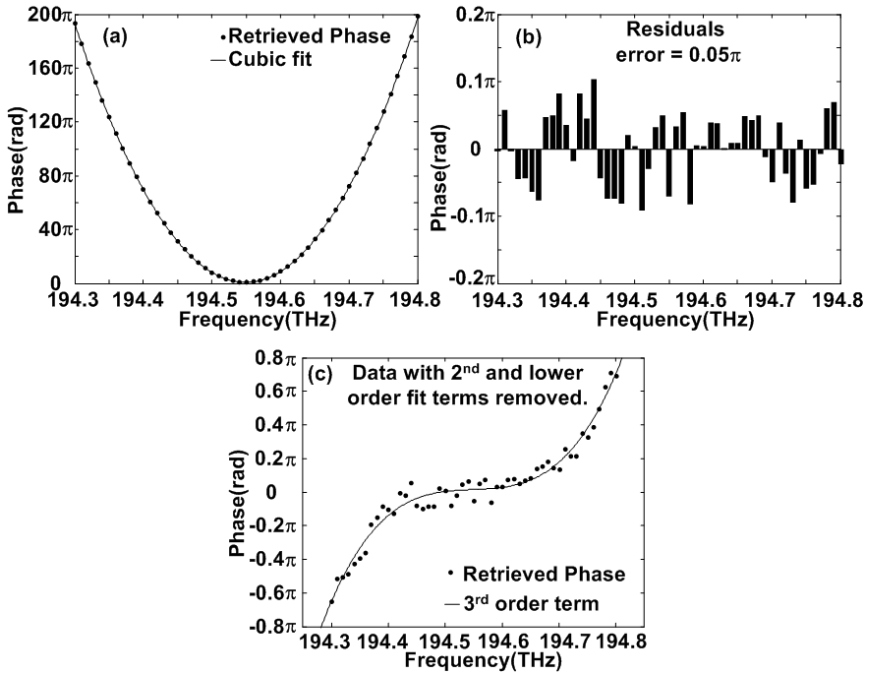

Fig. 3.5. 25km standard SMF, (a) Retrieved spectral phase and cubic fit; (b) Residuals of the fit; (c) Spectral phase plot after removing the quadratic phase component (dispersion).

The first set of experiments was done with a 25-km spool of standard SMF (OFS-Fitel). Fig 3.5(a) shows the retrieved spectral phase and a cubic fit to it. Fig 3.5(b) shows the residuals between the fit and the retrieved spectral phase. The error, defined as the standard deviation of the residuals, is 0.05π, indicating a very good fit. The choice of using a cubic function was made because at this bandwidth both the cubic term (which is

related to the dispersion slope) and the quadratic term (which gives the dispersion) are expected to be significant. This was confirmed by significantly higher errors (more than twice) obtained while fitting a quadratic only curve to the retrieved phase. However since the quadratic contribution dominates the cubic contribution, the curve still looks largely like a parabola. To show the presence of the cubic we subtracted the quadratic term and plot the difference in Fig 3.5(c). We see a clear cubic behavior from this figure. From the parameters of the fit we estimate the dispersion to be 393.6 ps/nm and the dispersion slope to be 1.50 ps/nm^2.

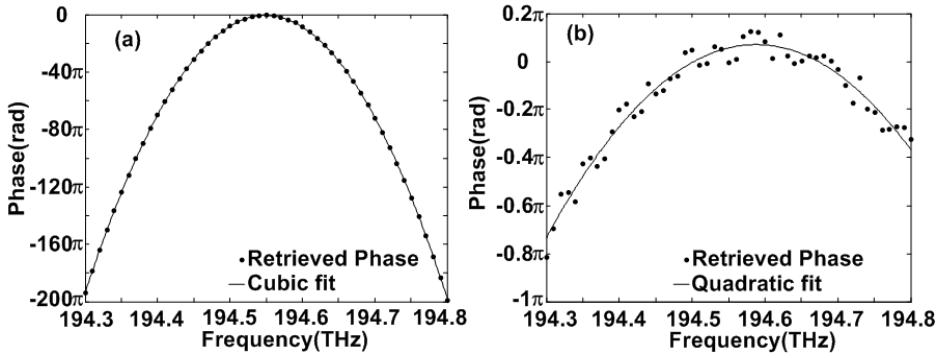

Fig. 3.6 (a) Retrieved spectral phase for a DCF module for the 25km SMF link with a cubic fit; (b) Retrieved spectral phase for the dispersion compensated link with a quadratic fit.

The next experiment is done to check the dispersion properties of a dispersion compensating fiber (DCF) module that is designed to compensate the 25-km link (OFS-Fitel, module type – EWBDK: 404). Fig. 3.6(a) shows the retrieved spectral phase and the cubic fit. From the parameters of the fit we obtain the total dispersion as -395.3 ps/nm and dispersion slope -1.39ps/nm^2. The data provided by the vendor for the DCF fiber module is a dispersion of -394ps/nm and a dispersion slope is -1.36ps/nm^2 at 1542nm. Our results and the numbers provided by the vendor show very good agreement.

Although the vendor specifications for the SMF module say that it is “matched in dispersion to the DCF module,” our measured dispersion values show slight differences between the SMF and DCF. To further investigate, we performed an experiment with the concatenation of the 25-km SMF link and the DCF module. Adding the dispersion values obtained from our measurements of the SMF and DCF taken one at a time, we expect a small net dispersion of -1.7 ps/nm and a net slope of 0.11 ps/nm^2. The retrieved

spectral phase of the concatenated link is shown in Fig 3.6(b). The quadratic fit to the data gives a net dispersion of -1.5 ps/nm, very close to what we expected, while the cubic phase term is negligible (below our measurement sensitivity). These experiments are indicative of the high precision in our technique allowing us to measure small dispersion (better than ~1.5ps/nm) while also simultaneously being able to measure very large dispersion (~395ps/nm), thus providing a large dynamic range of operation.

3.4 Single frame characterization of optical arbitrary waveforms

As we described in section 1.2, by changing the pulse-shaping function at the repetition rate of the comb, potentially infinite record length waveforms with arbitrary temporal resolution can be generated. In this case every successive pulse of the pulse train constituting the frequency comb has a different shape. Measuring such waveforms is demanding for several reasons. Firstly, as discussed in previous sections, owing to the line-by-line shaped nature of such waveforms, abrupt phase and amplitude changes can occur from line-to-line requiring high spectral resolution together with the ability to handle wide spectral bandwidths. Conventional ultrafast measurement methods which work very well for wide bandwidth (short pulses) with smoothly varying spectra and phase do not work well in this regime. Secondly, because of the availability of only a single frame per measurement, very high sensitivity is necessary. Due to high repetition rates of the sources used, for a given average power, there is significantly less energy per pulse (for a 10GHz source, the energy per pulse is 100dB less than the average power) increasing the sensitivity requirement for a single-shot measurement. Thirdly, since acquisition times (limited by available cameras) are significantly slower than the repetition rate of the source, a high quality time-gating system is necessary to select the waveform frame of interest and suppress all the other frames with sufficient fidelity that they do not affect the measurement.

The experimental setup for single frame measurements consists of three parts. 1) The DQSI setup. 2) A gating system to select a single waveform frame from a pulse train and 3) A waveform generator to emulate fast switching waveforms. Firstly, the DQSI setup is the same as before (fig 3.1). The frequency comb source we use in these

experiments is the same source generated by sending a continuous wave (CW) laser through cascaded modulators. In some of our experiments, these pulses are then spectrally broadened and compressed using a soliton based dispersion decreasing fiber which generates ~300 fs pulses. The desired bandwidth (limited to ~1 THz in these experiments) is selected using a simple pulse shaper based filter. A fraction of the power is used as the reference pulse; the remaining power is used for signal waveform synthesis.

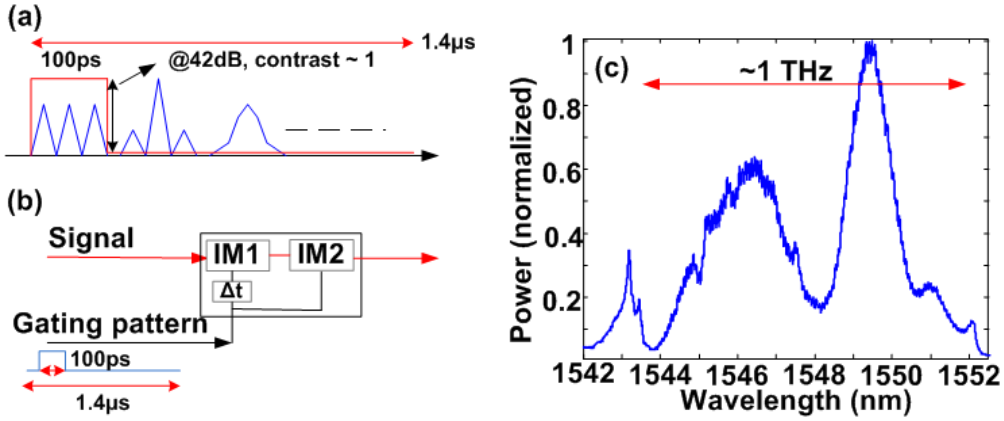

Fig. 3.7. (a) Schematic showing the need for high extinction gating, (b) Gating scheme, (c) Gated spectrum of a 10GHz pulse train.

The integration time of our camera is 1.4 μs while the repetition rate of the comb corresponds to 100 ps. When the waveforms are updated rapidly, to make a high quality measurement it becomes necessary to sufficiently suppress all other waveform periods in the integration window other than the period of interest. Fig. 3.7(a) shows a cartoon depicting this. The extinction requirement is dictated by the integration time of the available camera technology. Since the factor between the integration time and a single waveform frame (i.e., the comb period) is a factor of 14000 (or ~42dB) in our experiments, even if 1/14000 of the power leaks through during every waveform period, it will still integrate up to reduce the contrast between the waveform to be measured and the leakage to ~1. Since a high contrast is desirable to make clean measurements we achieve this by using a cascaded dual intensity modulator scheme (Fig. 3.7(b)). Here we first use a high extinction ratio modulator (>45dB extinction) followed by a conventional telecommunications modulator with >20dB extinction. The series extinction ratio is >65 dB, which corresponds to a signal to leakage contrast of >100. Both the intensity modulators are driven by an Agilent 13.5Gbps BERT based pattern generator which

produces a ‘1’ for 100ps (limited by rise and fall times) and ‘0’s for the remaining part of the 1.4μs window. Fig. 3.7(c) shows the spectrum of a single pulse gated from a 10 GHz frequency comb. The spectrum is taken through an OSA with a resolution of 1.25GHz. What was initially a spectrum made of sharp discrete lines spaced by 10 GHz is now a smooth spectrum with no sign of residual discrete line structure. This is one signature of high quality single pulse gating.

Now, let us briefly look into more detail on the gating system. It is composed of a high extinction intensity modulator followed in series by a more conventional intensity modulator and a natural question would be whether this can be achieved with just a single modulator. It turns out that we need both the modulators for two reasons. 1. To achieve high enough extinction ratios to get a good SNR between the signal being measured and the noise due to improper gating, and 2. To achieve a sharp fall time in the time domain so that the gating system can select only the frame of interest.

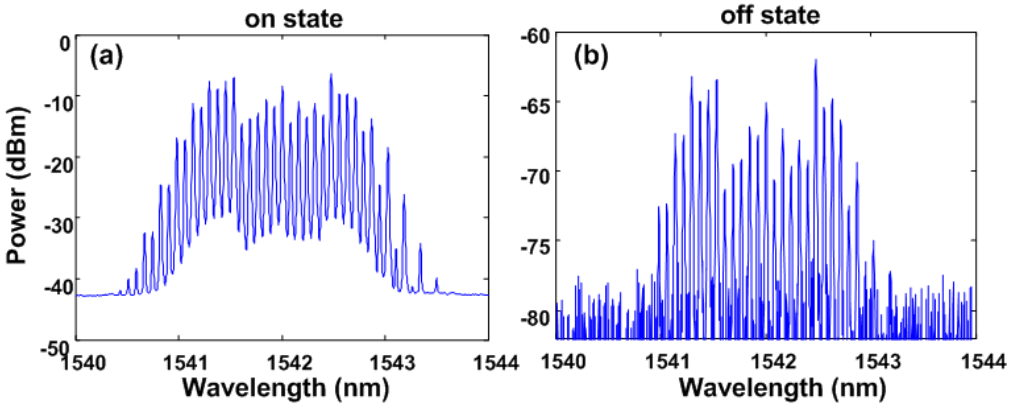

Fig. 3.8. (a) Optical comb spectrum with the high extinction modulator turned to ON state , (b) turned to OFF state

Fig 3.8 shows the behavior of just the high extinction modulator. The results shown are for a smaller bandwidth comb and at DC ON and OFF states (meaning, there is no fast modulaton of the transmission function of the modulator). The extinction ratio achieved was quite good at ~54dB, which is 12-dB greater than the 42 dB extinction ratio required for a SNR of 1. In the fast modulation case (i.e. at 10GHz) this number is slightly smaller, but still we can expect a ~10-dB SNR with just the high extinction modulator. However, we wanted to achieve >20dB of contrast (1%) between the signal

and the noise due to improper gating to ensure high quality pulse retrieval. This was the first reason to move towards a modulator series.

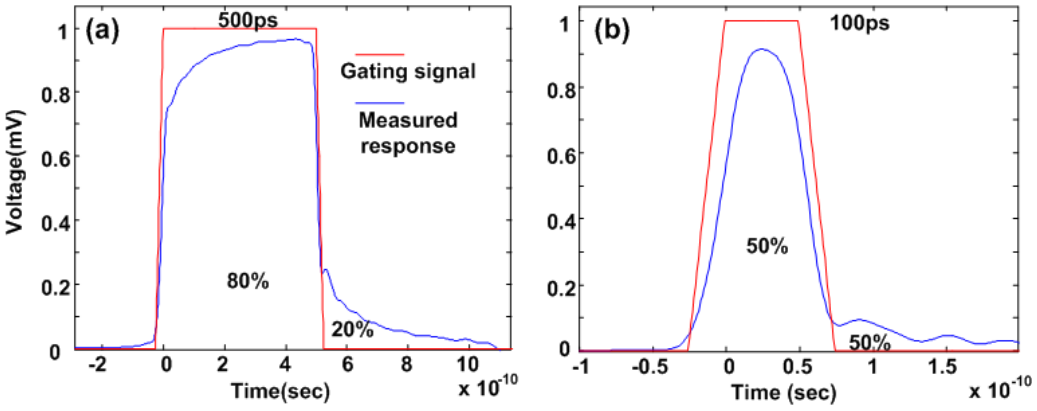

Fig. 3.9. Time domain gating signal and measured response from the high extinction modulator for (a) gating signal of 500ps wide (b) 100ps wide

The 2nd aspect is the time domain behavior of the modulators. The electro-optic response specifications for the high extinction modulator show a structured fall in the response of ~6-dB from 1GHz to 10GHz RF drive frequencies. The effect of this is that, when we drive the modulator with a sharp gating signal, the actual response will be a smoothened and structured output obtained due to the filtering effect from the modulator. An easy way to look at this is to use a continuous wave laser and modulate it with the gating function and then look at the output using a fast photo-diode and an oscilloscope. Fig 3.9 (a) and (b) show the applied gating signals and the actually measured gating functions. We can see the effect of the frequency response smoothening out the gating as well as creating a long tail instead of a sharp fall we want. In (a) where the gating function is 500ps wide, the power in the tail outside the gating window is ~20% which is quite significant. However, in the case of 100ps gating signal (corresponding to 10-GHz which is our final objective), we see that ~50% is outside in the tail regions. What this does is to corrupt the measurement with significant junk from adjacent frames and this will prevent proper measurement when there is update on a frame to frame basis.

We overcome these difficulties by using a more conventional intensity modulator (but with a much wider bandwidth - < 3-dB drop in electro-optic response from 1GHz to 10GHz) in series with the high extinction modulator. By suitably tuning the relative timing between the two modulators, we can ensure that the fall time is significantly

reduced as required for a single frame gating at 10-GHz. To demonstrate this we have the comb and the single frame gated version of the comb in fig 3.10 (a) and (b). We see that, as previously, the gated version has no comb like structure in contrast to the spectrum before gating indicated high quality gating. This effect can be easily understood by the fact that periodic time domain signals have discrete lines in frequency domain and perfectly aperiodic signals (as expected in the single frame gating) have a smooth continuous spectrum.

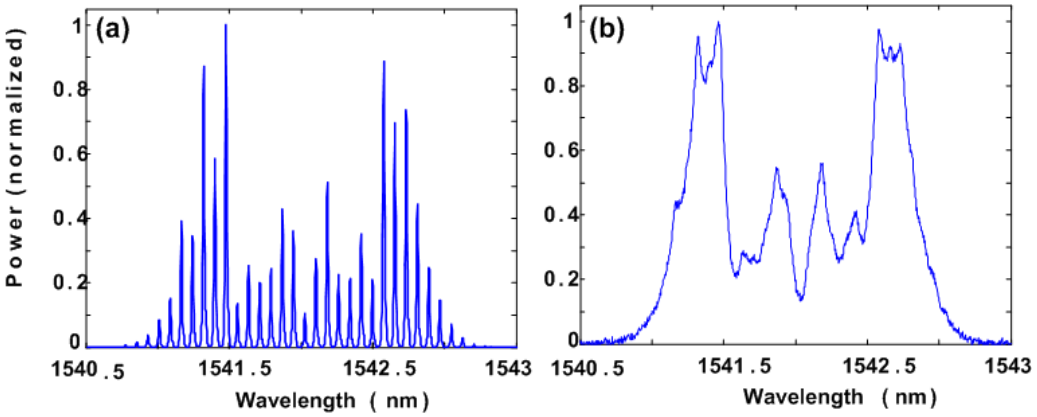

Fig. 3.10. comb spectrum before gating (a), and after gating a single frame (b)

Ideally, if the acquisition time of the camera (which gives the response time of the spectrometer) is the same as the repetition rate of the comb, we would have a continuous time acquisition system without the need for gating (the simple retrieval algorithm from the interferogram data allows us to assume the computation also to be real time). Such a system can measure potentially infinite record length waveforms without any dead spacing. Current camera technology though is still far away from the GHz class acquisition times necessary. However, if required by the application, it is possible to increase the record length per acquisition. Since this depends on the resolution of the spectrometer, by using high resolution spectral dispersers like the virtually imaged phase array (VIPA) possibly in conjunction with other dispersers (to obtain simultaneous high resolution – broad bandwidth operation) sub GHz resolution can be obtained, which in turn corresponds to temporal record lengths of >1ns. Temporal demultiplexing can be used to further increase the record lengths. We expect that in future, any candidate for continuous operation would probably involve all these aspects simultaneously to push

towards its objective. The longer record lengths per acquisition afforded by the higher spectral resolution and temporal demultiplexing allows for relatively slower cameras to be used in the spectrometer.

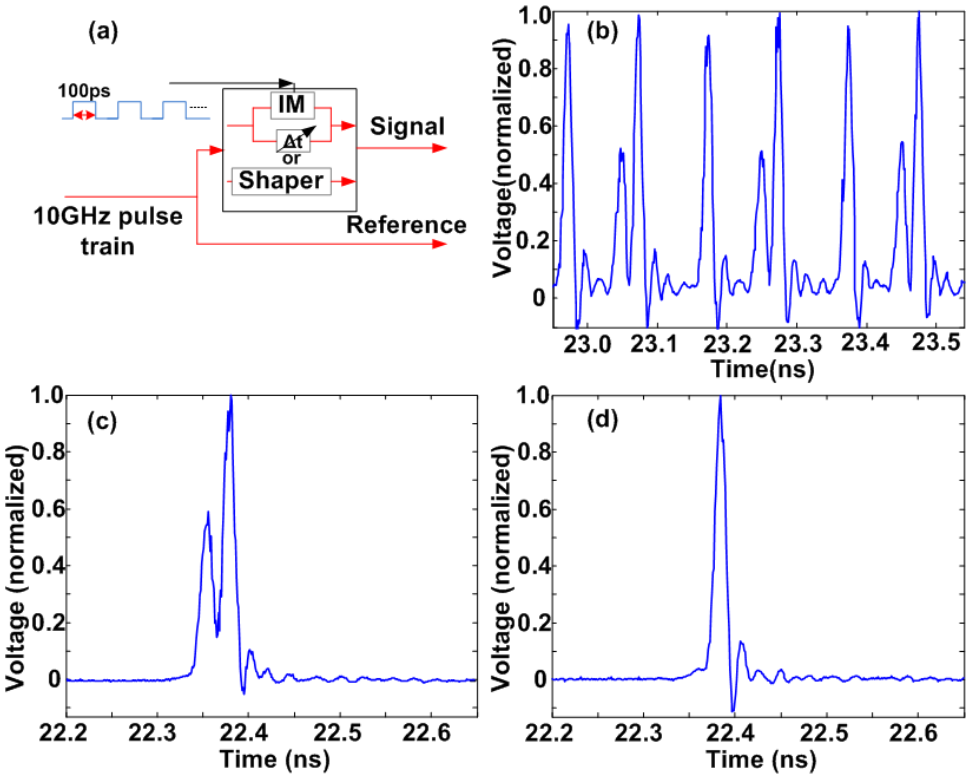

Fig. 3.11. (a) Scheme for waveform generation, (b) 60 GHz sampling scope trace of waveform without gating, (c) Gated pulse pair, (d) Gated single pulse

With respect to the choice of waveforms for measurement, an OAWG encoder which can generate arbitrary waveforms over a large number of spectral lines and update them at the repetition rate of the comb would be ideal. However, until such technology is available, other simple schemes can be used to generate adequate test waveforms. Some desirable attributes are: (i) abrupt or sharp variations of amplitude and phase in the spectral domain (since ours is a spectral domain based technique), and (ii) fast update since we saw previously that a true single shot operation can only be verified with dynamic waveforms. Our scheme to achieve this is shown in Fig. 3.11(a). An input 10GHz pulse train is split into two arms; in one arm an intensity modulator removes every alternate pulse. The relative heights of the pulses can also be controlled using attenuators present in each arm. These pulses are then combined with a delay to form a

quasi-dynamic signal. Fig. 3.11(b) shows the sampling scope trace taken using a 60 GHz photodiode showing alternate periods of single pulses and pulse pairs. Though in the time domain they look relatively simple, in the frequency domain these waveforms have rapid amplitude fringes characteristic of two temporally separated pulses interfering with each other and a linear spectral phase with abrupt 0-π jumps whenever the amplitude of the interference signal changes sign. Another motivation to choose such a waveform pattern is that, when we retrieve the single pulse waveform, if the gating is not ideal, leakage from adjacent periods is expected to show up as a small satellite pulse at the position of the 2nd pulse of the pulse pair waveform. Absence of this can be interpreted as sign of high qualtiy single waveform gating. Figs. 3.11(c) and 3.11(d) respectively show sampling scope traces taken of a pulse pair and of a single pulse waveform when the gating is switched on. By varying the delay of the gating pattern from the pattern generator, different waveform frames can be selected. The gated waveforms are amplified using an erbium doped fiber amplifier (EDFA) prior to measurement.

In addition to dynamic waveform measurements confirming true single shot operation as described above, we have also performed experiments where the dynamic pulse pair generator is replaced with a static line-by-line pulse shaper. (Fig. 3.11(a) bottom part). In this case we can program the pulse shaper to generate more complex text waveforms which are still measured in single-shot operation but without waveform update. Since waveform update is more a test of the gating system than of the spectral interferometry setup, once the gating system is verified we are free to measure more complex waveforms in static situations.

Figure 3.12 shows the experimental results for dynamic waveforms. Fig. 3.12(a) shows the measured spectral amplitude and phase for a gated single pulse. The phase is relatively flat as expected for a bandwidth limited pulse. As expected the retrieved spectrum resembles the spectrum for the gated pulse as shown in Fig. 3.7(c) (but flipped because it is plotted in frequency). The spectrum is relatively noisy and this we believe is due to amplified spontaneous emission (ASE) noise added by the amplifier before the spectral broadening process and by the EDFA which amplifies the waveforms after gating. However as far as the measurement is concerned, this is the spectrum of the

source in that waveform period. Also we see that the phase plot deviates slightly from its flat nature at places where the signal spectrum is small; this is likely due to reduced signal to noise ration (SNR) at these points causing extra phase errors. Perhaps a better way to look at the data is to calculate the time domain waveform using the retrieved spectrum and phase. This is shown in Fig. 3.12(b). A clean pulse is seen as expected. Also, no satellite pulse is seen which, as discussed earlier, demonstrates high qualtiy single waveform gating and unambiguous single-shot measurement.

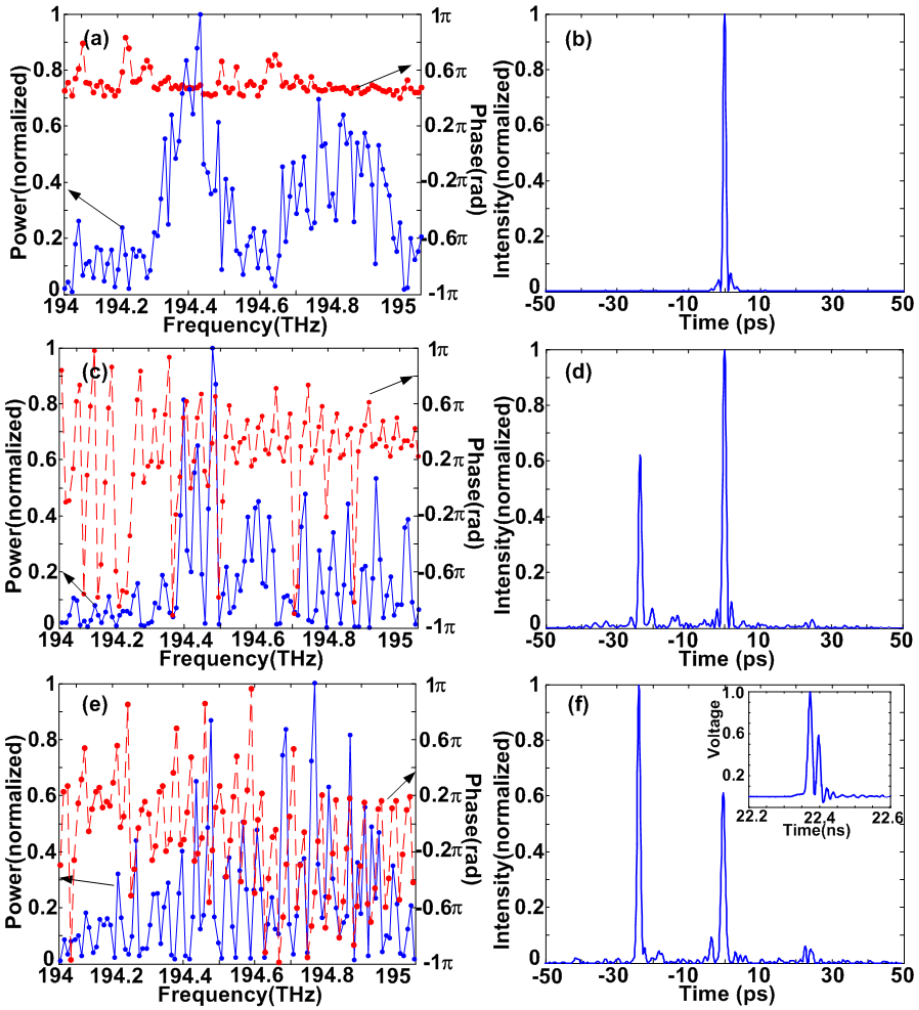

Fig. 3.12. (a),(b) Retrieved spectrum, phase and generated time domain trace for gated single pulse, (c), (d) For a gated pulse pair, (e), (f) For a gated pulse pair with different relative heights (inset – RF scope trace)

Figures 3.12(c) and 3.12(d) show the retrieved spectrum and phase and the generated time domain waveform for the gated pulse pair whose RF scope trace was shown in Fig. 3.11(c). In the spectral domain we see fast variations both in spectral

amplitude and phase - no easily discernible pattern exists, but when the time domain waveform is calculated, we see that it agrees very well with what was expected. This gives strong evidence of proper phase retrieval. Another point to note is that in our experiments the pulse at t=0 is left unchanged, while the pulse at t ~ -27ps is modulated. This point is exactly consistent with our waveform retrieval data, which gives additional evidence of correct phase measurement (a delay in time causes a linear spectral phase). Figs. 3.12(e) and 3.12(f) shows the retrieved spectrum and phase and the calculated time domain waveform for a different gated pulse pair waveform where the amplitude of the earlier, gated pulse is increased relative to the ungated pulse at t=0. The sampling scope trace is shown as the inset in Fig. 3.12(f). Excellent waveform retrieval is observed as indicated by the agreement between the calculated time domain waveform and the scope trace.

After the waveform generation and gating, the energy in a single gated pulse pair waveform was ~5pJ (for a gated single pulse it was roughly half of that). The spectrometer loss in our setup was around 10 dB which leads to about 500 fJ of signal energy distributed over 400 pixels on the camera (200 pixels per channel). The reference pulse energy was chosen such that the spectral intensity of the reference pulse was at least twice as strong as that of the signal pulse. This condition is necessary for unambiguous retrieval (section 3.2). The efficiency of the camera was around 70% which corresponds to an average of ~6700 photoelectrons from the signal waveform per pixel. The specified noise for the camera is ~600 photoelectrons per pixel. Since this is an interferometric measurement, depending on the coherent sum of the reference waveform and the signal waveform at each pixel (which depends on the phase difference) the SNR varies for different pixels. In cases where the sum is low, the SNR is lower leading to reduced accuracy of measurement. On average we observed an SNR of around 5 (20% contribution by noise) which corresponds to a higher noise contribution than by just considering camera noise. This we believe is due to amplifier ASE noise.

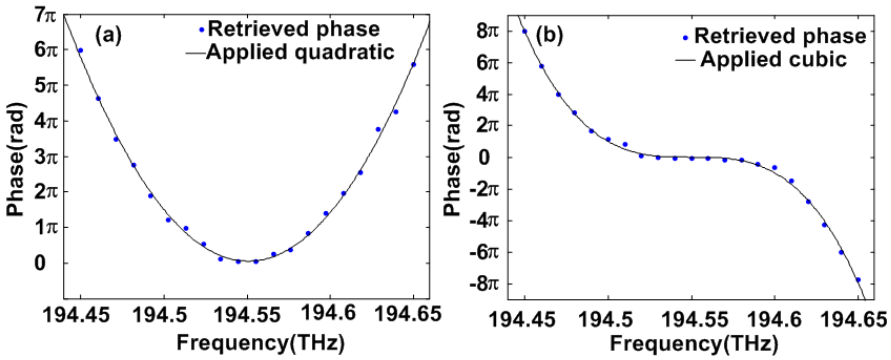

Fig. 3.13. (a) Applied quadratic phase and retrieved phase, (b) Applied cubic phase and retrieved phase.

Fig. 3.13 shows measurement results with user defined waveforms generated using a line-by-line pulse shaper. The bandwidth in these experiments is around 200GHz limited largely by the bandwidth available in the frequency comb before spectral broadening. Fig. 3.13(a) shows the retrieved spectral phase (circles) and the applied phase (a quadratic, shown as solid line). Excellent agreement is observed. Fig. 3.13(b) show the retrieved phase when cubic spectral phase is applied. The errors (standard deviation of differences between applied and retrieved phase) are 0.11π and 0.13π, respectively. These are only slightly higher than the errors of approximately 0.1π observed in previous measurements at higher average power in which spectral interferometry data were acquired for static waveforms over multiple waveform periods by integrating over the 1.4 μsec camera integration time (corresponds to $>10^4$ waveform periods) (section 3.2).

3.5 A simple implementation of spectral shearing interferometry for self referenced waveform characterization

In previous sections we demonstrated a fast characterization method using dual-quadrature spectral interferometry for optical arbitrary waveforms which can also characterize dispersion of long fiber links. However, this method requires a frequency-locked, pre-characterized reference frequency comb. For some applications a self-referenced scheme is needed (meaning the signal does not require a premeasured reference and an absolute phase is measured). Here we demonstrate a very easy to implement, low-power self-referenced scheme to characterize arbitrarily complex

periodic waveforms over wide bandwidths. Our scheme based on an elegant method proposed in [49] introduces an implementation of spectral shearing interferometry [50] utilizing only a Mach-Zehnder intensity modulator and an optical spectrum analyzer.

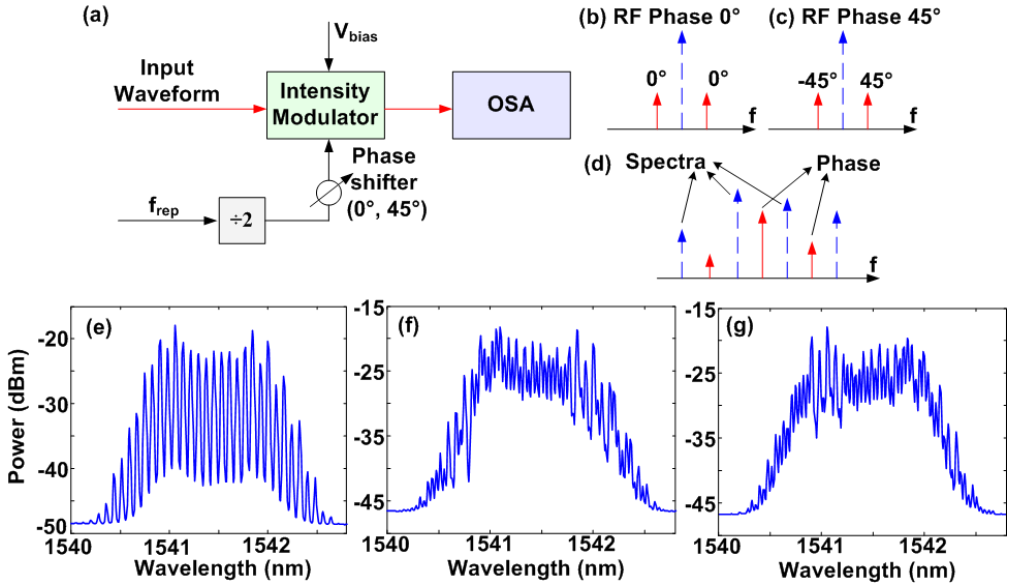

Fig. 3.14 (a) Experimental Setup; (b), (c) Relative phases between sidebands with RF phase shift; (d) Spectrum – from carriers, Phase – from interference between sidebands (e) OSA spectra with no modulation; (f) 0° "cos" modulation; (g) 45° "sin" modulation

Fig 3.14(a) shows the experimental setup. The input waveform is sent to a Mach-Zehnder intensity modulator (we use a x-cut LiNOb3 modulator from JDS Uniphase), which is driven by a weak sinusoidal RF signal with half the frequency as the input frequency comb (depending on availability, this can be either from a local oscillator or derived from the signal itself). The drive signal passes through a tunable RF phase shifter. Two spectra are recorded by the OSA with the RF phase shifter settings spaced 45° apart (this can be converted into a parallel measurement using a 0-45° hybrid, two intensity modulators and a dual-channel spectrometer). From these two spectra, unambiguous spectrum and phase can be retrieved.

To understand how this technique works, let us first consider only a single frequency which goes through the intensity modulator. Assuming a small RF signal, only first order sidebands at half the repetition rate are created on either side of the carrier with relative phases that depend on the RF phase shift (figs 3.14(b), 3.14(c)). With a frequency comb, at every possible sideband position contributions from two adjacent comb lines (at

higher and lower optical frequency) will interfere, yielding sideband intensities that depend on the phase difference. Through this interference, the sideband spectra provide us unambiguous phase information, while the spectra remaining at the carrier positions provide spectral amplitude information. If spectral resolution is a concern for lower repetition rate combs, another easy change would be to run the modulator in a carrier suppressed scheme and making 3 measurements – 1 for spectra and 2 for phase.

Let us now briefly look at why we need the phase shifter and two spectra. Whenever we look at the frequency resolved interference between two waveforms, a phase ambiguity arises preventing phase retrieval (just the "cosine" or "sine" interference components are not enough). So, in conventional implementations of both spectral interferometry and spectral shearing interferometry, this problem is overcome by setting the delay of the interfering pulses to be larger than the individual temporal widths. However, for wide temporal window waveforms this makes large demands on spectral resolution; for >50% duty factors, complete separation of the interfering waveforms by delay is impossible. Another way is to obtain both the components of the interference ("cos" and "sin"); this also makes unambiguous retrieval possible. In our scheme we obtain both interference components simply by changing the relative phases between the sidebands by 90°, which is achieved by a phase shift of 45° at the RF phase shifter. This is an important difference between our technique and electro-optic spectral shearing interferometry (EOSI) [51], a linear technique which emulates conventional spectral shearing interferometry, but instead uses a phase modulator to generate the spectral shear between a pair of pulses separated by a delay. In EOSI too, similar problems arise as the duty factor of the pulses increase, EOSI breaks down for >50% duty factor waveforms common in OAWG.

Now the expression for the interference between the sidebands of two adjacent lines ('n' and 'n+1') are -

$$I_{inphase} = c[|a_n|^2 + |a_{n+1}|^2 + 2|a_n||a_{n+1}|\cos(\psi_n - \psi_{n+1})] \tag{3.6}$$

$$I_{quadrature} = c[|a_n|^2 + |a_{n+1}|^2 + 2|a_n||a_{n+1}|\sin(\psi_n - \psi_{n+1})] \tag{3.7}$$

Where '$|a_i|$' and 'ψ_i'are the spectral amplitude and phase of the input comb lines and 'c' is a modulation parameter defined as the ratio between the sideband and the carrier for a single frequency input. This parameter depends on the modulator settings and can be easily extracted just from the two spectra without the need for any additional measurements. This ratio experimentally corresponds to the height of the sidebands w.r.t the carrier when a continuous wave (CW) input is used. In our experiments we adjust the modulator parameters like input RF voltage and bias voltage to have a low value for 'c' between 0.1- 0.2 to minimize the possible effects of higher order sidebands. For the above expressions we have assumed that the phases of sidebands in each case to be (0°, 0°) and (-45°, 45°), but in general there may be a constant offset phase. However, it can be easily shown that this only contributes a constant and linear term to the retrieved phase. Since this is only a constant phase and a constant delay in the time domain, we will ignore it. Figs 3.15(e) – (g) show representative spectra from OSA for the cases of no modulation and with "cos" and "sin" modulation.

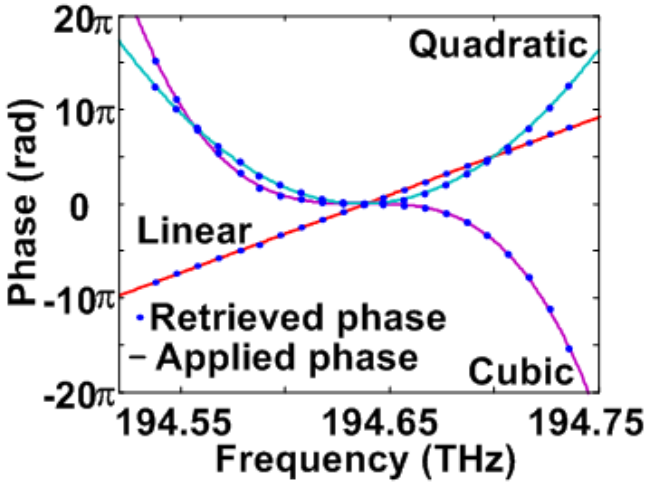

Fig 3.15 – Applied spectral phase – Solid lines, measured spectral phases – dots

Fig 3.15 shows the results of an experiment where we used a line-by-line pulse shaper to apply different spectral phases onto the comb, after which we measured the reshaped pulses. The figure shows examples of linear, quadratic, and cubic spectral phase. An excellent agreement was seen between applied phases and retrieved phases.

3.6 Characterization of novel optical frequency comb sources

In this section, we will utilize the method we discussed in section 3.5 to characterize a novel optical frequency comb source. As we discussed previously, modelocked lasers which have been the primary means of generating short pulses do not conveniently scale to high repetition rates (10GHz and above) while maintaining optical frequency stability and so novel techniques have been developed to generate high repetition rates without mode-locking [for e.g. 5-8]. Although these sources may provide wide optical bandwidth, they do not generate short pulse outputs due to abrupt spectral phase variations. Therefore characterization is essential if one wishes to compress these sources to the bandwidth limit [8]. To do this, it is desirable to have a self referenced measurement technique since it is harder to ensure that the reference source used in a relative measurement scheme has the same repetition rates and center frequencies. In general, usually the reference to derived from the same source and hence it becomes harder to characterize the absolute spectral phase. In this section we will use our technique to characterize two optical frequency comb sources. 1) An optical frequency comb generator,2) Frequency comb generated by cascaded Phase and Intensity modulators which we have used for other experiments previously.

First we will look into the optical frequency comb generator (OFCG). An optical frequency comb generator is made of a Fabry-Perot cavity with an intra-cavity phase modulator [5]. A stable CW laser is incident into the cavity and when the frequency of the RF signal driving the phase modulator is in resonance with the round trip time of the cavity, multiple side bands are created generating a frequency comb with the repetition rate given by the RF drive frequency. However, by the nature of the source, two pulses are created per round trip, the time and relative heights between them depending on the settings. For many applications, particularly for optical communications it is required to have a stable periodic pulse train with equal height pulses and this requires precise adjustment of the OFCG and phase correction [52]. This makes it necessary to exactly evaluate the change in pulse shapes as the settings are changed. Fast electronic oscilloscopes fail to do this since the bandwidths involved are more than 10times bigger.

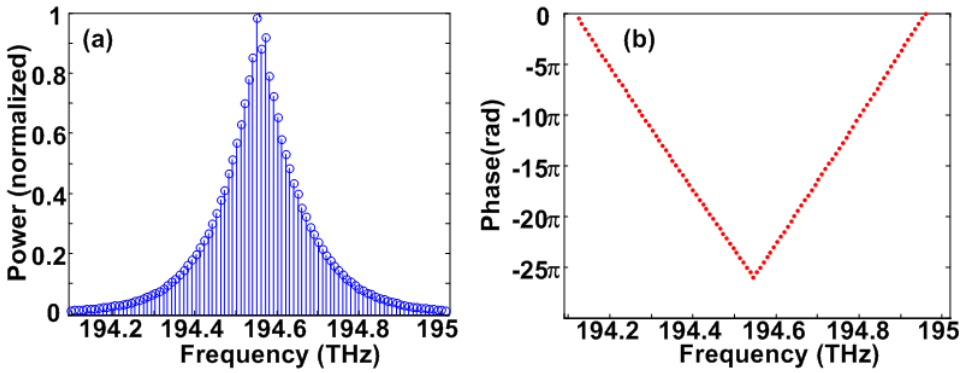

Fig 3.16 (a) A representative output spectrum from the OFCG, (b) spectral phase indicating two different slopes corresponding to two pulses with different frequency content

Fig 3.16(a) shows a retrieved representative output spectrum from the OFCG driven at a frequency of ~10GHz and 3.16(b) shows the corresponding spectral phase. In this case the pulses are roughly spaced half the distance apart at around 50ps. From the above picture it is hard to visualize the time domain behavior and so let us look at them in the time domain.

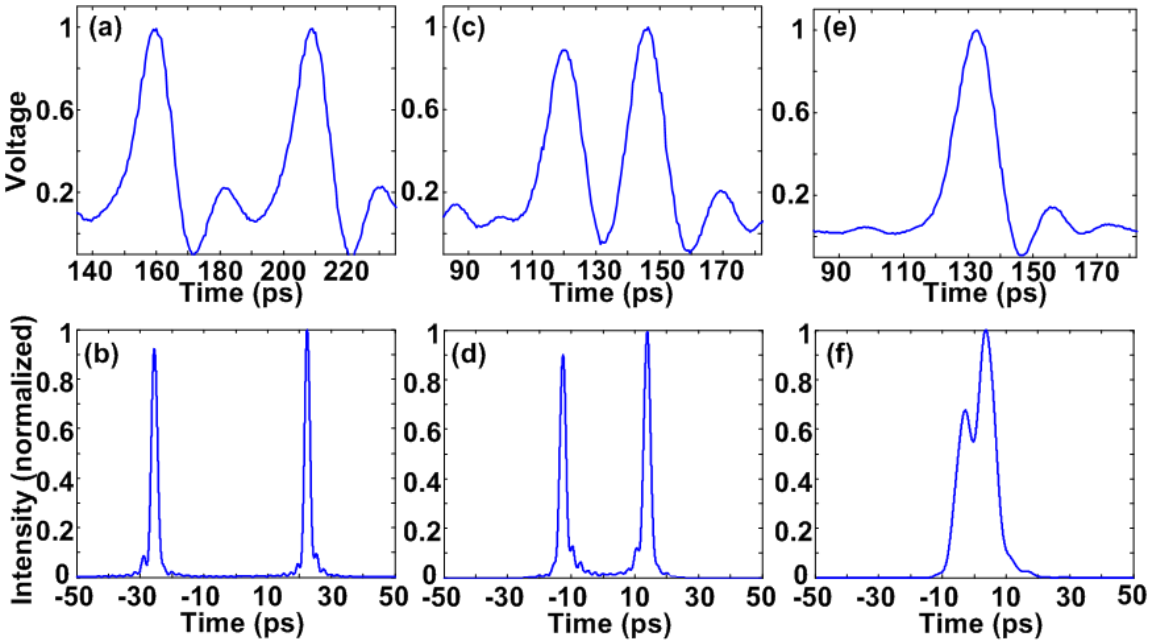

Fig 3.17 Variation of output with varying setting parameters of the OFCG, (a), (c), (e) RF scope traces obtained with a 60GHz photodiode and (b), (d), (f) Retrieved time domain signals using our measurement technique.

Fig 3.17(a), (b) shows the RF scope trace obtained with a 60GHz photodiode and the retrieved time domain signal using our measurement technique for the spectrum and

phase shown in fig 3.17. We see two pulses in the time domain as expected. The time difference between them is ~50ps. From the retrieved time domain picture we see that the bandwidth of the pulses is significantly wider than the 60GHz bandwidth of the photodiode, indicated by a much shorter pulse compared to the RF scope trace. Fig 3.17 (c) and (d) show a different setting where the pulses have come closer. In fig 3.17(e), (f) we have an interesting situation where the settings are adjusted such that the pulses now are very close to each other. In the RF trace it looks like a single pulse with no additional structure, however when we look at the time domain retrieval, we see that it is still two pulses with small delay between them. Another point to note is that the bandwidth of the pulses has reduced due to the changing of parameters and now the pulses are wider in time. This again is clearly visible in the retrieved time domain trace but not in the RF scope trace.

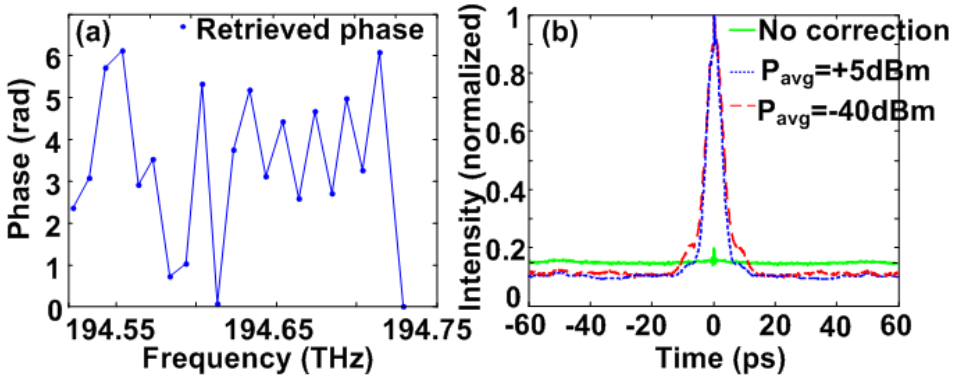

Fig. 3.18 (a) Retrieved phase of uncompensated comb; (b) Autocorrelation of uncompensated comb, compensated comb with phase measured at 5dBm (~4mW) and -40dBm (~100nW)

Fig 3.18(a) shows the retrieved spectral phase for a 10GHz frequency comb generated by the cascaded Phase and Intensity modulator scheme. The autocorrelation of the output is shown in fig 3.18(b) (no correction) indicating a flat envelope (100% duty factor). This is because phase modulation does not affect the time domain intensity, though in frequency domain a comb is generated (this corresponds to varying spectral phase). Using a line-by-line shaper, we then compensated the phase (retrieved at 2 different power levels, +5 and -40dBm). We expect a good phase retrieval to manifest as a bandwidth limited compressed pulse in the autocorrelation and this is confirmed in experiments (fig 3.18(b)) even down to average power levels of -40dBm=100nW (corresponding to 10aJ/pulse at 10GHz). The background level is due to amplifier and detector noise.

In summary, in this chapter we discussed characterization techniques for optical arbitrary waveforms. We proposed two different techniques. The first one based on dual-quadrature spectral interferometry is a relative phase measurement technique which measures the waveform relative to a characterized reference. Low power, fast measurements were demonstrated and utilizing this we could monitor dispersion and dispersion slopes of long fiber links quickly. We then extended this technique with fast temporal gating to measure very rapidly changing waveform updating at a frame to frame basis. We then proposed a new technique related to spectral shearing interferometry for characterization applications which require a self referenced technique. We used this to characterize two novel optical frequency comb sources. This technique too consumes very low power and we demonstrated good phase retrieval down to a few aJs/pulse level. Together with our waveform generation capabilities we now have a complete test-bed for high complexity waveform generation and characterization.

4. NOVEL GENERATION TECHNIQUES FOR OPTICAL FREQUENCY COMBS AND PULSE SOURCES USING PHASE MODULATION

Modelocked lasers have long been the primary means of generating optical frequency combs and short pulses. However, as we move into higher repetition rates, they run into problems of maintaining optical frequency stability as well as increased complexity in design and operation. Furthermore, they have many limitations, some of them being – the inability to tune the repetition rate easily, the inability to tune the optical center frequency and complex control mechanisms required to keep the system stable. To overcome these limitations, in recent years there has been significant work on novel techniques for frequency comb generation. A primary contender has been optical frequency combs generated by direct phase modulation with the required repetition rate of an input CW laser using Lithium-Niobate modulators. This has been made possible owing to recent advances in the modulator technology making them reliable, cheap and easily operable.

Strong sinusoidal phase modulation of a continuous wave (CW) laser creates multiple sidebands leading to generation of a frequency comb [6]. Advantages of this technique include the ability to create high repetition rate combs with stable optical center frequencies given by the source laser and convenient tuning of the repetition rate and optical center frequency. Therefore, such combs become a source of choice for some applications in optical communications [53], Radio frequency (RF) photonics [54] and optical arbitrary waveform generation (OAWG) [4].

4.1 Technique for frequency comb generation with very flat spectral profiles, high pulse quality and tunable repetition rate

By phase modulation alone, the spectral flatness of the comb is quite poor. The amplitudes of successive comb lines follow successive Bessel function dependences on drive voltage; for drive voltages large enough to generate a significant number of comb lines, the line to line amplitude variation can be quite large. A flat frequency comb is

generally desired. For example, if the comb is used as a multi-wavelength source, it is desirable to have equal power in different wavelengths. For applications such as RF photonic filtering requiring a specific spectral shape [55], apodization is much easier with minimal excess loss if we start off with a flat comb. Also, for time domain applications where a short pulse is needed, abrupt comb line to line variations result in poor pulse quality. Some examples of recent research activity aimed at generating flatter combs can be found in [56-60]. Though all of these schemes improve the flatness significantly compared to phase-only modulation, they still provide either limited flatness over the bandwidth of interest or limited number of comb lines over which flatness can be maintained. In this section, we will demonstrate a scheme which can produce very flat combs over large bandwidths in a easily scalable fashion. We achieve this using a cascade of two intensity modulators together with the phase modulators driven by tailored RF waveforms. In particular, we will generate a 10 GHz comb with 38 comb lines in a 1-dB bandwidth (corresponding to a bandwidth of 400GHz) and ~60 comb lines above the noise floor of the OSA (60-dB bandwidth). The number of comb lines can be scaled by increasing the RF drive power without sacrificing spectral flatness. Also, the spectral phase of the comb generated in our technique is almost purely quadratic, which allows for generation of high quality pulses via compression in a simple dispersive fiber or chirped fiber Bragg grating.

Our research draws on the interesting theoretical work of V. Torres-Company and coworkers [61], which proposed a novel way of understanding the spectral flatness achieved in previous schemes such as [56] and [57]. When a flat topped pulse is subjected to a strong, periodic, quadratically varying temporal phase, it undergoes time-to-frequency mapping [62, 63], resulting in a flat comb due to the shape being similar to the time domain intensity of the input waveform. A convenient approach to generate flat topped pulses is to use an intensity modulator driven with a sinusoid with an amplitude $V = V_\pi / 2$ of the modulator and a DC bias corresponding to a phase shift of $\phi_{dc} = -\pi / 2$ (the envelope of the output field after the intensity modulator is given by the relation $(1 + \exp(j\phi_{dc}) \exp(j\pi V / V_\pi \cos \omega_{rf} t))$ which in our case, after substitution simplifies to

$(1+\exp(-j\frac{\pi}{2})\exp(j\frac{\pi}{2}\cos\omega_{rf}t))$. Generating a periodic quadratic temporal phase though is hard; however, a sinusoidal temporal phase can be approximated by a quadratic function around its peak or its valley and to a first order provides a means to generate the required quadratic temporal phase.

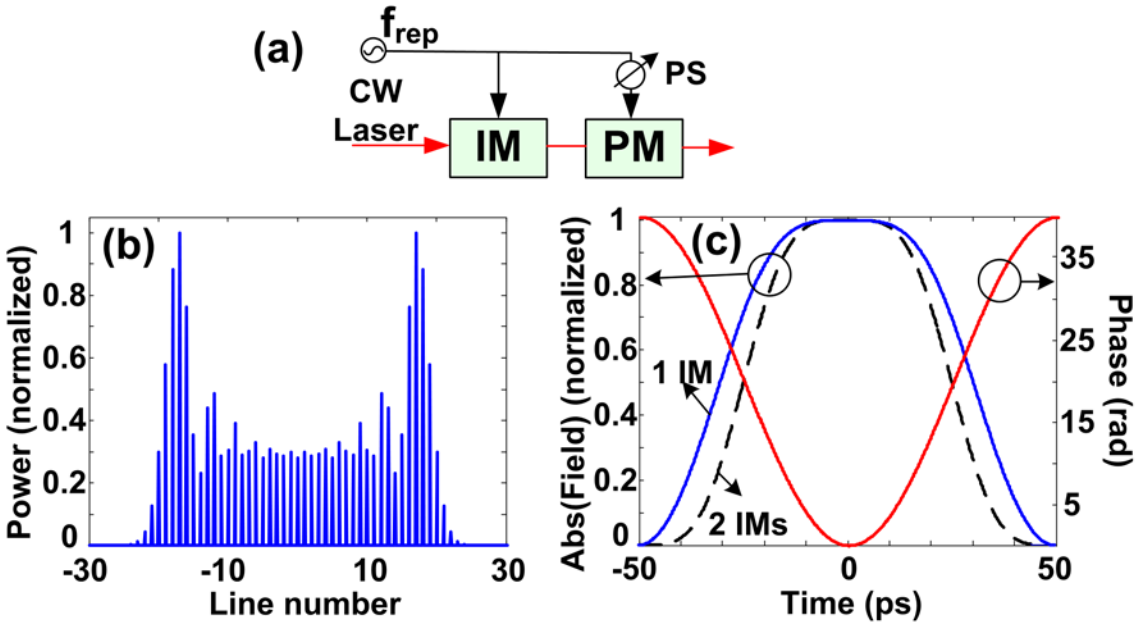

Fig.4.1 (a) Experimental scheme for flattening frequency combs generated by phase modulation using cascaded intensity modulator (IM) and phase modulator (PM), PS – RF phase shifter (b) Simulated output spectrum for this scheme, (c) Time domain plot showing the temporal phase applied by the PM (red, solid) to the outputs after 1 IM (blue, solid) and 2 IMs (black, dashed)

Fig 4.1(a) shows this scheme combining the two aspects, and Fig 4.1(b) shows the spectrum simulated assuming the phase modulator is driven with a sinusoidal voltage whose amplitude V satisfies the relation $\pi V / V_\pi = 20$ (i.e. the effect of the phase modulator can be written as a multiplication by $\exp(j\pi V / V_\pi \cos\omega_{rf}t) = \exp(j20\cos\omega_{rf}t)$). In Fig. 4.1(b) we see a flat central section to the spectra, but towards the edges there are pronounced "bat ears." To understand this, we look at figure 4.1(c) (blue, solid) which shows the time domain signal, and 4.1(c) (red, solid) which shows the sinusoidal temporal phase. In the central part, the time domain signal is very flat and the phase is almost quadratic leading to good

spectral flatness. As we move away from the center and the phase starts deviating from a quadratic, the flatness is degraded. The strong peaks or bat-ears occur at the spectral extrema, where the instantaneous frequency, i.e., the time derivative of the temporal phase, is at a minimum or maximum. The bat-ears may be explained on the basis of the relatively long time for which the instantaneous frequency function dwells at the frequency extrema [21].

In order to obtain flat spectra, we need both a nice flat-topped pulse as well as a good quadratic temporal phase (for which the instantaneous frequency would be a linear without extrema). Accordingly, we propose two modifications to the above method. A first improvement would be to make the flat-topped pulse sharper, which will reduce the fraction of the waveform seeing a significant departure from quadratic temporal phase. This can be achieved using two intensity modulators in series driven with the same parameters as described previously. Figure 4.1(c) (black, dashed) shows the new sharper time domain waveform. Secondly, since the bat ears happen due to deviation from quadratic phase, we attempt to generate a phase profile that better approximates a quadratic. The expansion for the cosine around its maximum up to the first undesirable term is,

$$\cos(\omega_{rf} t) = 1 - \frac{(\omega_{rf} t)^2}{2!} + \frac{(\omega_{rf} t)^4}{4!} - \ldots \tag{4.1}$$

So we have

$$\cos(\omega_{rf} t) - \frac{1}{16}\cos(2\omega_{rf} t) = \frac{15}{16} - 0.75\frac{(\omega_{rf} t)^2}{2!} + 0 + \ldots \tag{4.2}$$

From eqn (4.2) we see that by using the first and 2nd harmonics (which can be easily generated with a X2 frequency multiplier) with a suitable ratio and phase shift between them, the 4th order term (which is the first non-ideal term) can be made zero. With regard to higher order terms, since the cascade of the intensity modulators creates a waveform with a sharper decay, they are less of an issue in the region of the flat topped pulse.

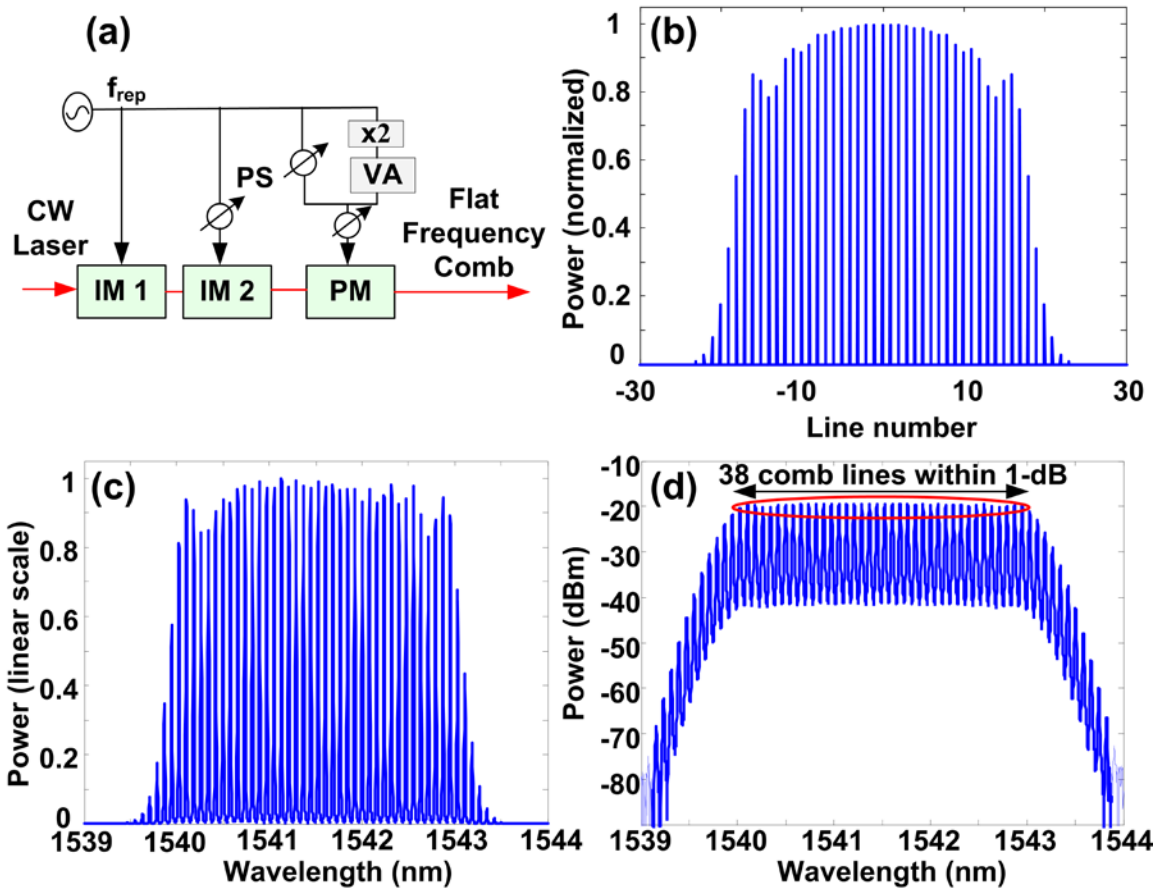

Fig.4.2 (a) Experimental scheme for comb generation with high spectral flatness, VA – variable attenuator, PS – RF phase shifters, (in our actual experiment, we use two phase modulators in series to generate greater number of lines) (b) Simulated output spectrum in this case, (c), (d) Output spectra of the experimentally generated comb in linear and log scale showing 38 comb lines within 1-dB variation

Figure 4.2(a) shows the scheme incorporating both the improvements we discussed. A tunable attenuator adjusts the ratio between the fundamental harmonic and the 2nd harmonic to the required value ((1/16)^2 ~ -24dB) and a tunable RF phase shifter ensures that they are 180degrees out of phase as required. We also have other tunable RF phase shifters to ensure that there is timing match between the different components. Figure 4.2(b) shows the simulated spectrum, which is now significantly flattened, with the absence of any bat-ear shape. In our actual experiment, a minor difference to the scheme shown in fig 4.2(a) is that we use two phase modulators in series instead of one. This is a common technique used (e.g., [57]) to overcome the RF power handling limit of the phase modulators. In our case we drive each phase modulator by its maximum RF

power of 1W; driving two phase modulators identically allows greater power handling and doubles the number of comb lines. The IM we use has a V_π of ~8V, the PM has a V_π of ~3V and all modulators are pigtailed with polarization maintaining fiber. The frequency of the RF oscillator is 10GHz. The X2 frequency multiplier used is a Ka band active X2 multiplier (Ducommun). The net optical loss of the whole apparatus is ~15dB (the unavoidable loss due to gating of the CW by the intensity modulators is only ~4dB, while the rest is mainly modulator insertion losses). Figures 4.2(c) and 4.2(d) show the experimental output comb spectra in linear and log scale, respectively. We observe a very flat spectral profile with 38 comb lines in a 1-dB bandwidth ($< \pm$ 10%) (circled in fig 4.2(d)) with much smaller variations in smaller bandwidths around the center.

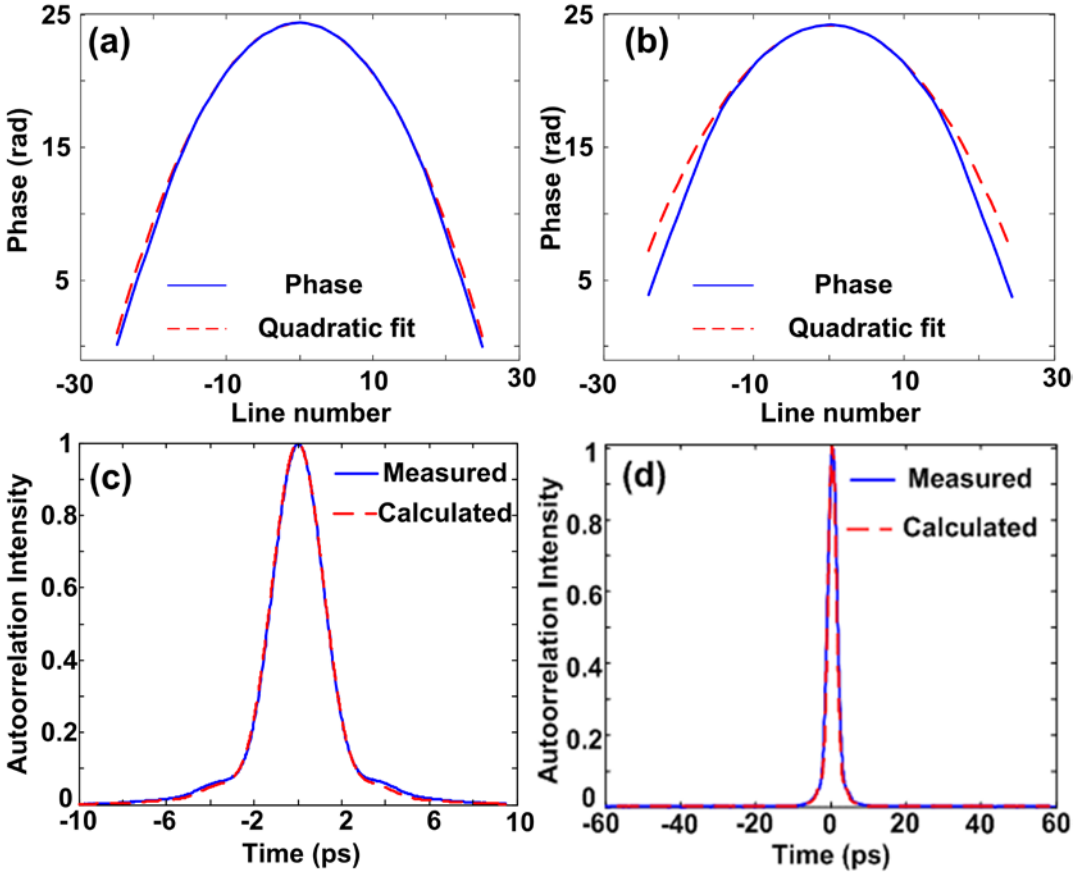

Fig.4.3, (a), (b) Simulated spectral phase and the quadratic fit to it for the case of phase modulation with tailored RF waveform (a) and a sinusoid (b). (c), (d) Short and long aperture time domain intensity autocorrelations of the output pulse (measured, blue, solid) (obtained after comb propagation through ~850m of SMF) superimposed with the autocorrelation calculated taking the spectra (2(c)) and assuming flat spectral phase. A very good agreement is seen between the two.

Another interesting aspect is that, in the large phase modulation limit, a waveform with a pure quadratic temporal phase corresponds to a spectrum with pure quadratic phase. This in turn corresponds to a pulse with a linear chirp, which can be compressed to the bandwidth limit with high quality just using an appropriate length of standard single mode fiber (compared to more complex pulse shaper based methods [64]). For the bandwidths involved, the effect of dispersion slope of the fiber is small. Figure 4.3(a) (blue, solid) which shows the simulated spectral phase of the comb together with a quadratic fit (red, dashed) clearly indicates this by showing an excellent agreement between them. This idea was first discussed in [65] and the process of making the drive more quadratic is referred to as aberration correction. To demonstrate it's superiority over a pure sinusoid, fig 4.3(b) shows the simulated spectral phase for the same configuration with the phase modulator now driven by a pure sinusoid. In this case, the spectral phase of the comb differs more significantly from a quadratic; this is expected to translate into lower quality pulse compression.

We measured the spectral phase of the comb using our frequency comb characterization technique based on a linear implementation of spectral shearing interferometry, described in detail in chapter 3 [30]. The measured phase indicated that pulse compression could be accomplished using ~850m of SMF. Fig 4.3(c) and 4.3(d) (blue, solid) show the measured intensity autocorrelation of the pulse resulting after fiber propagation in a short and wide temporal window. The theoretical intensity autocorrelation (red, dashed) taking into account the measured comb spectrum and assuming flat phase is also plotted. We see excellent agreement, indicating high quality pulse compression to a bandwidth-limited pulse. The obtained pulse has an intensity autocorrelation full width at half maximum (FWHM) of ~2.8ps, which corresponds to an intensity FWHM of ~2.1ps assuming the sinc^2 intensity profile appropriate for the nearly flat-topped spectrum.

In summary, we have demonstrated a new, easily scalable scheme for generating very flat optical frequency combs using cascaded intensity and phase modulators driven by tailored RF waveforms. In this work we demonstrated a 10 GHz comb with 38 comb lines in a 1-dB bandwidth and around 60 comb lines in total. Another attractive aspect of

our scheme is the ability to achieve very high quality compression (in our experiments resulting in a ~2.1 ps bandwidth-limited pulse) simply through propagation in standard single-mode fiber.

4.2 Simple scheme for bandwidth scaling of frequency combs using cascaded four-wave mixing in high non-linear fiber

In schemes involving direct phase modulation for frequency comb generation like the one we discussed, there is still significant limitation with regard to bandwidth scalability. The number of spectral lines scales linearly with the RF voltage driving the phase modulator. The RF power handling of the modulators are limited and hence would require a cascade of phase modulators to generate more lines. For example, good, commercially available low Vpi phase modulators (~3V) usually have a RF power limit of ~1W which limits the number of lines to ~20 (which at 10GHz is a bandwidth of 200GHz) in a 3-dB bandwidth. However, to reach the 100 line level, we would have to cascade 5 modulators, which then needs 5 high power RF amplifiers etc which is prohibitive and inefficient.

There have been some methods to scale the bandwidth involving first compressing the comb to a short pulse and then spectral broadening in dispersion decreasing fiber or highly nonlinear fiber (HNLF) [8, 59, 66]. A version of this is utilized in section 2.6. However, the spectral flatness of such combs is poor and also owing to subtle interplay between dispersion and nonlinearity, the generated spectrum is not very stable. In this section, we will demonstrate a simple scheme which can scale the bandwidth of the comb by several times (5, 7, --) in a stable and known fashion while simultaneously enhancing spectral flatness. We will demonstrate this by generating a comb which requires just one phase modulator and can create over 100 lines within 10-dB out of which, a record 75 of them are in a 1-dB bandwidth. Furthermore, similar to our previous technique, this scheme allows for simple compression of the comb to a bandwidth limited pulse using just a quadratic dispersion media (like single mode fiber). In comparison to the previous method, we achieve this without utilizing the aberration correction which makes it simple and enhances the scalability to much higher repetition rates (like 40GHz and above) where having a X2 multiplier is significantly more difficult.

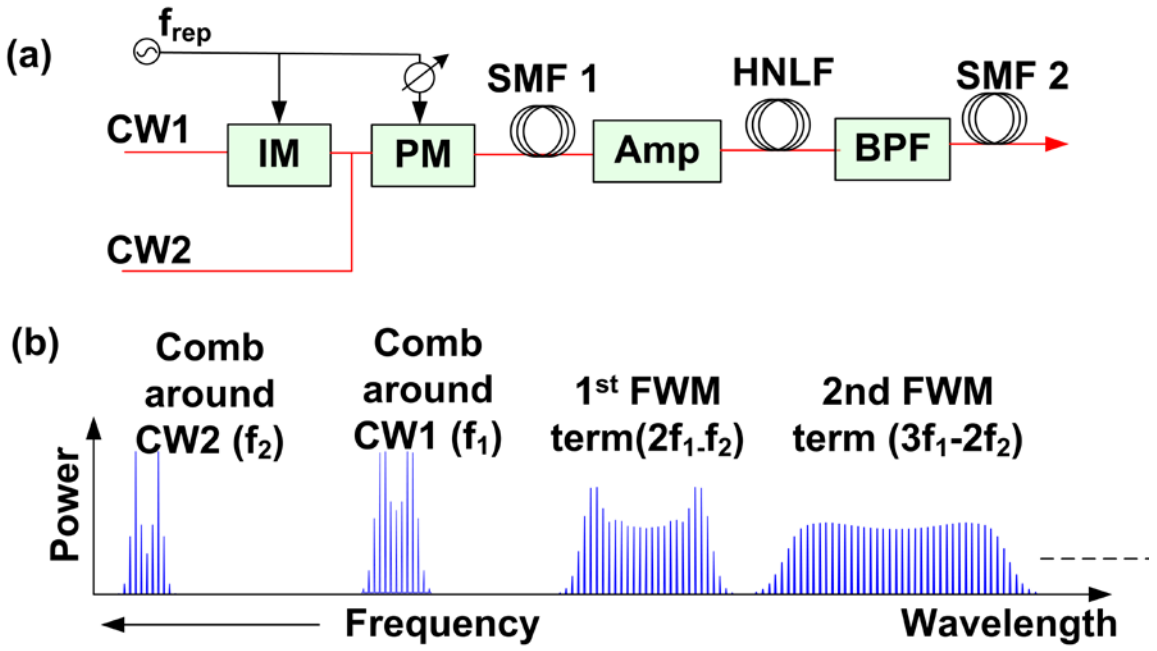

Fig. 4.4 (a) Experimental Setup, CW – continuous wave laser, IM – Intensity modulator, PM – phase modulator, SMF – single mode fiber, HNLF – Highly nonlinear fiber, Amp – High power amplifier, BPF – band pass filter, (b) Bandwidth scaling of the comb and enhanced spectral flattening

Fig. 4.4(a) shows the experimental setup. Like the previous scheme, a CW laser (CW 1) at frequency f_1 is driven using a cascade of intensity and phase modulators. If $a_1(t)$ (which is close to a flat-topped pulse) and $\phi(t)$ (which is a sinusoid) are the amplitude and phase modulation, the output after the IM and PM is $a_1(t)\exp(j\phi(t))$. We include a 2nd CW laser at frequency f_2 which is only phase modulated ($a_2(t)\exp(j\phi(t)) = \exp(j\phi(t))$). This is followed by a length of SMF whose length is chosen such that, it delays one frequency by half a period (i.e. 50ps for a 10GHz repetition period) relative to the other (i.e. $\exp(j\phi(t)) \rightarrow \exp(-j\phi(t))$). The reason for this is to ensure constructive bandwidth addition in the four wave mixing terms between the two frequencies. We assume that the frequency difference is much higher than the comb bandwidth created around each frequency. This is followed by a higher power amplifier followed by a near zero dispersion, low dispersion slope, highly nonlinear fiber (HNLF) and a band pass filter to select an appropriate frequency band. Assuming, a short length of HNLF with near zero dispersion and low loss, the propagation regime is pure self-phase modulation, which creates a cascade of four wave-mixing terms. Looking

towards the side of f_1, we will have new frequency components created at $2f_1 - f_2$, which would go as,

$$[a_1(t)\exp(j\phi(t))^2][\exp(-j\phi(t))^*] = a_1(t)^2\exp(3j\phi(t)) \quad (4.3)$$

We clearly see that the bandwidth has tripled in this case. The next term in the cascade of four wave mixing terms will occur at $3f_1 - 2f_2$, which would be dominated by the term corresponding to mixing between 1 photon of the first FWM term, one photon at f_1 and 1 photon at f_2, which goes as

$$[a_1(t)^2\exp(3j\phi(t))][a_1(t)\exp(j\phi(t))][\exp(-j\phi(t))^*] = a_1(t)^3\exp(5j\phi(t)) \quad (4.4)$$

This indicates a bandwidth scaling of five times. Similarly, if we look at the higher order terms, we will have bandwidths scaling as 7 times, 9 times and so on. However, the efficiency reduces owing to increasing phase mismatch for the nonlinear process. An interesting aspect is that, the amplitude coefficient of the above terms successively rises to higher powers and this creates a reduction of the duty cycle of the time domain waveform. As we discussed previously, this allows better time to frequency mapping and hence with proper choice of the IM drive conditions, flatter combs. Fig 4.4(b) is the cartoon showing the bandwidth scaling and increasing spectral flatness in this scheme. In this discussion above, our arguments have been more qualitative and doing so, we have largely neglected the effect of dispersion slope and other effects affecting the comb generation process. However, we have seen that these effects don't play a significant role in our experiment as confirmed by numerical simulations of the non-linear schrodinger equation. Fig 4.5 shows the numerical simulation assuming the dispersion is 0 at the wavelength position of CW1, dispersion slope, loss corresponding to specifications provided by the HNLF vendor and the power levels similar to what we used in our experiment. We see similar behavior to what we expected with our simple quantitative model above.

Another advantage of this method is that, since a better approximation to a quadratic temporal phase also creates a quadratic spectral phase, we can compress the comb using a just a calculated length of SMF (SMF 2 in fig 4.4(a)). This effect occurs naturally in this scheme without the need for phase correction of the sinusoid to better approximate a quadratic.

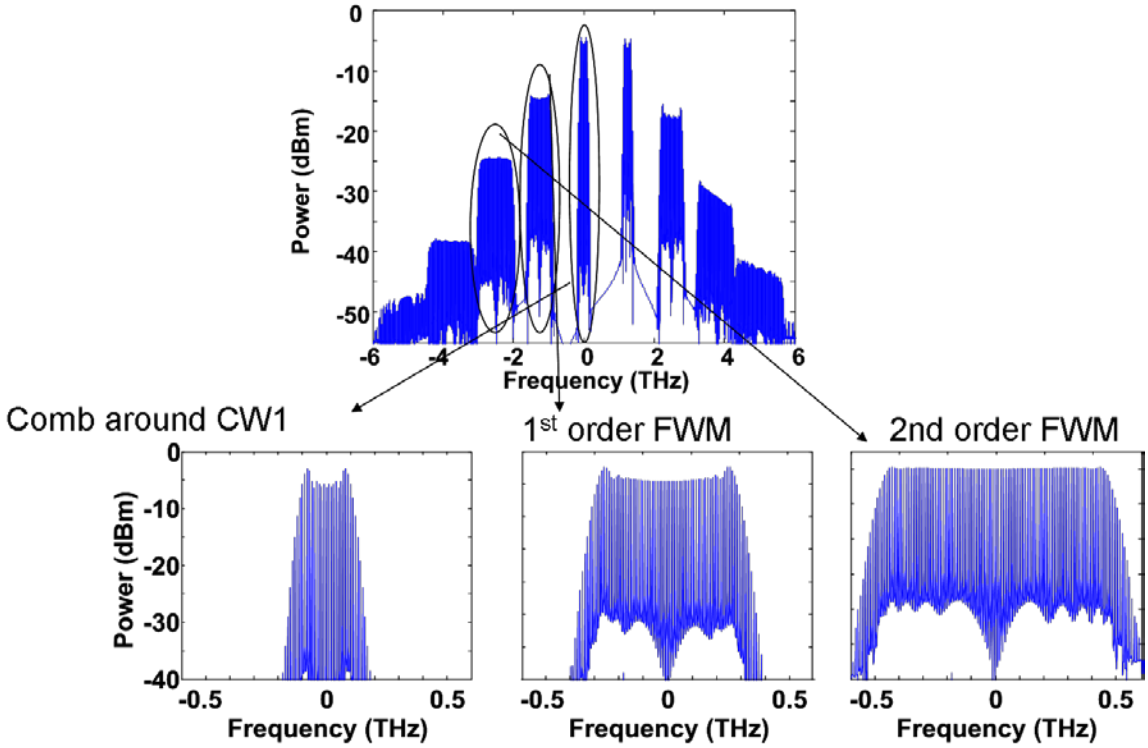

Fig. 4.5 Simulations incorporating the effect of dispersion slope, and loss of the HNLF demonstrating the bandwidth scaling and spectral flattening due to cascaded four-wave mixing

In our experiment, we choose the wavelength difference between the lasers such that there is no spectral overlap between the term we are interested in and its adjacent terms. Fig 4.6 demonstrates our experimental result where we look at the 2nd order FWM term. The initial lasers have ~100 KHz linewidth and are spaced ~10nm apart (1542 nm and 1532 nm). The initial comb generator provides < 20 lines in a 3-dB bandwidth with mediocre flatness (Fig. 4.6(a)). The RF oscillator has a 10GHz frequency and the first SMF spool is ~300m creating the 50ps delay. We use a high power optical amplifier with ~1.5W output power. The HNLF we use has a length of 100m, D = 0.66ps/nm/km and S = 0.02ps/nm^2/km. Fig 4.6(a) shows the comb around 1542nm with ~ 22 lines in a 10-dB

bandwidth. The comb around 1532 nm is of similar bandwidth but with further deteriorated flatness owing to pure phase modulation.

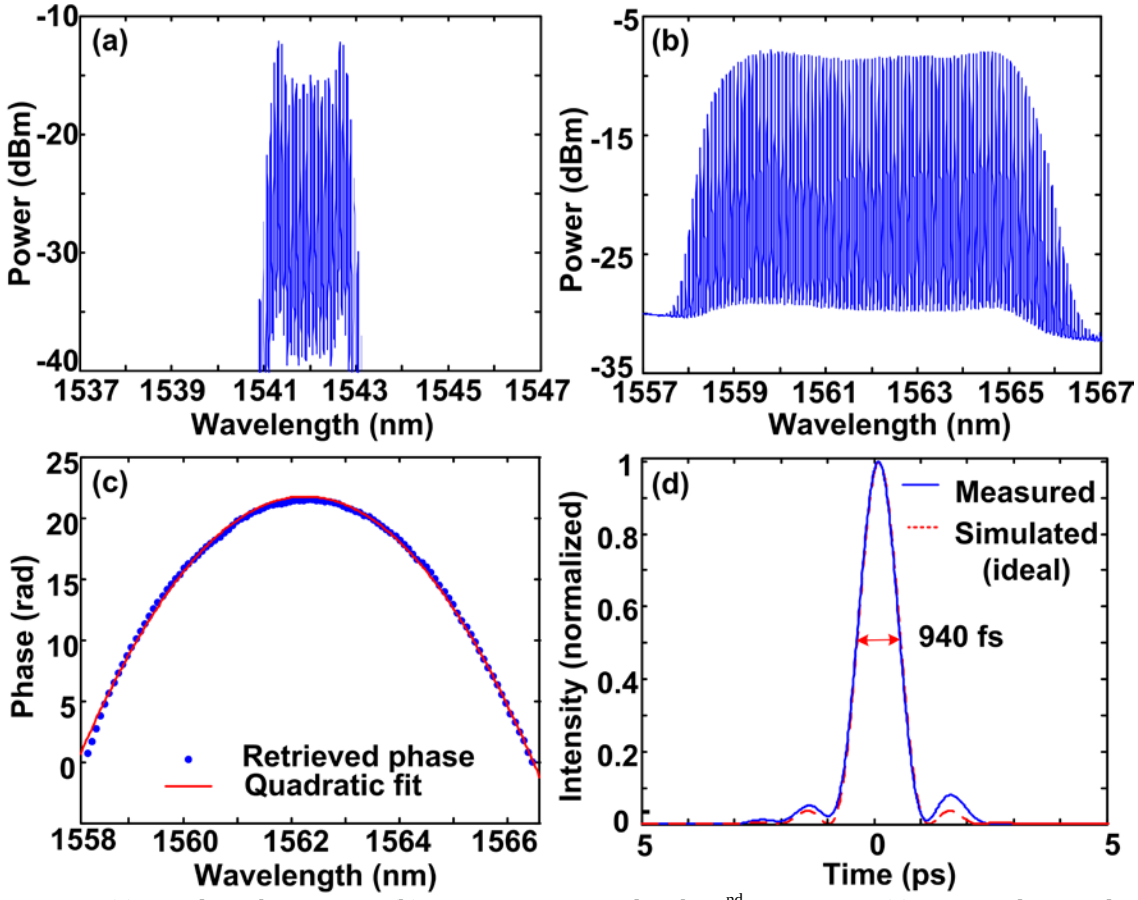

Fig. 4.6 (a) Initial comb spectrum, (b) Spectrum generated at the 2nd FWM term, (c) Measured spectral phase and a quadratic fit to it, (d) Measured time domain intensity with a simulation taking the spectrum and assuming flat spectral phase.

Fig 4.6(b) shows the 2nd FWM term centered on 1562 nm. We get around 20 mW of power in this region. We can clearly see the significant improvement in spectral flatness and scaling of bandwidth. The new comb has >100 lines in a 10-dB bandwidth with a record 75 of them within 1-dB. Fig 4.6(c) shows the measured spectral phase using our waveform measurement apparatus for frequency combs based on half-repetition rate modulation [30] and we see an excellent fit to a quadratic. We compensated this using ~200m of SMF and fig 4.6(d) shows the measured pulse intensity having a FWHM of ~940fs. It also matches very well with a simulated time domain intensity taking the spectrum into account and assuming flat spectral phase demonstrating good phase

correction. In this scheme, by increasing the repetition rate, the generated bandwidth can also be easily scaled (for example at 40GHz, the bandwidth should be four times as much and should be able to generate a < 250fs pulse).

In summary, we have demonstrated a simple scheme to significantly scale the bandwidth of phase modulated CW combs while enhancing spectral flatness. This scheme preserves all the previous advantages like easy tunability of optical center frequency and repetition rate. Furthermore, owing to having a nearly quadratic spectral phase this scheme allows for easy compression to a bandwidth limited pulse. In this work we demonstrated a 10GHz comb with >1THz of bandwidth (with >750 GHz in a 1-dB bandwidth) using just a single intensity and phase modulator. The generated comb was easily compressed to 940fs pulses. The work described in this chapter is detailed in the papers [67] and [68].

5. SUMMARY AND FUTURE WORK

Our work demonstrates new techniques and provides a tested recipe for an OAWG system. To this effect, we

- We proposed a new methodology using phase modulation of CW lasers, to generate high repetition rate frequency combs which are used as sources for OAWG applications. These combs are significantly flatter and generate pulses of high quality, both qualities highly desirable and prior to this work, not achieved in a direct fashion. Extending this work, we also provided a method to significantly scale the bandwidth of such combs by several times while keeping all the desirable attributes intact. The ability to achieve broad-bandwidths together with the convenience of these frequency comb sources also makes it a desirable source for several applications in optical communications and RF photonics.
- We proposed a new class of apparatii utilizing dual spectral dispersers to achieve line-by-line control of frequency combs in a programmable fashion. This scheme allowed for significant increase in addressable lines. In optical signal processing applications, this scheme allows for implementation of almost arbitrary linear filters directly in the optical domain. This capacity makes it an attractive option for a variety of tasks in optical systems and equipment.
- A key requirement for high repetition rate frequency comb sources and OAWG systems are characterization apparatii to measure the properties of the source or the waveform. Such apparatii also serve as decoders necessary for a complete system. Existing pulse measurement schemes are difficult to apply to such waveforms owing to their unique requirements. We proposed techniques to measure OAWG waveforms and also utilized their unique advantages for an application in fiber optics.

For future work, some immediate enhancements of each aspect would be –

- **Generation techniques –** To enhance the bandwidth of phase modulated frequency combs to very broad bandwidths to achieve the levels of Femtosecond modelocked lasers. This would make our source extremely useful not only for applications requiring high repetition rates where they are already being used but also for many other ultrafast applications which require a simple, tunable source for very short pulses.
- **Characterization techniques –** We demonstrated characterization results for frequency combs and OAWG waveforms both in the averaged regime (where they are shaped frequency combs) as well as in the single-shot regime. However, owing to the limitation in the update rate of the apparatus, in the single-shot regime, though the waveform is measured on a frame by frame basis, the measurement is not real time. This would be a limitation for practical applications as a decoder in communication and LIDAR applications. So a very useful addition would be to achieve not only single shot by real time measurement capabilities for THz bandwidth optical arbitrary waveforms.
- **Manipulation techniques –** Our demonstrations were limited by the sources available, while the apparatus itself can achieve shaping over much broader bandwidths. We anticipate practical difficulties scaling the bandwidth and hence demonstration of further enhancement in pulse shaping complexity would be a great addition to this work. Further more, as an apparatus which can achieve arbitrary linear filters in the optical domain, many applications can be imagined. Here is one example -

Spectroscopic gas sensing with spectrally matched waveforms generated using the 2D pulse shaper

Spectroscopic sensing provides an excellent method for fast and accurate determination of trace amounts of gases which is useful for a variety of environmental and industrial applications. Here, the frequency resolved absorption signal of a broadband light source by a sample is analyzed to look for features characteristic of different

gaseous species. Also, the strength of the absorptions can be used to evaluate the concentrations. Fig 5.1 shows a representative absorption spectrum for a gaseous mixture of Ammonia, Acetylene and Carbon monoxide (from [69]).

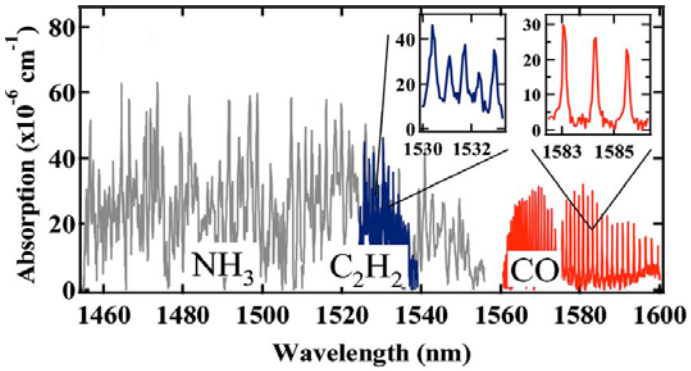

Fig 5.1 A representative absorption spectrum for a gaseous mixture of Ammonia, Acetylene and Carbon monoxide (from [69]).

However, as the gas concentrations become smaller and the gases become more numerous, a few problems arise. Firstly, the spectrometer used to frequency resolve the signal needs to have very high sensitivity to measure small absorptions and secondly, with increasing number of gaseous components, the decision making to identify components and relative concentrations of each becomes a difficult task. To increase the sensitivity, there has been recent work on utilizing an enhancement cavity to significantly increase the absorption features [70]. However there still remains the effect of identifying different gaseous components from a mixture absorption spectrum.

We can look at this problem in a different way. Instead of looking for all the gases in the sample, another way is to ask whether any particular gas is present in the sample and if it is, by what amount. If such a measurement can be done, then these measurements can be done in series for an arbitrarily long list of gases as required. This is related to the well known spectroscopic technique called optical correlation spectroscopy [71]. Here, simultaneously a broadband light source is sent through one cell with an unknown gas sample and through another cell with a known concentration of a gas that needs to be detected. By looking at the correlations between the two outputs, presence or absence and concentration of the gas that is being checked can be determined. This technique though still requires a spectrometer and is also quite cumbersome since the measurement has to be repeated several times for each gas component that needs to be measured.

There is however another method of checking for individual gases. Instead of illuminating the gas sample with the entire broadband source, we can just send a source whose spectrum is tailored to match with absorption features of a particular gas. The output can now be looked at through a simple point detector. The relative change in measured output would allow us to make decisions on existence of the particular gas in the sample and if it is, then the concentration. Effectively, it is enhancing spectroscopic response by utilizing shaped waveforms matched only to the gas that needs to be characterized. The 2D pulse shaper which has fine spectral resolution with large operating bandwidth provides us an excellent system to create such waveforms. The spectral resolution can be sub GHz in the 2D shaper which is sufficient since the Doppler limited line width for gases is usually of that scale and any higher resolution than that is not useful. Used in a programmable fashion with a 2D spatial light modulator, different patterns corresponding to different gases can be loaded onto the SLM from memory and simple power measurements can be done to look for different gaseous samples. A schematic of this is shown in fig 5.2.

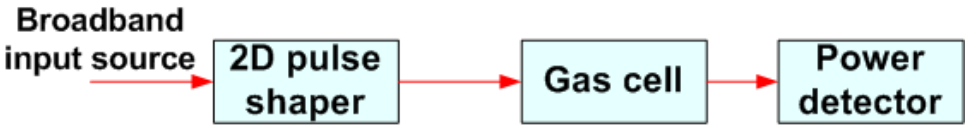

Fig 5.2 A spectroscopic gas sensing system with spectrally matched waveform generation

The different patterns corresponding to absorption characteristics of different gases can be generated using published data on their absorption characteristics [72]. Another advantage in this technique is that, point detectors are significantly less sensitive and easier to use to sensor arrays used in spectrometers thus further reducing implementation complexities.

LIST OF REFERENCES

LIST OF REFERENCES

[1] D. J. Jones, S. A. Diddams, J. K. Ranka, A. Stentz, R. S. Windeler, J. L. Hall, S. T.Cundiff, “Carrier-envelope phase control of femtosecond mode-locked lasers and direct optical frequency synthesis,” Science, vol. 288, pp. 635-639, April 2000.

[2] T. Udem, R. Holzwarth, T. W. Hansch, “Optical frequency metrology,” Nature, vol.416, pp. 233-237, March 2002.

[3] A. M. Weiner. “Femtosecond pulse shaping using spatial light modulators,” Rev. Sci. Instr. 71, 1929–1960 (2000).

[4] Z. Jiang, C.-B. Huang, D. E. Leaird and A. M. Weiner. “Optical Arbitrary Waveform Processing of More than 100 Spectral Comb Lines,” Nature Photonics 1, 463-467 (2007).

[5] Kourogi, M.; Nakagawa, K.; Ohtsu, M., "Wide-span optical frequency comb generator for accurate optical frequency difference measurement," Quantum Electronics, IEEE Journal of , vol.29, no.10, pp.2693-2701, Oct 1993.

[6] H. Murata, A. Morimoto, T. Kobayashi, and S. Yamamoto, “Optical pulse generation by electroopticmodulation method and its application to integrated ultrashort pulse generators,” IEEE J. Sel. Top. QuantumElectron. 6, 1325-1331 (2000).

[7] P. Del’Haye, A. Schliesser, O. Arcizet, T. Wilken, R. Holzwarth and T. J. Kippenberg, "Optical frequency comb generation from a monolithic microresonator," Nature 450, 1214-1217 (2007).

[8] C.-B. Huang, S.-G. Park, D.E. Leaird, and A.M. Weiner, "Nonlinearly broadened phase-modulated continuous-wave laser frequency combs characterized using DPSK decoding," Opt. Express 16, 2520-2527 (2008).

[9] J. A. Salehi, A. M. Weiner, and J. P. Heritage, "Coherent ultrashort light pulse code-division multiple access communication systems," J. Lightwave Technol., vol. 8, pp. 478-491, 1990.

[10] Z. Jiang, D. S. Seo, S. D. Yang, D. E. Leaird, R. V. Roussev, C. Langrock, M. M. Fejer and A. M. Weiner, "Four user 10 Gb/s spectrally phase-coded O-CDMA

system operating at \sim 30 fj/bit", IEEE Photon. Technol. Lett., vol. 17, no. 3, pp. 705-707, Mar. 2005.

[11] M. Shirasaki. “Large angular dispersion by a virtually imaged phased array and it’s application to a wavelength division multiplexer,” Opt. Letters. 21, 366–368, (1996).

[12] G-H. Lee, S. Xiao and A. M. Weiner. “Optical Dispersion Compensator with >4000 ps/nm Tuning Range Using a Virtually Imaged Phase Array (VIPA) and Spatial Light Modulator,” IEEE Phot. Tech. Lett, 18, 1819-1821 (2006).

[13] V. R. Supradeepa, Chen-Bin Huang, Daniel E. Leaird, and Andrew M. Weiner, "Femtosecond pulse shaping in two dimensions: Towards higher complexity optical waveforms," Opt. Express **16**, 11878-11887 (2008).

[14] V. R. Supradeepa, D. E. Leaird, and A. M. Weiner, "Programmable High Resolution Broadband Pulse Shaping Using a 2-D VIPA-Grating Pulse Shaper with a Liquid Crystal on Silicon (LCOS) Spatial Light Modulator," in International Conference on Ultrafast Phenomena, OSA Technical Digest (CD) (Optical Society of America, 2010), paper TuF3.

[15] Takahashi, H.; Suzuki, S.; Kato, K.; Nishi, I., "Arrayed-waveguide grating for wavelength division multi/demultiplexer with nanometre resolution," Electronics Letters , vol.26, no.2, pp.87-88, (1990).

[16] Hill, K.O.; Meltz, G., "Fiber Bragg grating technology fundamentals and overview," Lightwave Technology, Journal of, vol.15, no.8, pp.1263-1276, (1997).

[17] S. Xiao and A. M. Weiner. “2-D wavelength demultiplexer with potential for >= 1000 channels in the C-band,” Optics Express 12, 2895-2902, (2004).

[18] S. X. Wang, S. Xiao and A. M. Weiner. “Broadband, High Spectral Resolution 2-D Wavelength-Parallel Polarimeter for Dense WDM Systems,” Optics Express 13, 9374-9380 (2005).

[19] S. A. Diddams, L. Hollberg, and V. Mbele. “Molecular fingerprinting with the resolved modes of a femtosecond laser frequency comb,” Nature 445, 627-630 (2007).

[20] O. E. Martinez, J. P. Gordon, and R. L. Fork, "Negative group-velocity dispersion using refraction," J. Opt. Soc. Am. A 1, 1003- (1984).

[21] A. M. Weiner. “Ultrafast Optics,” Wiley Publishing, ISBN: 9780471415398 (2009).

[22] Ghang-Ho Lee and Andrew M. Weiner, "Programmable Optical Pulse Burst Manipulation Using a Virtually Imaged Phased Array (VIPA) Based Fourier Transform Pulse Shaper," J. Lightwave Technol. **23**, 3916- (2005)

[23] K. Goda, K. K. Tsia, and B. Jalali, “Serial time-encoded amplified imaging for real-time observation of fast dynamic phenomena,” Nature 458, 1145 (2009).

[24] A. Lohmann and D. P. Paris. “Binary Fraunhofer holograms, generated by computer,” Appl. Opt. 6, 1739 (1967).

[25] http://www.holoeye.com/phase_only_modulator_heo1080p.html.

[26] E. Frumker and Y. Silberberg, "Femtosecond pulse shaping using a two-dimensional liquid-crystal spatial light modulator," Opt. Letters. 32, 1384 (2007).

[27] V. R. Supradeepa, Daniel E. Leaird, and Andrew M. Weiner, "Optical arbitrary waveform characterization via dual-quadrature spectral interferometry," Opt. Express **17**, 25-33 (2009)

[28] V. R. Supradeepa, C. M. Long, D. E. Leaird, and A. M. Weiner, “Fast Characterization of Dispersion and Dispersion Slope of Optical Fiber Links Using Spectral Interferometry With Frequency Combs,” IEEE Photon. Technol. Lett. 22(3), 155–157 (2010)

[29] V. R. Supradeepa, Daniel E. Leaird, and Andrew M. Weiner, "Single shot amplitude and phase characterization of optical arbitrary waveforms," Opt. Express 17, 14434-14443 (2009)

[30] V. R. Supradeepa, Christopher M. Long, Daniel E. Leaird, and Andrew M. Weiner, "Self-referenced characterization of optical frequency combs and arbitrary waveforms using a simple, linear, zero-delay implementation of spectral shearing interferometry," Opt. Express 18, 18171-18179 (2010)

[31] D. J. Kane; R. Trebino, "Characterization of arbitrary femtosecond pulses using frequency-resolved optical gating," IEEE J. Quantum Electron. 29, 571-579 (1993).

[32] P. O’Shea, M. Kimmel, X. Gu, and R. Trebino, "Highly simplified device for ultrashort-pulse measurement," Opt. Lett. 26, 932-934 (2001).

[33] C. Iaconis and I. A. Walmsley, "Spectral phase interferometry for direct electric-field reconstruction of ultrashort optical pulses," Opt. Lett. 23, 792-794 (1998).

[34] L. Lepetit, G. Cheriaux, and M. Joffre, "Linear techniques of phase measurement by femtosecond spectral interferometry for applications in spectroscopy," J. Opt. Soc. Am. B 12, 2467- (1995).

[35] E. Frumker, E. Tal, Y. Silberberg, and D. Majer, "Femtosecond pulse-shape modulation at nanosecond rates," Opt. Lett. 30, 2796-2798 (2005).

[36] J. T. Willits, A. M. Weiner, and S. T. Cundiff, "Theory of rapid-update line-by-line pulse shaping," Opt. Express 16, 315-327 (2008).

[37] Z. Jiang, D. E. Leaird, and A. M. Weiner, "Optical Arbitrary Waveform Generation and Characterization Using Spectral Line-by-Line Control," J. Lightwave Technol. 24, 2487- (2006).

[38] R. P. Scott, N. K. Fontaine, J. Cao, K. Okamoto, B. H. Kolner, J. P. Heritage, and S. J. B. Yoo, "High-fidelity line-by-line optical waveform generation and complete characterization using FROG," Opt. Express 15, 9977-9988 (2007).

[39] R. Trebino, “Frequency resolved optical gating: The measurement of ultrashort optical pulses,” Springer publications (2002).

[40] F.K. Fatemi, T.F. Carruthers, J.W. Lou, "Characterisation of telecommunications pulse trains by Fourier-transform and dual-quadrature spectral interferometry," Electron. Lett. 39, 921-922 (2003).

[41] A.D. Ellis; F.C.G. Gunning, "Spectral density enhancement using coherent WDM," Photonics Technology Letters, IEEE, vol.17, no.2, pp.504-506, Feb. 2005.

[42] Gunning, F.C.G.; Healy, T.; Ellis, A.D., "Dispersion tolerance of coherent WDM," Photonics Technology Letters, IEEE, vol.18, no.12, pp.1338-1340, June 2006.

[43] G. Li, "Recent advances in coherent optical communication," Adv. Opt. Photon. 1, 279-307 (2009).

[44] S. M. Foreman, K. W. Holman, D. D. Hudson, D. J. Jones, and J. Ye, “Remote transfer of ultrastable frequency references via fiber networks,” Rev. Sci. Instrum. 78, 021101 (2007).

[45] F. Narbonneau, M. Lours, S. Bize, A. Clairon, G. Santarelli, O. Lopez, Ch. Daussy, A. Amy-Klein, and Ch. Chardonnet, “High resolution frequency standard dissemination via optical fiber metropolitan network,” Rev. Sci. Instrum. 77, 064701 (2006).

[46] J. Kim, J. A. Cox, J. Chen, and F. X. Kärtner, “Drift-free femtosecond timing synchronization of remote optical and microwave sources,” Nature Photonics 2, 733-736 (2008).

[47] L. Cohen, "Comparison of single-mode fiber dispersion measurement techniques," Lightwave Technology, Journal of , vol.3, no.5, pp. 958-966, Oct 1985.

[48] J. Y. Lee and D. Y. Kim, "Versatile chromatic dispersion measurement of a single mode fiber using spectral white light interferometry," Opt. Express 14, 11608-11615 (2006).

[49] Jean Debeau, Benoît Kowalski, and Rémi Boittin, "Simple method for the complete characterization of an optical pulse," Opt. Lett. 23, 1784-1786 (1998).

[50] Ian A. Walmsley and Christophe Dorrer, "Characterization of ultrashort electromagnetic pulses," Adv. Opt. Photon. 1, 308-437 (2009).

[51] Christophe Dorrer and Inuk Kang, "Highly sensitive direct characterization of femtosecond pulses by electro-optic spectral shearing interferometry," Opt. Lett. 28, 477-479 (2003).

[52] Z. Jiang, D. E. Leaird, C.-B. Huang, H. Miao, M. Kourogi, K. Imai, A. M. Weiner, “Spectral line-by-line pulse shaping on an optical frequency comb generator,” IEEE J. Quantum Electron., vol. 43, no. 12, pp. 1163-1174, Dec. 2007.

[53] Takuya Ohara, Hidehiko Takara, Takashi Yamamoto, Hiroji Masuda, Toshio Morioka, Makoto Abe, and Hiroshi Takahashi, "Over-1000-Channel Ultradense WDM Transmission With Supercontinuum Multicarrier Source," J. Lightwave Technol. 24, 2311- (2006).

[54] J. Capmany and D. Novak, "Microwave photonics combines two worlds," Nat. Photonics 1, 319-330 (2007).

[55] Ehsan Hamidi, Daniel E. Leaird, and Andrew M. Weiner, “Tunable Programmable Microwave Photonic Filters based on an Optical Frequency Comb,” IEEE Transactions on Microwave Theory and Techniques, special issue on Microwave Photonics, Vol. 58, No. 11, pp. 3269-3278, November 2010.

[56] Masamichi Fujiwara, Mitsuhiro Teshima, Jun-ichi Kani, Hiro Suzuki, Noboru Takachio, and Katsumi Iwatsuki, "Optical Carrier Supply Module Using Flattened Optical Multicarrier Generation Based On Sinusoidal Amplitude and Phase Hybrid Modulation," J. Lightwave Technol. 21, 2705- (2003).

[57] Takashi Yamamoto, Tetsuro Komukai, Kazunori Suzuki, and Atsushi Takada, "Multicarrier Light Source With Flattened Spectrum Using Phase Modulators and Dispersion Medium," J. Lightwave Technol. 27, 4297-4305 (2009).

[58] Isao Morohashi, Takahide Sakamoto, Hideyuki Sotobayashi, Tetsuya Kawanishi, Iwao Hosako, and Masahiro Tsuchiya, "Widely repetition-tunable 200 fs pulse source using a Mach–Zehnder-modulator-based flat comb generator and dispersion-flattened dispersion-decreasing fiber," Opt. Lett. 33, 1192-1194 (2008).

[59] R. P. Scott, N. K. Fontaine, J. P. Heritage, B. H. Kolner, and S. J. B. Yoo, " 3.5-THz Wide, 175 Mode Optical Comb Source," in Optical Fiber Communication Conference and Exposition and The National Fiber Optic Engineers Conference, OSA Technical Digest Series (CD) (Optical Society of America, 2007), paper OWJ3.

[60] S. Ozharar, F. Quinlan, I. Ozdur, S. Gee, and P. J. Delfyett, “Ultrafast Optical Comb Generation by Phase-Only Modulation of Continuous-Wave Light,” Photonics Technology Letters, vol. 20, no. 1, pp. 36-38, (2008).

[61] Víctor Torres-Company, Jesús Lancis, and Pedro Andrés, "Lossless equalization of frequency combs," Opt. Lett. 33, 1822-1824 (2008).

[62] Brian H. Kolner and Moshe Nazarathy, "Temporal imaging with a time lens," Opt. Lett. 14, 630-632 (1989).

[63] M. T. Kauffman, W. C. Banyai, A. A. Godil, and D. M. Bloom, "Time-to-frequency converter for measuring picosecond optical pulses," Appl. Phys. Lett. 64,270-272 (1994).

[64] C.-B. Huang, Z. Jiang, D. E. Leaird, and A. M. Weiner, "High-Rate Femtosecond Pulse Generation via Line-by-Line Processing of a Phase-Modulated CW Laser Frequency Comb," Electron. Lett. 42, 1114-1115 (2006).

[65] James van Howe, Jonas Hansryd, and Chris Xu, "Multiwavelength pulse generator using time-lens compression," Opt. Lett. 29, 1470-1472 (2004)

[66] K. R. Tamura, H. Kubota, and M. Nakazawa, "Fundamentals of stable continuum generation at high repetition rate," IEEE J. Quantum Electron. , vol. 36, 773-779, 2000.

[67] Rui Wu, V. R. Supradeepa, Christopher M. Long, Daniel E. Leaird, and Andrew M. Weiner, "Generation of very flat optical frequency combs from continuous-wave lasers using cascaded intensity and phase modulators driven by tailored radio frequency waveforms," Opt. Lett. 35, 3234-3236 (2010)

[68] V. R. Supradeepa, Andrew M. Weiner, “A Broadband, Spectrally Flat, High Rep-rate Frequency Comb: Bandwidth Scaling and Flatness Enhancement of Phase Modulated CW through Cascaded Four-Wave Mixing”, arXiv:1010:2527, (2010)

[69] Michael J. Thorpe, Darren D. Hudson, Kevin D. Moll, Jacob Lasri, and Jun Ye, "Cavity-ringdown molecular spectroscopy based on an optical frequency comb at 1.45-1.65 μm," Opt. Lett. **32**, 307-309 (2007)

[70] Michael J. Thorpe, David Balslev-Clausen, Matthew S. Kirchner, and Jun Ye, "Cavity-enhanced optical frequency comb spectroscopy: application to human breath analysis," Opt. Express **16**, 2387-2397 (2008)

[71] J. Dakin, M. Gunning, P. Chambers, and Z. Xin, “Detection of gases by correlation spectroscopy,” Sens. Actuators B 90, 124-131 (2003).

[72] L. S. Rothman, et al., "The HITRAN 2004 molecular spectroscopic database," J. Quant. Spectrosc. Radiat. Transfer 96, 139-204 (2005).

[73] Shijun Xiao; Weiner, A.M.; Lin, C., "A dispersion law for virtually imaged phased-array spectral dispersers based on paraxial wave theory," IEEE Journal of Quantum Electronics 40, no.4, 420-426 (2004).

[74] “Wolfram Alpha”, http://www.wolframalpha.com

[75] V. R. Supradeepa, Ehsan Hamidi, Daniel E. Leaird, and Andrew M. Weiner, "New aspects of temporal dispersion in high-resolution Fourier pulse shaping: a quantitative description with virtually imaged phased array pulse shapers," J. Opt. Soc. Am. B 27, 1833-1844 (2010)

APPENDICES

A. QUANTITATIVE ANALYSIS OF TEMPORAL DISPERSION PROPERTIES OF VIPA BASED PULSE SHAPERS

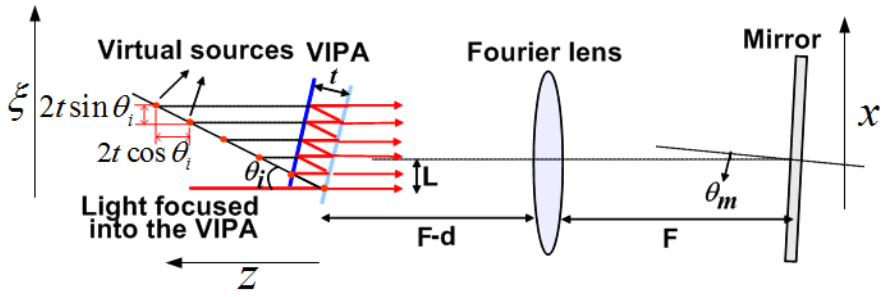

Fig. A.1 A general configuration of a VIPA pulse shaper.

In this section we will calculate the additional dispersion effects in VIPA based pulse shapers and characterize the new zero dispersion condition. The analysis in this section is built on the framework introduced in [73] to analyze demultiplexing properties of the VIPA. Fig. A1 shows a general configuration of a VIPA pulse shaper. We will use ξ and z to represent the transverse and longitudinal position coordinates in the object plane and x to represent the transverse coordinate in the Fourier plane. An air spaced VIPA with a thickness t is considered and an input Gaussian beam is coupled into the VIPA at an angle of θ_i. The front side of the VIPA has ~100% reflectivity while the back side is partially reflecting (between 0.95-0.98). Multiple reflections occur inside the VIPA etalon and due to partial reflecting nature of the back surface, at every reflection a fraction of the beam escapes as shown in the figure. This phenomenon is best modeled by using virtual sources having Gaussian profiles to represent the successive beams, having a longitudinal separation and vertical separation of

$$\Delta z = 2t\cos\theta_i \tag{A1}$$

$$\Delta\xi = 2t\sin\theta_i \tag{A2}$$

between successive sources. We will allow the VIPA – lens distance to be different from the focal length and let this change be d. Let us assume that the first virtual source is

offset from the optic axis by L and the mirror is tilt at an angle given by θ_m . The distance between the mirror and the Fourier lens is maintained at F since this ensures minimum loss and also the best spectral resolution in case of pulse shapers.

Assuming that the power loss from the top end of the etalon is negligible, we can model the field on the Fourier plane as a superposition of contributions from an infinite number of virtual sources whose profiles go as

$$E_n(\xi) = (R)^n E_0 \exp(-\frac{(\xi - \Delta\xi_n + L)^2}{w_0^{\,2}}) \tag{A3}$$

Where, R is the effective reflection coefficient per bounce inside the VIPA (around 0.95 – 0.98), $\Delta\xi_n$ is the vertical position of the nth virtual source given by

$$\Delta\xi_n = n * 2t \sin\theta_i \tag{A4}$$

L is the vertical offset and w_0 is the focused beam size at the back surface of the VIPA for the input beam. The field on the Fourier plane can be written as [73]

$$\begin{aligned} E_{out}(x,k) \propto \sum_{n=0}^{\infty} \exp(-ik(\Delta z_n - d)) \exp(ik\frac{(\Delta z_n - d)}{2F^2}x^2) \\ \times \int_{-\infty}^{\infty} E_n(\xi) \exp(\frac{ikx\xi}{F}) d\xi \end{aligned} \tag{A5}$$

Where k = $2\pi/\lambda$ and d is the distance by which the VIPA lens distance is of focus (d > 0 indicates that the lens to VIPA distance is closer than the focal length of the lens (F)). Δz_n is the horizontal position of the nth virtual source given by

$$\Delta z_n = n * 2t \cos\theta_i \tag{A6}$$

Substituting eqn (A3) in eqn (A5) and making the transformation $\xi' = \xi + L$, eqn (A5) can be written as

$$E_{out}(x,k) \propto \exp(ikd)\exp(\frac{-ikL}{F}x)\exp(\frac{-ikd}{2F^2}x^2)\sum_{n=0}^{\infty}\exp(-ik\Delta z_n)\exp(\frac{ik\Delta z_n}{2F^2}x^2) \times \int_{-\infty}^{\infty}(R)^n E_0 \exp(-\frac{(\xi'-\Delta\xi_n)^2}{w_0^2})\exp(\frac{ikx\xi'}{F})d\xi' \quad \text{(A7)}$$

We would like to look at the above equation as being constituted of two relevant terms. The expression inside the summation corresponds to the demultiplexing property of the VIPA with the L=0, d=0 condition as discussed in [73]. However the introduction of the new parameters has introduced certain extra spatial phase terms, a linear phase term corresponding to L and as expected a quadratic phase term corresponding to d. Now in order to obtain the introduced spectral phases we will go through the following scheme. The demultiplexer part of the equation (included in the summation) gives us the wavelength to space mapping in the Fourier plane and using this mapping we will evaluate the spectral phases corresponding to the additional spatial phases.

From using the simplification for the demultiplexer part [73], we have the expression as –

$$E_{out}(x,k) \propto \exp(ikd)\exp(\frac{-ikL}{F}x)\exp(\frac{-ikd}{2F^2}x^2) \exp(\frac{-x^2}{w'^2})\left(\frac{1}{1-\mathrm{R}\,exp(-ik(2t\cos\theta_i - 2t\sin\theta_i\frac{x}{F} - t\cos\theta_i\frac{x^2}{F^2}))}\right) \quad \text{(A8)}$$

Where w' is an effective width of the intensity envelope on the Fourier plane. This depends on the input beam size and the focal lengths of other lenses used in the system. More details on this can be obtained in [73].

From eqn (8) we have the additional spatial phase terms as

$$\exp(-ikL\frac{x}{F})\exp(-ikd\frac{x^2}{2F^2}) \quad \text{(A9)}$$

Here we have neglected the constant phase term since it does not contribute to any

observable phenomenon.

From the VIPA demultiplexer part, we see that the equation for the VIPA demultiplexer becomes-

$$k(2t\cos\theta_i - 2t\sin\theta_i \frac{x}{F} - t\cos\theta_i \frac{x^2}{F^2}) = 2m\pi \quad \text{(A10)}$$

$$\text{i.e.} \quad 2t\cos\theta_i - 2t\sin\theta_i \frac{x}{F} - t\cos\theta_i \frac{x^2}{F^2} = m\lambda \quad \text{(A11)}$$

λ is the wavelength and m is the order of diffraction. We clearly see the nonlinear relation connecting the position and wavelength. It is necessary here to mention on how the diffraction order m is obtained. From eqn (A8) we see that the nature of spectral dispersion by the VIPA causes the intensity profile on the Fourier plane to be a Gaussian centered around x=0. So, for a given frequency the diffraction order which disperses it near x=0 will have the most intensity. This is schematically shown in fig A2.

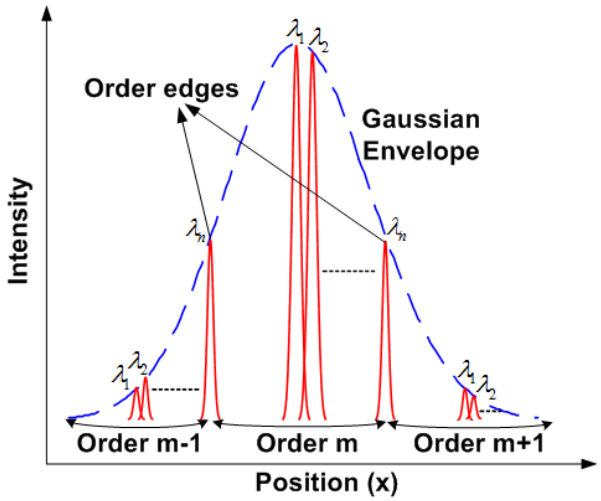

Fig A.2 – Schematic of diffraction by a VIPA seen on the Fourier plane

For a given wavelength λ, we have from eqn (A11) that the diffraction order given by $m = \{2t\cos\theta_i / \lambda\}$ ({} representing closest integer) causes it to disperse around $x = 0$ (obtained by substituting x=0 in the equation) and hence has the highest intensity. Given a wavelength, we will refer to the order which has the highest intensity as the main order

and let us also denote the center wavelength of each order as $\lambda_m = 2t\cos\theta_i / m$ (which would fall on x=0). For a center wavelength which is an FSR higher or lower (i.e. $\lambda_{m\pm1} = \lambda_m \pm \Delta\lambda$, where $\Delta\lambda$ is the FSR) will also correspond to x=0 and the main order in this case will be $m\pm1$ and so on.

Since a linear spatial phase term also leads to higher order spectral phases, the issue now is why don't we just work at L=0 and avoid the additional term in the first place. To explain why we need L>0 we have pictorially represented the three possible cases in fig(A3). For the power to couple back into the VIPA it is necessary to have overlap between the VIPA and the reflected virtual sources. The optical system inverts the vertical position of the sources and because of this the overlap is only possible when L>0. Fig A3(A) and A3(B) shows the cases for L=0 and L< 0 and we see no overlap while for L>0 there is overlap. Depending on the parameters like the input angle, VIPA design parameters etc there is an optimal L necessary to maximize the overlap. Though we discussed this using a reflective configuration, this effect is independent of the geometry being reflective (with a mirror) or transmissive (with another lens and spectral disperser). In any configuration of the VIPA pulse shaper, w.r.t the VIPA, the first virtual source on the output side cannot be at the same position as the first virtual source on the input side and hence a linear spatial phase is always present. However the coefficients of the phase might change relative to the geometry being used.

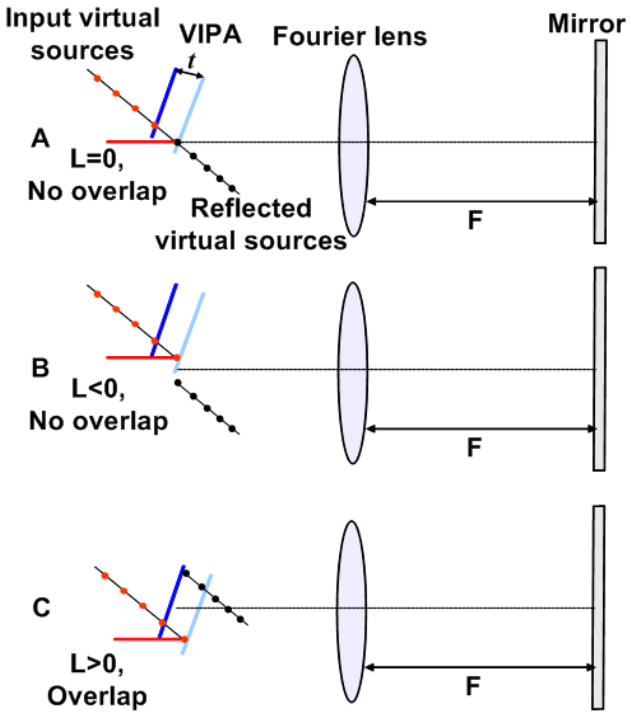

Fig. A.3 Figure showing overlap conditions between input and reflected sources for varying L. (A) L=0, no overlap, (B) L<0, No overlap, (C) L>0, overlap.

Eqn(A8) which gives the spatial phases is still incomplete. We need to incorporate two more factors. 1) A pulse shaper is a dual pass system and by reciprocity, the magnitudes of the phases need to be doubled. 2) In eqn (A8) only the parameters L and d are present and we still haven't incorporated the mirror angle θ_m. To do this let us look at the physical effect of a mirror with a small tilt. What the mirror does is tilt the wavefront by an angle twice the mirror angle causing an additional linear spatial phase given by

$$\exp(-ik\tan 2\theta_m) \tag{A12}$$

and so θ_m has a similar effect as L. Conversely this can also be looked at as effectively causing a vertical offset of the reflected virtual sources by an amount $F\tan 2\theta_m$ (comparing the linear term of eqn(A9) with eqn(A12)). Also for the case of the mirror we don't need to multiply it by 2 since it is only in the return path. A way of visualizing this is, for L>0 and θ_m = 0, the distance between the incident and reflected

first virtual source is 2L, but for L=0, $\theta_m \neq 0$ it will only be $F \tan 2\theta_m$ and not twice that. A rigorous derivation of this can be obtained by looking at the expressions for the wave fronts but the essential idea is as we described above. Including these effects, the expression for the spatial phase becomes

$$\exp(-ik(2L + F\tan 2\theta_m)\frac{x}{F})\exp(-ikd\frac{x^2}{F^2}) \tag{A13}$$

To obtain the expressions for spectral phases, first let us solve the for eqn(A11) in terms of λ and then substitute this in eqn (A13). The solution for eqn (A11) is –

$$\frac{x}{F} = \frac{-2t\sin\theta_i + 2t\sin\theta_i\sqrt{1-\frac{\cos\theta_i(m(\lambda-\lambda_m))}{t\sin^2\theta_i}}}{2t\cos\theta_i} \tag{A14}$$

Where $\lambda_m = 2t\cos\theta_i / m$ is the center wavelength for order m and we have chosen the solution closer to x=0, which as we discussed before is the relevant solution due to the intensity envelope. For a given order m, the maximum excursion for the term $(\lambda - \lambda_m)$ is $\Delta\lambda/2$ where $\Delta\lambda$ is the FSR. So we have,

$$\frac{\cos\theta_i(m(\lambda-\lambda_m))}{t\sin^2\theta_i} < \frac{\cos\theta_i(m\Delta\lambda)}{2t\sin^2\theta_i} \sim \frac{\lambda\cos\theta_i}{2t\sin^2\theta_i} \tag{A15}$$

Where we have used $m \sim 2t\cos\theta_i/\lambda$. For the space of operating parameters in our experiment, which is $\theta_i \sim$ 4degrees and t=0.75mm, we have

$$\frac{\cos\theta_i(m(\lambda-\lambda_m))}{t\sin^2\theta_i} < \frac{\lambda\cos\theta_i}{2t\sin^2\theta_i} \sim 0.2 \tag{A16}$$

Since this is reasonably smaller than 1 in our case and also for a reasonable space of

operating parameter space, we will expand the expression inside the square root sign using the binomial expansion rule $\sqrt{1-\alpha} = 1 - \alpha/2 - \alpha^2/8 - \alpha^3/16 - 5\alpha^4/128....$ [74] up to the 4th order term, since by the 5th order term its negligibly small and this gives us-

$$\frac{x}{F} \sim \frac{1}{2t\sin\theta_i} m(\lambda-\lambda_m) + \frac{\cos\theta_i}{8t^2\sin^3\theta_i} m^2(\lambda-\lambda_m)^2 + \frac{\cos^2\theta_i}{16t^3\sin^5\theta_i} m^3(\lambda-\lambda_m)^3 + \frac{5\cos^2\theta_i}{128t^4\sin^7\theta_i} m^4(\lambda-\lambda_m)^4 \tag{A17}$$

Using this expression in the expression for the spatial phases (eqn (A10)) and grouping the corresponding spectral phases by order we have the expression for spectral phases as - Linear phase -

$$\exp\left(i\frac{2\pi}{\lambda}\frac{(L+\frac{F}{2}\tan 2\theta_m)}{2t\sin\theta_i} m(\lambda-\lambda_m)\right) \tag{A18}$$

Quadratic phase -

$$\exp\left(i\frac{2\pi}{\lambda}\frac{(L+\frac{F}{2}\tan 2\theta_m - d\tan\theta_i)\cos\theta_i}{4t^2\sin^3\theta_i} m^2(\lambda-\lambda_m)^2\right) \tag{A19}$$

Cubic phase -

$$\exp\left(i\frac{2\pi}{\lambda}\frac{(L+\frac{F}{2}\tan 2\theta_m - d\tan\theta_i)\cos^2\theta_i}{8t^3\sin^5\theta_i} m^3(\lambda-\lambda_m)^3\right) \tag{A20}$$

Biquadratic phase –

$$\exp\left(i\frac{2\pi}{\lambda}\frac{(L+\frac{F}{2}\tan 2\theta_m - d\tan\theta_i)5\cos^3\theta_i}{64t^4\sin^7\theta_i} m^4(\lambda-\lambda_m)^4\right) \tag{A21}$$

Converting these expressions from the wavelength domain to the frequency domain, we get the equivalent expressions for spectral phases as

Linear phase -

$$\exp(-i*2\pi\frac{(2L+F\tan 2\theta_m)}{2t\sin\theta_i}m\frac{(\omega-\omega_m)}{\omega_m}) \tag{A22}$$

Quadratic phase -

$$\exp(i*2\pi\frac{(L+\frac{F}{2}\tan 2\theta_m-d\tan\theta_i)\cos\theta_i}{4t^2\sin^3\theta_i}(\frac{2\pi c}{\omega})m^2\frac{(\omega-\omega_m)^2}{\omega_m{}^2}) \tag{A23}$$

Cubic phase -

$$\exp(-i*2\pi\frac{(L+\frac{F}{2}\tan 2\theta_m-d\tan\theta_i)\cos^2\theta_i}{8t^3\sin^5\theta_i}(\frac{2\pi c}{\omega})^2m^3\frac{(\omega-\omega_m)^3}{\omega_m{}^3}) \tag{A24}$$

Biquadratic phase -

$$\exp(-i*2\pi\frac{(L+\frac{F}{2}\tan 2\theta_m-d\tan\theta_i)5\cos^3\theta_i}{64t^4\sin^7\theta_i}(\frac{2\pi c}{\omega})^3m^4\frac{(\omega-\omega_m)^4}{\omega_m{}^4}) \tag{A25}$$

Here ω_m is the frequency corresponding to λ_m, $\Delta\omega$ is the FSR of the VIPA expressed in frequency units and c is the velocity of light. The order number can also be represented in the frequency domain as $\omega_m/\Delta\omega$

We are not interested in the linear spectral phase since that is just a pulse delay in the time domain but 2nd and higher order spectral phases affect the temporal envelope of the pulse. In this case along with 2nd order spectral phase which causes temporal dispersion, we also have higher order spectral phases which cause pulse distortion. We notice that in all the eqns (A23-A25) which give the expressions for the quadratic, cubic and bi-

quadratic phases, they have a common coefficient which is $L+\frac{F}{2}\tan 2\theta_m - d\tan\theta_i$. In fact, we will now show that this coefficient is in every term of degree>1. From eqn(A14) we have $\frac{x}{F}$ in the functional form –

$$\frac{x}{F} = 2t\tan\theta_i(\sqrt{1-\alpha}-1) \tag{A26}$$

Where $\alpha = \frac{\cos\theta_i(m(\lambda-\lambda_m))}{t\sin^2\theta_i}$. Substituting this in the equation for the spatial phases (eqn (A9)) we have the expression for spectral phases as

$$e^{(-ik(L+\frac{F}{2}\tan 2\theta_m - d\tan\theta_i)4t\tan\theta_i(\sqrt{1-\alpha}-1)-i4kdt^2\tan^2\theta_i\alpha)} \tag{A27}$$

It is clear from the above the expression that when the expression is expanded in a power series in terms of α, except for the first order term (since it includes the additional term to the right), for all orders of α>1, the coefficient will contain the term $L+\frac{F}{2}\tan 2\theta_m - d\tan\theta_i$. If we can adjust the parameters of the experiment to make this term zero, then all 2nd and higher order phases will go to zero. This will provide us a configuration with no dispersion or pulse distortion and will be the true zero dispersion condition for a VIPA based pulse shaper.

Zero dispersion condition

$$L+\frac{F}{2}\tan 2\theta_m - d\tan\theta_i = 0 \tag{A28}$$

It is interesting to look at the physical interpretation of the zero dispersion condition. By nature of the VIPA based pulse shaper configuration, a linear spatial phase is unavoidable and hence the non linear sampling of this linear phase will force higher order

spectral phase terms. However the distance between the VIPA and Fourier lens which introduces a quadratic spatial phase, on non linear sampling, will also introduce second and higher order spectral phases. So what we are doing here is to change the VIPA lens distance to create phases which are of opposite sign to compensate the phases created due to the spatial linear phase and thus producing a net zero dispersion configuration.

The constants in equation (A28) give us an idea of the importance of individual parameters. Since the input angle to the VIPA is usually small (< 5deg) and the focal length of the Fourier lens is tens of centimeters, we see that the temporal dispersion is much more sensitive to L and θ_m than it is to d and so it becomes important to control these parameters precisely. To get an idea of the numbers involved, for a VIPA with an incident angle of 5 degrees, an aperture of 11mm, a Fourier lens of focal length 20cm and $\theta_m = 0$, the value of L to obtain minimum loss is ~ 4mm [74]. To compensate the temporal dispersion caused by this, the distance the lens has to be moved from the 4-F configuration is ~4.5cm. We see that the change that needs to be done to compensate these effects is significant (more than 20% of the focal length of the lens in this case).

Now let us quantitatively describe the spectral manifestation of dispersion. Let $\psi^m(\lambda)$ and $\psi^{m+1}(\lambda)$ be the spectral phase for a wavelength λ for two adjacent diffraction orders 'm' and 'm+1'. As shown in fig A2, on the Fourier plane since there is a Gaussian envelope which decides the intensity distribution, interference effects will largely be limited to two adjacent diffraction orders dispersed around x=0. So we are justified in modeling this with only two orders. The output power at the wavelength λ now depends on the coherent sum of the two orders which is a function of their phase difference. If the phase difference becomes a function of λ, then as the wavelength changes the interference condition may change from constructive to destructive etc causing spectral amplitude ripples. Firstly taking into consideration only the linear spectral phase (eqn A18) we have

$$\psi^{m+1}(\lambda) - \psi^m(\lambda) = 2\pi \frac{(L + \frac{F}{2}\tan 2\theta_m)}{2t \sin\theta_i} \tag{A29}$$

In the simplification we have used $\lambda_m = 2t\cos\theta_i / m$ defined before. We see that the phase difference is independent of λ and hence does not contribute to spectral ripples. However if we take the quadratic spectral phase (eqn 19) we have

$$\psi^{m+1}(\lambda) - \psi^{m}(\lambda) = 2\pi \frac{(L + \frac{F}{2}\tan 2\theta_m - d\tan\theta_i)\cos\theta_i}{4t^2 \sin^3\theta_i}(2m(\lambda - \lambda_m) + \lambda) \qquad \text{(A30)}$$

Which we see is linearly related to λ and so as λ changes the coherent sum is expected to change. Another interesting point to note is that, for the case of quadratic spectral phase, since the phase difference is linearly proportional to λ, the spectral ripple is expected to be sinusoidal with a constant period. If we defined the period as P, then it has to satisfy –

$$[\psi^{m+1}(\lambda + P) - \psi^{m}(\lambda + P)] - [\psi^{m+1}(\lambda) - \psi^{m}(\lambda)] = 2\pi \qquad \text{(A31)}$$

Substituting this in eqn (A30) and again making use of $m \sim 2t\cos\theta_i / \lambda$, we get the expression for the constant ripple period as –

$$P = \frac{\lambda t \sin^3\theta_i}{(L + \frac{F}{2}\tan 2\theta_m - d\tan\theta_i)\cos^2\theta_i} \qquad \text{(A32)}$$

Similarly looking at 3rd and higher order spectral phases will show phase differences which vary with wavelength at order 2 and higher. However, the net magnitude of the phase contributions progressively reduce as we go higher in order and so we can visualize the spectral ripple formation as a constant period function due to the 2nd order phase with the period modified by the higher order spectral phases. More detail on this work can be found in our paper [75].

VITA

VITA

Supradeepa Venkata Subbaiah Ramakrishna received his B.Tech. degree in Engineering Physics from Indian Institute of Technology Madras, India, in 2006, and is currently a Ph.D. candidate in the School of Electrical and Computer Engineering at Purdue University, West Lafayette, IN. He has been a Research Assistant in the Ultrafast Optics and Optical Fiber Communications Laboratory since 2006. His current research interests include Ultrafast Optics, Optical signal processing, Fiber optics, Optical communications, Radio Frequency Photonics, Optical frequency combs and Optical Metrology.

During the course of his graduate study, Supradeepa has authored/co-authored over 30 publications in peer reviewed journals and international conferences. He was awarded the IEEE Photonics Society graduate fellowship for the year 2010-2011 for demonstrated excellence in graduate work. He is a student member of the Optical Society of America, IEEE Photonics Society and the electrical engineering honor society Eta Kappa Nu. He has served as a reviewer for Journal of Lightwave Technology, Optics Letters, Optics Express, Applied Optics and Optics Communications.